UNIVERSIDADE FEDERAL DE MINAS GERAIS

Escola de Engenharia

Programa de Pós-Graduação em Engenharia Metalúrgica, Materiais e de Minas

Taiane Guedes Fonseca de Souza

INFLUÊNCIA DO ALUMÍNIO NA ADSORÇÃO E IMOBILIZAÇÃO DE CONTAMINANTES POR FERRIDRITAS

Belo Horizonte

2022

Taiane Guedes Fonseca de Souza

INFLUÊNCIA DO ALUMÍNIO NA ADSORÇÃO E IMOBILIZAÇÃO DE CONTAMINANTES POR FERRIDRITAS

THE INFLUENCE OF ALUMINUM ON THE ADSORPTION AND IMMOBILIZATION OF CONTAMINANTS BY FERRIHYDRITES

Versão final

Tese de Doutorado apresentada ao Programa de PósGraduação em Engenharia Metalúrgica, Materiais e de Minas da Universidade Federal de Minas Gerais, como requisito parcial para obtenção do grau de Doutor em Engenharia Metalúrgica, Materiais e de Minas.

Área de concentração: Ciência e Engenharia de Materiais

Orientadora: Profª. Virginia S. T. Ciminelli

Co-orientadora: Profª. Nelcy D. S. Mohallem

Belo Horizonte

2022

Souza, Taiane Guedes Fonseca de.
S729i Influência do alumínio na adsorção e imobilização de contaminantes por ferridritas [recurso eletrônico] = The influence of aluminum on the adsorption and immobilization of contaminants by ferridrites / Taiane Guedes Fonseca de Souza. – 2022.
1 recurso online (141 f.: il., color.): pdf.

Orientadora: Virgínia Sampaio Teixeira Ciminelli.
Coorientadora: Nelcy D. S. Mohallem.

Tese (doutorado) - Universidade Federal de Minas Gerais, Escola de Engenharia.

Apêndices: f. 124-139.

Bibliografia: f. 102-123.
Exigências do sistema: Adobe Acrobat Reader.

1. Materiais - Teses. 2. Ciência dos materiais - Teses. 3. Alumínio - Metalurgia - Teses. 4. Adsorção - Teses. 5. Arsênio - Teses. 6. Antibióticos - Teses. I. Ciminelli, V.S.T. (Virgínia Sampaio Teixeira). II. Mohallem, Nelcy Della Santina. III. Universidade Federal de Minas Gerais. Escola de Engenharia. IV. Título.

CDU: 620(043)

Ficha catalográfica elaborada pela Bibliotecária Roseli Alves de Oliveira CRB/6 2121
Biblioteca Prof. Mário Werneck, Escola de Engenharia da UFMG

UNIVERSIDADE FEDERAL DE MINAS GERAIS
ESCOLA DE ENGENHARIA
Programa de Pós-Graduação em Engenharia Metalúrgica, Materiais e de Minas

A tese intitulada **"Influência do Alumínio na Adsorção e Imobilização de Contaminantes por Ferridritas"**, área de concentração: Ciência e Engenharia de Materiais, apresentada pela candidata **Taiane Guedes Fonseca de Souza**, para obtenção do grau de Doutora em Engenharia Metalúrgica, Materiais e de Minas, foi aprovada pela comissão examinadora constituída pelos seguintes membros:

Dra. Virginia Sampaio Teixeira Ciminelli
Orientadora (UFMG)

Dra. Nelcy Della Santina Mohallem
Coorientadora (UFMG)

Dr. Eduardo Henrique Martins Nunes
(UFMG)

Dr. Hélio Anderson Duarte
(UFMG)

Dra. Ana Cláudia Queiroz Ladeira
(CNEN/CDTN)

Dr. Fernando Luiz Pantuzzo
(SRK Consulting)

Coordenador do Programa de Pós-Graduação em Engenharia Metalúrgica, Materiais e de Minas/UFMG

Belo Horizonte, 27 de julho de 2022

AGRADECIMENTOS

À Deus, por me amparar, me guiar e colocar pessoas maravilhosas no meu caminho, sem as quais essa jornada teria sido impossível.

À minha família pelo incentivo e admiração. Agradeço em especial: ao meu pai, Sr Geraldo, pelo orgulho e apoio incondicional, ao Leo pelo carinho e à Marina pelo amor, pelos choques de realidade, pela companhia (no lab ou nos estudos) e por cuidar do João para eu trabalhar. À minha mãe (in memorian), dona Marlene, que me incentivou a ler e querer aprender desde sempre. Ao Breno por ser mais que um companheiro. Pela colaboração científica, pelos ensinamentos de físico-química e de redação científica, pelos conselhos (ainda que alguns fossem ignorados), por assumir integralmente o cuidado da nossa família nas tantas vezes que precisei me ausentar, por todo amor, incentivo e suporte. Ao João por me encher de amor e alegria, por me fazer crescer como pessoa e por me ajudar a levantar da cama nos dias difíceis. À Helena pela companhia involuntária nas madrugadas, por me colocar prazos e por me encher de expectativas e esperança. A Stru (*in memorian*) por ter sido meu exemplo de determinação com os estudos (às vezes, aprender dói). À Keliane que no início desta jornada trouxe pra nossa casa, cuidado, tranquilidade, encheu o João de carinho e, assim, permitiu que me dedicasse a esse trabalho.

Sou imensamente grata às minhas orientadoras. À Prof.ª Virginia pelo exemplo de excelência e dedicação. Por me fazer crescer enquanto pesquisadora e aluna, pelas críticas certeiras que me fizeram buscar melhorar e pelas longas horas (em curto espaço de tempo) dedicadas a esta tese, devido à minha ansiedade e vinda da Helena. À Prof.ª Nelcy que muito me ensinou sobre ciência, academia e pesquisa ao longo desses 16 anos. Pela serenidade e positividade ao lidar com meus desesperos e resultados ruins. Pelos puxões de orelha, conselhos, acolhimento e carinho que ultrapassam a relação orientadora e orientada.

Nessa caminhada contei com a ajuda e ensinamento de diversas pessoas. Agradeço especialmente à Sica (Profª Maria Sylvia Dantas) pelas aulas de Raman, cuidado com cada resultado, pássaros, conselhos para a vida e alegria compartilhadas na salinha do Raman. Apesar de ser a física mais doce que já conheci, por xingar minhas amostras e me mandar esquenta-las. Ao Érico Freitas por tamanha

generosidade ao me ensinar sobre TEM, pelas colaborações e pelas imagens mais lindas desta tese. Às Prof.ª Andreia Bicalho (que me socorreu em meio à pandemia) e Ângela Mello pelas análises de difração de raios X. Aos Prof. Witor Wolf e Renata Diniz pelos valiosos ensinamentos em microscopia e cristalografia e por sua maneira humana e humilde de ensinar. À Cida (Aparecida Pacheco) pela eficiência e presteza em ajudar sempre.

Aos amigos do Laborátório de Hidrometalurgia pelo convívio prazeroso, trocas de conhecimento e lanchinhos. Agradeço principalmente a Nathalia, Nelson, Saulo, Tamiris, Victor, Marina, Nathanael, Thaiara e Daísa pelos desabafos, polêmicas e descontrações. Ao Tio Nelson sou grata também companhia e colaboração no lab. Ao Sunday pelas colaborações e discussões acadêmicas, religiosas e pelos conselhos para a vida. À Ilda por espalhar alegria pelo laboratório e pela disponibilidade em nos socorrer. À Claudia Caldeira e Christina Salvador pela presteza e disponibilidade em ajudar sempre. À Patrícia e Guilhermina por me ensinarem sobre ICP-OES e de análise química. À Hellen e Filipe pelas análises químicas, pelos inúmeros socorros. Ao Prof. Emílio (*in memorian*) por todos os ensinamentos. Aos colegas do LMN pela receptividade e conhecimento trocados, em especial ao Gustavo e ao Luiz pelos ensinamentos e discussões em refinamento Rietveld e adsorção gasosa.

Aos amigos: Naira, Júnia, Bia, Núbia, Val, Ju, Lívia, os que a química trouxe, os da Nanum e os do barreiro. Por sempre acolheram minhas lerdezas, me encheram de carinho e fazerem parte da minha construção. À Roberta pelos inúmeros momentos compartilhados ao longo da vida pessoal e acadêmica.

Por fim, agradeço ao Curso de Pós-Graduação em Engenharia Metalúrgica, de Minas e Materiais e às agências: CNPq, INCT-Acqua, Fapemig e CAPES pelo suporte e apoio financeiro, essenciais à realização desta pesquisa e no crescimento da ciência e educação no país.

À todos, muito obrigada!!!

Nothing in life is to be feared, it is only to be understood. Now is the time to understand more, so that we may fear less.

(Marie Curie)

RESUMO

As ferridritas (Fh) são minerais metaestáveis, abundantes no solo e comumente encontradas contento Al substituindo parcialmente o Fe. Devido a sua elevada área superficial (até 650 m^2 g^{-1}), são excelentes candidatas para adsorção de contaminantes, além de impactarem no destino destes no solo. Por este motivo, a remoção de dois contaminantes por Fh (contendo ou não Al) foi estudada de maneira aprofundada neste trabalho: o arsênio-um metaloide extremante tóxico que, seja por origem natural ou antrópica, representa um problema para o abastecimento de água de muitas regiões- e a amoxicilina (AMX)- um contaminante emergente, cujo aumento da concentração no ambiente pode levar ao desenvolvimento de bactérias resistentes, um dos grandes problemas de saúde pública. As Fh mostraram capacidade de remoção superior a muitos adsorventes, tanto para As (8.6 µmol m^{-2}) quanto para AMX (75 mg g^{-1}). Identificou-se que o Al, isomorficamente substituído (até 15% em mol), aumentou a quantidade de hidroxilas na superfície das Fh e, com elas, a capacidade de adsorção de As (em até 28 %). Resultados similares foram encontrados em solos ricos em oxihidróxidos de Fe contendo Al. Já para a AMX o efeito do Al foi contrário. O principal mecanismo de interação foi identificado como complexação bidentada binuclear da carboxila com o Fe da superfície do adsorvente. Uma interação forte, a qual, em solos contaminados com AMX e ricos em Fh, pode retardar o transporte do antibiótico permitindo, assim, a degradação por bactérias do solo. Como o As não pode ser degradado, uma alternativa é sua imobilização nos resíduos. Neste contexto, foi estudado o envelhecimento dos resíduos da adsorção de As em Fh e FhAl. Inicialmente, o Al aumentou a mobilidade de As e o tempo de transformação de fase. Porém, sua presença alterou esse mecanismo, formando apenas hematitas (mais inertes que as goethitas formadas nas amostras sem Al) e formando agregados orientados. Nas FhAl sintéticas, após envelhecimento, e nos óxidos e hidróxidos contendo Al presentes no solo, o Al aumentou a fixação de As em 6 pontos percentuais, possivelmente pela incorporação de As dentro de agregados orientados formados devido à presença de Al.

Palavras chave: Ferridrita. Substituição isomórfica. Alumínio. Adsorção. Arsênio. Amoxicilina.

ABSTRACT

Ferrihydrites (Fh) are metastable minerals, abundant in soil and commonly found with Al-for-Fe isomorphic substitution. Due to their high surface area (up to 650 m^2 g^{-1}), they are excellent candidates for adsorption of contaminants. Ferrihydrites also influence the contaminants fate in the soil. For this reason, the removal of two contaminants by Fh (containing or not Al) was studied in depth. Arsenic - an extremely toxic metalloid that, either by natural or anthropogenic origin, represents a problem for the water supply of many regions- and amoxicillin (AMX)- an emerging contaminant, whose increase in the environment can lead to the development of resistant bacteria, one of the major public health problems. The synthesized Fh showed superior removal capacity than many adsorbents for both As (8.6 µmol m^{-2}) and AMX (75 mg g^{-1}). The isomorphically substituted Al (until 15 mol%) was found to increase the number of hydroxyls on the Fh surface and, in turn, As uptake (up to 28%). Similar results were found in soils rich in Fe oxyhydroxides containing Al. For AMX, the effect of Al was the opposite. The main mechanism of interaction was identified as binuclear bidentate complexation of the carboxyl group with the surface Fe of the adsorbent. This strong interaction can delay antibiotic transport, thus allowing degradation by bacteria in Fe- rich soils contaminated with AMX. As arsenic cannot be degraded, an alternative is its safe immobilization in waste. In this context, the aging of the residues of As adsorption in Fh and FhAl was studied. Initially, Al increased the As mobility and the time for phase transformation. However, Al also altered the aging mechanism, by forming only hematite as the end-product (more inert than the goethite also formed in the absence of Al) and oriented aggregates. In both the synthetic FhAl, after aging, and Al-containing oxides and hydroxides in soils, Al increased As fixation in 6 percentage points, by the incorporation of the metalloid within oriented aggregates produced in the presence of aluminum.

Keywords: Ferrihydrite. Isomorphic substitution. Aluminum. Adsorption. Arsenic. Amoxicillin.

LIST OF FIGURES

LIST OF TABLES

LIST OF ACRONYMS

AMX- Amoxicillin

ATR- Attenuated Total Reflectance

ASA- Apparent Surface Area

BE- Binding Energy

BET- Brunauer-Emmett-Teller method

DFT- Density Functional Theory

DFTB- Density Functional Tight-Binding method

EDS- X-Ray Dispersive Spectroscopy

Fh- Ferrihydrites

FFT- Fast Fourier Transform

FTIR- Fourier Transform Infra-Red spectroscopy

HRTEM- High Resolution Transmission Electron Microscopy

ICP-OES- Inductively Coupled Plasma Optical Emission Spectrometry

ICSD- Inorganic Crystal Structure Database- FIZ Karlsruhe Institut

IEP- Isoelectric Point

MLA- Mineral Liberation Analysis setup

OA- Oriented Attachment

OR- Ostwald Ripening

PDF- Powder Diffraction File

SAD- Selected Area Electron Diffraction

SEP- Sequential Extraction Protocol

SCC-DFTB- Density Functional Tight-Binding method, including the Self-Consistent Charge approach

SSA- Specific Surface Area

TEM- Transmission Electron Microscopy

XPS- X-Ray Photoelectron Spectroscopy

XRD- X-Ray Diffraction

SUMMARY

1. INTRODUÇÃO

1.1 Ferridrita: um mineral abundante e relevante no transporte ou remoção de contaminantes do ambiente

As ferridritas (Fh) são oxihidróxidos de Fe(III), nanocristalinos, metaestáveis, e extremante abundantes em solos, leitos de rios, afloramento de nascentes, sedimentos costeiros, lagoas de drenagem ácida de minas, entre outros (JAMBOR; DUTRIZAC, 1998; SCHWERTMANN, UDO; FRIEDL; STANJEK, 1999; WAYCHUNAS, GLENN A.; KIM; BANFIELD, 2005). Estes minerais só existem como nanopartículas (< 12 nm), as quais possuem elevada área superficial específica (até 650 m^2 g^{-1}), alta reatividade e grande quantidade de defeitos estruturais (BOILY; SONG, 2020; HIEMSTRA; VAN RIEMSDIJK, 2009; SASSI; CHAKA; ROSSO, 2021). Sua abundância e propriedades fazem esse mineral singular extremamente relevante para aplicações de remoção/imobilização de contaminantes, bem como, para o transporte e destino de poluentes no solo (CHEN, X. *et al.*, 2022; JOHNSTON; CHRYSOCHOOU, 2016; KUBICKI *et al.*, 2018; LI, B. *et al.*, 2021; NAMAYANDEH; KABENGI, 2019; PRASAD PANDA *et al.*, 2022).

As Ferridritas são classificadas como 2-linhas ou 6-linhas, quando sintetizadas, de acordo com o número de linhas dos seus respectivos padrões de difração. Porém, as formas naturais podem apresentar outros padrões (2-7 linhas) (SCHWERTMANN, UDO; FRIEDL; KYEK, 2004). Seu tamanho reduzido e defeitos estruturais fazem com que a estrutura cristalográfica e fórmula molecular da Fh sejam, ainda hoje, objeto de controvérsia (DRITS *et al.*, 1993; MANCEAU, A.; SKANTHAKUMAR; SODERHOLM, 2014; MANCEAU, ALAIN, 2019; MICHEL; EHM; ANTAO; *et al.*, 2007; SASSI; CHAKA; ROSSO, 2021). Os autores divergem entre si quanto a presença de hidroxilas estruturais além da existência e localização de átomos de Fe com coordenação tetraédrica. Neste trabalho serão adotadas a fórmula molecular $Fe_5O_8H.4H_2O$ e a estrutura proposta por Michel e colaboradores para Fh de 2-3 nm (MICHEL; EHM; ANTAO; *et al.*, 2007; MICHEL; EHM; LIU; *et al.*, 2007).

Os oxihidróxidos de ferro raramente existem em sua forma pura em ambientes naturais, estando associados, principalmente, a Si, Al e Mn (Cornell and

Schwertmann, 2003; Liang et al., 2019; Ye et al., 2020; Zoppi et al., 2008). O alumínio é abundante na natureza e pode influenciar a reatividade da Fh, afetando, assim, sua eficiência na remoção de contaminantes, bem como a estabilidade dos produtos adsorvidos visando a uma possível disposição. Os efeitos da substituição do Fe por Al na morfologia e na área superficial específica de hematitas também tem sido objeto de estudos, pois a alteração da morfologia, a quantidade e a distribuição dos grupos hidroxila de superfície alteram o comportamento na adsorção de poluentes (BARRON; HERRUZO; TORRENT, 1988; DI IORIO *et al.*, 2018; HA *et al.*, 2009; LIANG *et al.*, 2019).

O crescimento da população mundial traz consigo a demanda cada vez maior por água potável. Há regiões no mundo que já sofrem com o estresse hídrico (onde a demanda média de água por habitante é maior que a oferta por habitante), como mostra a Figura 1.**1**, e a perspectiva futura é que esse cenário se agrave como mostram as previsões do *World Resources Institute* (https://www.wri.org/tags/water-stress).

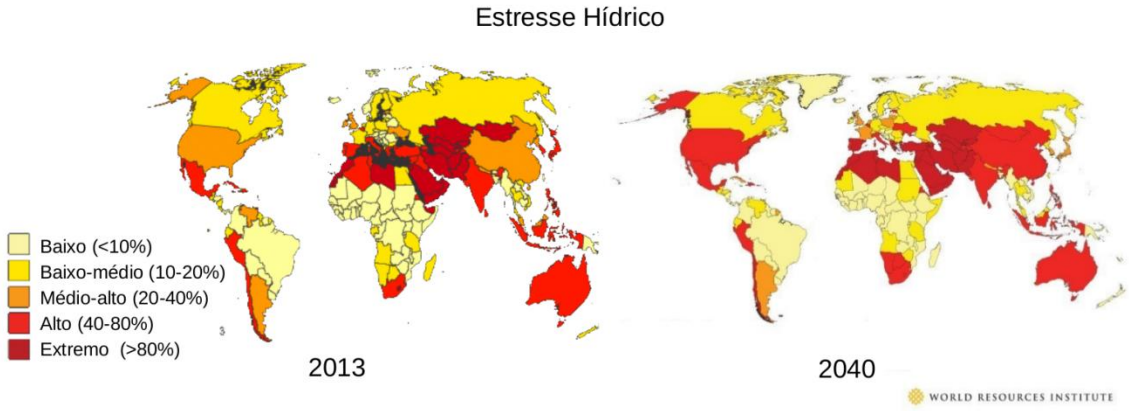

Figura 1.1: Demanda média de água por habitante em função da oferta (estresse hídrico) medido em 2013 e previsto para 2040. Adaptado de *World Resources Institute.*

Assim, o desenvolvimento de tecnologias eficientes para remediação e tratamento de águas e solos contaminados, bem como a efetiva imobilização dos rejeitos produzidos, se fazem cada vez mais necessários a fim de suprir a demanda crescente de água potável e evitar a contaminação dos solos e águas subterrâneas.

As águas impróprias para consumo podem ocorrer naturalmente ou pela disposição inadequada de contaminantes. O arsênio, por exemplo, pode contaminar águas por

ocorrência natural ou fruto de ações antrópicas (mineração, fundição, produtos de combustão de combustíveis fósseis, uso de pesticidas e fertilizantes fosfatados) (JUNGCHAROEN *et al.*, 2017; SMEDLEY; KINNIBURGH, 2002). O arsênio (As) pode ser encontrado no ambiente na forma inorgânica (sob a forma de oxiânions cuja carga e o número de oxidação dependem do pH e potencial redox do meio), associado a hidrogênios (arsina), ou a radicais orgânicos. Trata-se de um elemento extremamente tóxico e a sua presença na forma de traços (e.g., 100 μg/L) em água subterrânea usada para consumo humano, em Bangladesh, resultou no que é considerado o maior problema de contaminação em massa já reportado no mundo. O grau de toxicidade dos compostos de arsênio diminui na seguinte ordem: arsina (-3) > derivados orgânicos da arsina > arsênio inorgânico (+3) > arsênio orgânico (+3) > arsênio inorgânico (+5) > compostos orgânicos pentavalentes > compostos de arsênio e por último o arsênio elementar (VIRARAGHAVAN; SUBRAMANIAN; ARULDOSS, 1999). Estudos envolvendo remoção e fixação de As são de grande relevância para diversas regiões do estado de Minas Gerais, como Paracatu, Ouro Preto e Nova Lima, onde se observa a ocorrência natural de solos com alto teor de As, em geral associados à mineralização de ouro. A mineração de ouro é uma atividade antrópica capaz de mobilizar As e gerar grandes quantidades de rejeitos contendo o metalóide. As anomalias de As criam uma preocupação permanente para a população e governança local, principalmente após os desastres envolvendo barragens de mineração de ferro em Mariana e Brumadinho nos últimos anos.

É estimado que cerca de 100 milhões de pessoas estejam utilizando água subterrânea contaminada por arsênio (HENKE, 2009; JUNGCHAROEN *et al.*, 2017). A exposição crônica a níveis superiores a 10 μg/L As em água potável pode causar vários problemas de saúde, incluindo câncer (DODD *et al.*, 2006). Portanto, com o aumento da população mundial e a demanda por água, muitas técnicas para imobilizar As tem sido investigadas (BOSMAN *et al.*, 2006; CHEN, L. *et al.*, 2014; DI IORIO *et al.*, 2018; FRANKENBERGER, 2001; LIM *et al.*, 2013; XUE *et al.*, 2019). O custo do tratamento, a complexidade operacional do processo, a habilidade necessária para operá-lo e o descarte de resíduos de arsênio devem ser considerados antes da seleção do método de tratamento. E todas essas técnicas produzirão resíduos de arsênio, que deverão ser estáveis para evitar posterior contaminação do solo, dos aquíferos e, consequentemente, da população.

Outro objeto de preocupação na contaminação de águas são os chamados contaminantes emergentes. Dentre eles, os antibióticos, e alguns de seus produtos de degradação (ANASTOPOULOS *et al.*, 2020). Os antibióticos, mesmo em concentrações traço no ambiente, podem afetar os organismos aquáticos, causar distúrbios metabólicos e reprodutivos (BOJARSKI; KOT; WITESKA, 2020), e a morte ou inibição do crescimento de bactérias importantes no ecossistema, além de desenvolver microrganismos resistentes, o que constitui um problema crescente de saúde pública (COSTANZO; MURBY; BATES, 2005). Em 2015, o consumo de antibióticos foi estimado em mais de 42 bilhões de doses diárias e as projeções para 2030 são de um aumento de até 200% (KLEIN, E. Y. *et al.*, 2018). Os β-lactamas são os mais utilizados mundialmente devido ao seu amplo espectro de atividade antibacteriana (KÜMMERER, 2009; RODRIGUEZ-HERRERA *et al.*, 2019). A amoxicilina (AMX) é dos representantes relevantes da classe β-lactamas de antibióticos. A amoxicilina pode ser encontrada na natureza devido a atividades agropecuárias, resíduos industriais, de hospitais ou doméstico, devido a metabolismo incompleto (excreção de até 80% da dose ingerida) (AKSU DEMIREZEN; YILDIZ; DEMIREZEN YILMAZ, 2019; GRENNI; ANCONA; BARRA CARACCIOLO, 2018; KÜMMERER, 2009). Apesar disso, o mecanismo de adsorção de AMX em minerais encontrados nos solos permanece pouco investigado (KLEIN, A. R. *et al.*, 2021; PUTRA *et al.*, 2009; TRI; NGUYEN; TRUNG, 2020). Trabalhos anteriores sobre a adsorção de AMX em Fh não foram encontrados na literatura.

A substituição isomórfica de parte do alumínio por ferro em oxi-hidróxidos de ferro para remoção de contaminantes é controversa. Alguns consideram a presença de Al uma abordagem eficiente para a remoção do arsênio e chumbo (ADRA *et al.*, 2016; LIANG *et al.*, 2019; TUFO; AFONSO; SILEO, 2016) de águas contaminadas. Porém, há trabalhos que mostram que a introdução de Al pode diminuir a adsorção de As(V) (MASUE; LOEPPERT; KRAMER, 2007; SILVA *et al.*, 2010; VIOLANTE *et al.*, 2009). A substituição isomórfica de oxihidróxidos de Al por Fe é comumente observada em solos e tem sido correlacionada com elevadas concentrações de As no ambiente, conforme observado em trabalhos do grupo (ANTÔNIO, DAPHNE C. *et al.*, 2021; FREITAS *et al.*, 2015) e, portanto, tornou-se um dos focos desta investigação.

Apesar da importância das Fh substituídas por Al em sistemas ambientais, a caracterização da incorporação de Al ainda é deficiente bem como o entendimento de como a verdadeira substituição química afetará a adsorção de As. No que concerne à estabilidade dos produtos de adsorção de As, existem alguns trabalhos que estudaram a influência da presença de As ou Al no envelhecimento de Fh (Bolanz et al., 2013; Das et al., 2014; Li et al., 2016; Wang et al., 2022, 2015). Porém, os efeitos sinérgicos do Al e As nas transformações de fases de Fh contendo Al isomorficamente substituído, bem como na remobilização de As previamente adsorvido, permanecem desconhecidos.

No que concerne à remoção de amoxicilina por Fh, não foram encontrados estudos na literatura. Como mineral ubíquo no solo e leitos de rios, compreender a adsorção de AMX por Fh é relevante considerando o destino da AMX (de atividades agrícolas e rios contaminados, por exemplo) no meio ambiente e a prevenção da contaminação de águas subterrâneas. Além disso, os adsorventes à base de Fh são relativamente simples de produzir. Apesar das características atrativas da Fh (pura ou substituída com Al), a capacidade de adsorção e os mecanismos de interação com o AMX ainda precisam ser investigados.

Neste contexto, o principal objetivo deste trabalho é aprofundar a compreensão do papel do Al, em Fh isomorficamente substituídas, na remoção e imobilização de contaminantes, mais especificamente arsênio e amoxicilina, escolhidos como representantes de contaminante inorgânico e emergente, respectivamente, e objetos deste estudo. Pretende-se avaliar e compreender a influência do Al na capacidade de adsorção e possível remobilização dos contaminantes através da elucidação do mecanismo de adsorção da AMX, da investigação do papel do Al no envelhecimento da Fh e no destino do As nos produtos de envelhecimento de Fh contendo ou não Al.

1.2 Estrutura e organização da tese

A presente tese está organizada em 5 capítulos. O capítulo 1, intitulado Introdução, traz uma breve contextualização do trabalho. É feita uma breve apresentação da ferridrita. Em seguida, são evidenciadas as principais lacunas da literatura no que concerne (i) o uso de ferridritas isomorficamente substituídas na remoção de As (V),

(ii) o destino do As adsorvido em Fh ou AlFh durante a transformação de fases desses oxihidróxidos e (iii) o uso de Fh na remoção de AMX. São apresentados também os objetivos desta tese.

O Capítulo 2 apresenta os resultados e discussão da adsorção de As em Al-Ferridritas. Este capítulo deu origem à publicação “Defects induced by Al substitution enhance As(V) adsorption on ferrihydrites”, publicada no Journal of Harzardous Materials, volume 420, página 126544 (DOI: 10.1016/j.jhazmat.2021.126544). Esta etapa do trabalho aborda a síntese e caracterização de ferridritas contendo Al isomorficamente substituídos. O impacto da presença de Al na adsorção de As(V) foi estudado em pH 5 e 8. Mostrou-se um aumento de até 28% na adsorção de As e sua causa foi investigada por meio das técnicas de espectroscopia na região do infravermelho com transformada de Fourier (FTIR), difração de elétrons por área selecionada e espectroscopia fotoelétrons de raios X. O impacto ambiental desses resultados é discutido com base em análises de solos ricos em As e oxihidróxidos de Fe com diferentes teores de Al.

No Capítulo 3 as ferridritas substituídas, ou não, em Al foram testadas para a remoção de outro contaminante, a amoxicilina (AMX). Foi estimada a capacidade máxima de adsorção pelos adsorventes contendo 0 e 10% de Al, bem como a influência do pH e da força iônica no processo. Cálculos teóricos, utilizando DFTB (*Density Functional Based Tight Binding method*), combinados com resultados de FTIR e espectroscopia Raman ajudaram na elucidação do principal mecanismo envolvido na remoção. Este trabalho foi submetido para publicação em revista científica da área e está sob revisão de pares.

Os estudos apresentados no Capítulo 4 buscam melhorar o entendimento da presença de Al na fixação de As adsorvido nas Fh. Os experimentos abordam o envelhecimento de Fh (contendo ou não Al e As) e as transformações de fases decorrentes deste envelhecimento. Os mecanismos envolvidos no crescimento das partículas são discutidos a luz das técnicas de difração de raios X e microscopia eletrônica de transmissão. Buscando entender o particionamento do As nas fases formadas, bem como sua possível mobilidade no ambiente e a intensidade da ligação As-FhAl, amostras envelhecidas ou não foram submetidas a ensaios de extração sequencial (SEP). Os resultados das amostras sintéticas foram, então,

correlacionados com resultados (de SEP) de solos ricos em As, óxidos e hidróxidos de Fe, contendo diferentes teores de Al.

No capítulo 5 são destacados os resultados principais obtidos por esta pesquisa e sugeridos tópicos para futuras investigações.

Por fim, os apêndices A, B e C trazem informações e figuras complementares a cada capítulo (2, 3 e 4 respectivamente) e o apêndice D mostra um pequeno resumo dos trabalhos realizados em colaboração com outros pesquisadores. A tese é finalizada com um pequeno memorial da autora e as referências bibliográficas utilizadas no trabalho.

2. INTRODUCTION

2.1 Ferrihydrite: an abundant and relevant mineral in the transport or removal of contaminants from the environment

Ferihydrites (Fh) are nanocrystalline Fe(III) oxyhydroxides, metastable, extremely abundant in soils, river beds, outcrops of river sources, coastal sediments, acid mine drainage lagoons, among others (JAMBOR; DUTRIZAC, 1998; SCHWERTMANN, UDO; FRIEDL; STANJEK, 1999; WAYCHUNAS, GLENN A.; KIM; BANFIELD, 2005). They only exist as nanoparticles (< 12 nm), which have a high specific surface area (até 650 m^2 g^{-1}), high reactivity and large amount of structural defects (BOILY; SONG, 2020; HIEMSTRA; VAN RIEMSDIJK, 2009; SASSI; CHAKA; ROSSO, 2021). Its abundance and properties make this unique mineral extremely relevant for contaminant removal/immobilization applications, as well as for the transport and fate of soil pollutants (CHEN, X. *et al.*, 2022; JOHNSTON; CHRYSOCHOOU, 2016; KUBICKI *et al.*, 2018; LI, B. *et al.*, 2021; NAMAYANDEH; KABENGI, 2019; PRASAD PANDA *et al.*, 2022).

Ferrihydrites are classified as 2-line or 6-line, when synthesized, according to the number of lines in their respective diffraction patterns. However, natural shapes may have other patterns (2-7 lines) (SCHWERTMANN, UDO; FRIEDL; KYEK, 2004). Its reduced size and structural defects make the crystallographic structure and molecular formula of Fh still controversial (DRITS *et al.*, 1993; MANCEAU, A.; SKANTHAKUMAR; SODERHOLM, 2014; MANCEAU, ALAIN, 2019; MICHEL; EHM; ANTAO; *et al.*, 2007; SASSI; CHAKA; ROSSO, 2021). The authors differ among themselves regarding the presence of structural hydroxyls in addition to the existence and location of Fe atoms with tetrahedral coordination. In this work, the molecular formula $Fe_5O_8H.4H_2O$ and the structure proposed by Michel and collaborators for 2-3 nm Fh will be adopted. (MICHEL; EHM; ANTAO; *et al.*, 2007; MICHEL; EHM; LIU; *et al.*, 2007).

Iron oxyhydroxides rarely exist in their pure form in natural environments, being mainly associated with Si, Al and Mn (Cornell and Schwertmann, 2003; Liang et al., 2019; Ye et al., 2020; Zoppi et al., 2008). Aluminum is abundant in nature and can

influence the reactivity of Fh, thus affecting its efficiency in removing contaminants, as well as the stability of the adsorbed products aiming at a possible disposal. The effects of replacing Fe by Al on the morphology and specific surface area of hematites have also been the object of studies, since the change in morphology, quantity and distribution of surface hydroxyl groups alters the behavior in the adsorption of pollutants (BARRON; HERRUZO; TORRENT, 1988; DI IORIO *et al.*, 2018; HA *et al.*, 2009; LIANG *et al.*, 2019).

The growth of the world population brings with it the increasing demand for clean water. There are regions in the world that already suffer from water stress (where the average demand for water per inhabitant is greater than the supply per inhabitant), as shown in Figure 1.1, and the future perspective is that this scenario will worsen as shown by the forecasts of the *World Resources Institute* (https://www.wri.org/tags/water-stress).

Thus, the development of efficient technologies for the remediation and treatment of contaminated water and soil, as well as the effective immobilization of the waste produced, are increasingly necessary in order to meet the growing demand for drinking water and avoid contamination of soils and groundwater.

Waters unfit for consumption can occur naturally or through the inadequate disposal of contaminants. Arsenic, for example, can contaminate water by natural occurrence or as a result of human actions (mining, smelting, combustion products of fossil fuels, use of pesticides and phosphate fertilizers)(JUNGCHAROEN *et al.*, 2017; SMEDLEY; KINNIBURGH, 2002). Arsenic (As) can be found in the environment in inorganic form (in the form of oxyanions whose charge and oxidation number depend on the pH and redox potential of the medium), associated with hydrogens (arsine), or with organic radicals. It is an extremely toxic element and its presence, in traces quantities (e.g., 100 μg/L), in groundwater used for human consumption in Bangladesh, has resulted in what is considered the biggest mass contamination problem ever reported in the world. The degree of toxicity of arsenic compounds decreases in the following order: arsine (-3) > organic arsenic derivatives > inorganic arsenic (+3) > organic arsenic (+3) > inorganic arsenic (+5) > pentavalent organic compounds > arsenic and finally elemental arsenic (VIRARAGHAVAN; SUBRAMANIAN; ARULDOSS, 1999). Studies involving As removal and fixation are

of great relevance for several regions of the state of Minas Gerais, such as Paracatu, Ouro Preto and Nova Lima, where the natural occurrence of soils with high As content, generally associated with gold mineralization, is observed. Gold mining is an anthropic activity capable of mobilizing As and generating large amounts of tailings containing the metalloid. Arsenic anomalies create a permanent concern for the population and local governance, especially after the recent disasters involving iron mining dams in Mariana and Brumadinho.

It is estimated that around 100 million people are using arsenic-contaminated groundwater (HENKE, 2009; JUNGCHAROEN *et al.*, 2017). Chronic exposure to levels higher than 10 μg/L As in drinking water can cause a number of health problems, including câncer (DODD *et al.*, 2006). Therefore, with the increase of the world population and the demand for water, many techniques to immobilize As have been investigated.(BOSMAN *et al.*, 2006; CHEN, L. *et al.*, 2014; DI IORIO *et al.*, 2018; FRANKENBERGER, 2001; LIM *et al.*, 2013; XUE *et al.*, 2019). The treatment cost, the operational complexity of the process, the skill required to operate it, and the disposal of arsenic residues must all be considered before selecting the treatment method. And all these techniques will produce arsenic residues that must be stable to avoid further contamination of the soil, aquifers and, consequently, the population.

Another object of concern, in water contamination, are the so-called emerging contaminants. Among them, antibiotics, and some of their degradation products (ANASTOPOULOS *et al.*, 2020). Antibiotics, even at trace concentrations in the environment, can affect aquatic organisms, cause metabolic and reproductive disorders (BOJARSKI; KOT; WITESKA, 2020), in addition to killing or inhibiting the growth of important bacteria in the ecosystem, and to developing resistant microorganisms, which constitutes a growing public health problem (COSTANZO; MURBY; BATES, 2005). In 2015, antibiotic consumption was estimated at more than 42 billion of daily doses and projections for 2030 are for an increase of up to 200% (KLEIN, E. Y. *et al.*, 2018). The β-lactams are the most used worldwide due to their broad spectrum of antibacterial activity (KÜMMERER, 2009; RODRIGUEZ-HERRERA *et al.*, 2019). Amoxicillin (AMX) is one of the relevant representatives of β-lactams antibiotics. Amoxicillin can be found in nature due to agricultural activities,

industrial, hospital or domestic waste, due to incomplete metabolism (excretion of up to 80% of the ingested dose) (AKSU DEMIREZEN; YILDIZ; DEMIREZEN YILMAZ, 2019; GRENNI; ANCONA; BARRA CARACCIOLO, 2018; KÜMMERER, 2009). Despite this, the mechanism of adsorption of AMX in minerals found in soils remains poorly investigated (KLEIN, A. R. *et al.*, 2021; PUTRA *et al.*, 2009; TRI; NGUYEN; TRUNG, 2020). Previous works on the adsorption of AMX on Fh were not found in the literature.

The isomorphic replacement of part of the iron by aluminum in iron oxyhydroxides for removal of contaminants is controversial. Some consider the presence of Al an efficient approach for the removal of arsenic and lead from contaminated water (ADRA *et al.*, 2016; LIANG *et al.*, 2019; TUFO; AFONSO; SILEO, 2016). However, there are works that show that the introduction of Al can decrease the adsorption of As(V) (MASUE; LOEPPERT; KRAMER, 2007; SILVA *et al.*, 2010; VIOLANTE *et al.*, 2009). The isomorphic substitution of oxyhydroxides of Al by Fe is commonly observed in soils and has been correlated with high concentrations of As in the environment, as observed in studies by the group (ANTÔNIO, DAPHNE C. *et al.*, 2021; FREITAS *et al.*, 2015) and, therefore, became one of the focuses of this investigation.

Despite the importance of Fh replaced by Al in environmental systems, the characterization of Al incorporation is still deficient as well as the understanding of how the true chemical substitution will affect the adsorption of As. Regarding the stability of As adsorption products, there are some works that have studied the influence of the presence of As or Al on the aging of Fh (Bolanz et al., 2013; Das et al., 2014; Li et al., 2016; Wang et al., 2022, 2015). However, the synergistic effects of Al and As on the transformations of Fh phases containing isomorphically substituted Al, as well as on the remobilization of previously adsorbed As, remain unknown.

Regarding the removal of amoxicillin by Fh, no studies were found in the literature. As a ubiquitous mineral in soil and river beds, understanding AMX uptake by Fh is relevant considering the fate of AMX (from agricultural activities and contaminated rivers, for example) in the environment and the prevention of groundwater contamination. Furthermore, Fh-based adsorbents are relatively simple to produce. Despite the attractive characteristics of Fh (pure or substituted with Al), the

adsorption capacity and the mechanisms of interaction with AMX still need to be investigated.

In this context, the main objective of this work is to deepen the understanding of the role of Al, in isomorphically substituted Fh, in the removal and immobilization of contaminants, more specifically arsenic and amoxicillin, chosen as representatives of inorganic and emerging contaminants, respectively, and objects of this study. It is intended to evaluate and understand the influence of Al on the adsorption capacity and possible remobilization of contaminants through the elucidation of the adsorption mechanism of AMX, the investigation of the role of Al in the aging of Fh, and in the fate of As in the aging products of Fh containing or not Al.

2.2 Thesis structure and organization

This thesis is organized into 5 chapters. Chapter 1, entitled Introduction, provides a brief contextualization of the work. A brief presentation of ferrihydrite is given. Then, it is presented the main gaps in the literature regarding (i) the use of isomorphically substituted ferrhydrites in the removal of As(V), (ii) the fate of As adsorbed on Fh or AlFh during the phase transformation of these oxyhydroxides and (iii) the use of Fh in the removal of AMX. The objectives of this thesis are also presented.

Chapter 2 presents the results and discussion of the adsorption of As on Al-Ferrihydrites. This chapter gave rise to the publication “Defects induced by Al substitution enhance As(V) adsorption on ferrihydrites”, published in the Journal of Harzardous Materials, volume 420, page 126544 (DOI: 10.1016/j.jhazmat.2021.126544). This stage of the work addresses the synthesis and characterization of ferrihydrites containing isomorphically substituted Al. The impact of the presence of Al on the adsorption of As(V) was studied at pH 5 and 8. An increase of up to 28% in the adsorption of As was shown and its cause was investigated using spectroscopy techniques in the infrared region with Fourier transform (FTIR), selected area electron diffraction and X-ray photoelectron spectroscopy. The environmental impact of these results is discussed based on analyzes of soils rich in As and Fe oxyhydroxides with different Al contents.

In Chapter 3, ferrihydrites substituted or not in Al were tested for the removal of

another contaminant, amoxicillin (AMX). The maximum adsorption capacity by the adsorbents containing 0 and 10% Al was estimated, as well as the influence of pH and ionic strength in the process. Theoretical calculations, using DFTB (Density Functional Based Tight Binding method), combined with FTIR and Raman spectroscopy results, helped to elucidate the main mechanism involved in the removal. This work has been submitted for publication in a scientific journal in the area and is under peer review.

The studies presented in Chapter 4 seek to improve the understanding of the presence of Al in the fixation of As adsorbed on Fh. The experiments approach the aging of Fh (containing or not Al and As) and the transformations of phases resulting from this aging. The mechanisms involved in particle growth are discussed in light of X-ray diffraction and transmission electron microscopy techniques. Seeking to understand the partitioning of As in the phases formed, as well as its possible mobility in the environment and the intensity of the As-FhAl binding, samples aged or not were submitted to sequential extraction assays (SEP). The results of the synthetic samples were then correlated with the results (of SEP) of soils rich in As, Fe oxides and hydroxides, containing different contents of Al.

In chapter 5, the main results obtained by this research are highlighted and topics for future investigations are suggested.

Finally, appendices A, B and C provide additional information and figures for each chapter (2, 3 and 4 respectively) and appendix D shows a small summary of the work carried out in collaboration with other researchers. The thesis ends with a small memorial of the author and the bibliographic references used in the work.

3. DEFECTS INDUCED BY AL SUBSTITUTION ENHANCE AS(V) ADSORPTION ON FERRIHYDRITES[1]

Highlights

Up to 20 mol % Al isomorphically substituted in 2-line ferrihydrite-Fh shown by SAD.

Up to 15 mol % Al increases 28 % As(V) uptake and decreases adsorption energy.

Surface M-OH sites (45% to 77%) increase with Al content (0 to 20% mol Al).

Al-for-Fe substitution induces structural defects filled by OH.

Increase in As(V) uptake ascribed to the increase of OH induced by Al substitution.

Graphical abstract

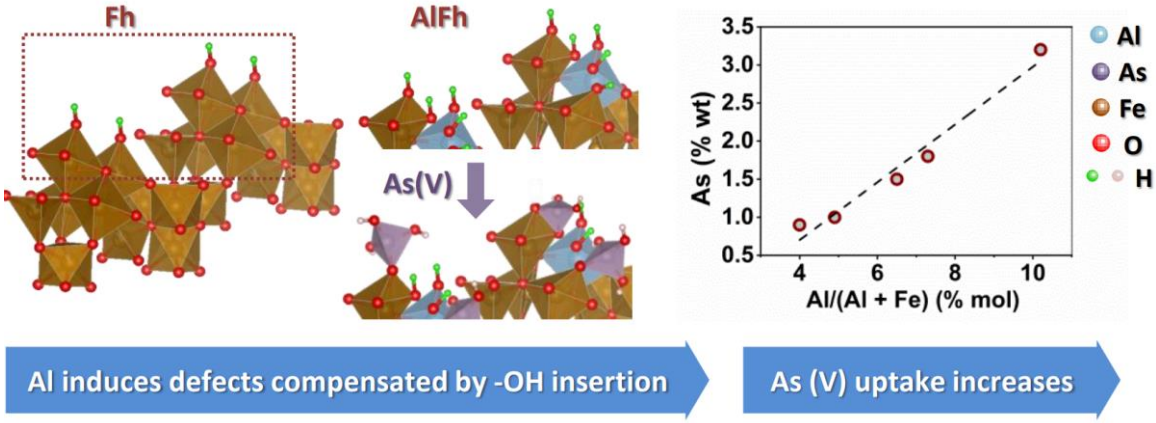

[1] This chapter is published as: Souza, T.G.F., Freitas, E.T.F., Mohallem, N.D.S., Ciminelli, V.S.T., 2021. Defects induced by Al substitution enhance As (V) adsorption on ferrihydrites. J. Hazard. Mater. 420, 126544.

Abstract

An original rationale is proposed to explain the controversial role of aluminum, a common substitutive element in ferrihydrite (Fh), on arsenic adsorption. The adsorption of arsenic on synthetic Al-for-Fe substituted Fh (AlFh) with up to 20 mol% Al was investigated at pH 5 and 8. The reduced interplanar spacings observed by selected area electron diffraction show that all AlFh samples have chemically incorporated up to 20 mol% Al. A 15 mol% Al incorporation increases the arsenic uptake by 28%. In contrast, the Langmuir binding constants decrease, suggesting weaker bonds. Arsenic uptake reduces by 50% as pH rises from 5 to 8. The Al-for-Fe substitution in ferrihydrite causes structural defects, proton-compensated by OH groups, as indicated by the Vegard rule deviation. X-ray photoelectron spectroscopy demonstrates the increase in the relative amount of surface M-OH sites (45% to 77%) with Al concentration (AlFh-0 to AlFh-20), respectively. The enhanced As(V) uptake was ascribed to the insertion of hydroxyls on the Fh structural defects. Fourier-transformed-infrared spectroscopy showed that the sites modified by Al introduction are involved in As adsorption. These findings help to understand aluminum's role in arsenic adsorption, fixation, and fate in the environment.

3.1 Introduction

Ferrihydrite (Fh) is a nanocrystalline Fe oxyhydroxide commonly found in natural environments. The mineral plays a crucial role in the fate and transport of environmental nutrients and contaminants (FAIVRE, 2016; HIEMSTRA; VAN RIEMSDIJK, 2009; JOHNSTON; CHRYSOCHOOU, 2016; NAMAYANDEH; KABENGI, 2019). Its highly specific surface area and high density of reactive surface-sites turn Fh into an attractive material for the removal of contaminants and industrial wastewater treatment (Adra et al., 2016; Hao et al., 2018; Harrington et al., 2011; Jambor and Dutrizac, 1998; Kumar et al., 2019) . Nevertheless, in natural systems, Fh seldom exists as a pure phase. The nature and content of associated impurities may affect properties, such as structure (ADRA *et al.*, 2013; CISMASU *et al.*, 2011, 2012, 2013, 2014; PINNEY; MORGAN, 2013b; SCHWERTMANN, UDO *et al.*, 2000), reduction potential (ADRA *et al.*, 2016; EKSTROM *et al.*, 2010), Fe bioavailability (CISMASU *et al.*, 2012; EKSTROM *et al.*, 2010), phase transformation to hematite and goethite (BAZILEVSKAYA *et al.*, 2011; HANSEL *et al.*, 2011;

SCHWERTMANN, UDO *et al.*, 2000; YANG, Z. *et al.*, 2021a; YU *et al.*, 2020), solubility (HANSEL *et al.*, 2011; MASUE; LOEPPERT; KRAMER, 2007), and its adsorptive capacity (ADRA *et al.*, 2016; CISMASU *et al.*, 2014; HARVEY; RHUE, 2008; JOHNSTON; CHRYSOCHOOU, 2016).

Aluminum is among the most common substitutive elements in naturally occurring Fh (ADRA *et al.*, 2013; CISMASU *et al.*, 2011; CORNELL, R. M.; SCHWERTMANN, 2003; JENTZSCH; PENN, 2006; MANCEAU, A.; GATES, 2013; PINNEY; MORGAN, 2013a; SCHWERTMANN, UDO *et al.*, 2000). Although Al in the Fh structure is widely studied, many studies do not clearly demonstrate to what extent Al is incorporated through true chemical (isomorphous) substitution or merely sorbed on the tiny and poor crystalline Fh phase (JOHNSTON; CHRYSOCHOOU, 2016; NAMAYANDEH; KABENGI, 2019; NI *et al.*, 2016; YE, C. *et al.*, 2020). One must remember that it is also challenging to confirm the chemical substitution using diffraction and imaging methods. Some studies indicate that coprecipitation promotes Al-rich hydroxide segregation, primarily on the Fh surface (which precipitates first), due to kinetics and solubility effects (ANDERSON; BENJAMIN, 1990; HARVEY; RHUE, 2008). Phase separation could occur at scales similar to or below Fh particle sizes and may remain undetected, even with powerful microscopy techniques such as high-resolution TEM (CISMASU *et al.*, 2012). In some cases, an isomorphic substitution of Fe^{3+} by Al^{3+} is indicated by the broadening of the X-ray diffraction peaks (CHADWICK *et al.*, 1986; NAMAYANDEH; KABENGI, 2019) or by increased stability of these precipitates concerning thermal decomposition (MASUE-SLOWEY; LOEPPERT; FENDORF, 2011; SCHWERTMANN, UDO *et al.*, 2000). The Mössbauer technique was used to discuss the possibility of segregation of Al-rich domains within 6-line Fh (CHADWICK *et al.*, 1986). Synchrotron-based techniques have also been applied to provide pieces of evidences of Al isomorphic substitution (ADRA *et al.*, 2013; CISMASU *et al.*, 2011, 2012; MASSEY *et al.*, 2014), but these are tools not readily available as XRD or electronic microscopies.

The control of the coprecipitation rate proved to affect the Al incorporation into Fh and phase separation (CISMASU *et al.*, 2012). Maximum concentrations of Al in synthetic 2-line Fh have been reported to vary from 20 mol% Al (MASUE; LOEPPERT; KRAMER, 2007) to 25 mol% Al (SCHWERTMANN, U. *et al.*, 1979) and

to 82 mol% Al (HARVEY; RHUE, 2008). It is unclear whether Al-for-Fe substitution is the primary mechanism of association in these cases, especially in Al contents as high as 82 mol% Al, in which case the formation of an aluminous surface precipitate was proposed by the authors. In either case, crystalline aluminum oxyhydroxides (gibbsite, boehmite) were detected above the mentioned Al concentrations. Environmental samples, from acid mine drainage systems and those formed in volcanic settings, were reported to contain up to 30 mol % Al (ADRA *et al.*, 2013; CISMASU *et al.*, 2011; HENMI *et al.*, 1980).

Determining the manner in which Al is associated with Fh, and its effect on Fh structural and physical properties, is essential in understanding its surface reactivity. Aluminum has been shown not only to alter the physicochemical properties of ferrihydrite, such as solubility, bioavailability, and secondary mineralization to more thermodynamically stable Fe oxyhydroxides phases, like goethite and hematite, but also to affect the retention of aqueous contaminants, such as arsenic (ADRA *et al.*, 2016; MASUE; LOEPPERT; KRAMER, 2007), chromium (NI *et al.*, 2016), phosphorus (LIU, YU-TING; HESTERBERG, 2011), and uranium (MASSEY *et al.*, 2014).

Our previous works have demonstrated that Al favors As immobilization within the structure of oriented aggregates of Al-for-Fe oxyhydroxide-substituted nanoparticles, found both in natural and synthetic samples (FREITAS *et al.*, 2015, 2016; LADEIRA, ANA C.Q.; CIMINELLI, 2004). Freitas and coworkers suggested that As first adsorbs onto AlFh nanoparticles and then is incorporated into the crystalline nanoparticles' aggregates, hindering further release into the environment. Nevertheless, this previous work did not explore the role of Al in the primary adsorption process.

The binding structure of adsorbed As on iron oxyhydroxides is still the object of many studies (SOLDOOZY *et al.*, 2020; WANG, S. *et al.*, 2019). Ferrihydrite has a unique polyhedral surface structure with a high density of singly coordinated surface groups (Hiemstra and Zhao, 2016). These groups may interact with oxyanions, forming either monodentate or binuclear bidentate complexes. Extended X-ray absorption fine structure (EXAFS) studies on As(V) adsorption on gibbsite, iron oxyhydroxides, and Al-substituted Fh indicate inner-sphere bidentate-binuclear complexation (ADRA *et al.*, 2013; DANTAS *et al.*, 2011; LADEIRA, A C Q *et al.*, 2001; SHERMAN;

RANDALL, 2003). The inner-sphere monodentate complex was suggested for arsenate adsorption on 2-line Fh (WAYCHUNAS, G. A. *et al.*, 1993; WAYCHUNAS, GLENN A.; DAVIS; FULLER, 1995). The recent work of Wang et al. (2019) showed that these sites predominate in weak alkaline pH values. Hiemstra and Zhao (2016) report the predominance of bidentate complexes at higher pH against an increasing proportion of monodentate for acid environments. Adra et al. (2013) studied As(V) adsorption on natural and synthetic FhAl and found that the arsenate is bound to Fe (rather than Al) by binuclear bidentate inner-sphere complexes. The authors further proposed that the increased As(V) adsorption on FhAl would likely be due to the formation of outer-sphere complexes that form hydrogen bonds with =Al-OH or =Fe-OH (Adra et al., 2016). Ladeira and Ciminelli (2004) studied arsenic adsorption and desorption on different soils and minerals. Leaching with some salt solutions showed very low As(V) release from goethite and an Al-rich oxisol, which indicate that the hydrogen bonds are not the main complexation mechanism. The authors suggest inner-sphere complexation for both goethite and Al-rich oxisol.

In the context of adsorption capacity, the literature reveals disagreements regarding whether the presence of Al in Fh enhances arsenic removal (ADRA *et al.*, 2016; MASUE; LOEPPERT; KRAMER, 2007). Adra and coworkers (2016), who studied Al-substituted ferrihydrites, found increasing As(V) adsorption capacity with an Al-increasing content. These authors focused only on two Al:Fe (22 and 39%) molar ratios and observed the presence of Al-oxyhydroxide in the latter. Therefore, the influence of Al incorporated through chemical substitution on arsenate adsorption could only be assessed in the 22% Al-Fe sample. Conversely, Masue et al. (2007) observed no variation in the As(V) adsorption capacity between the sample without Al and the sample with 20% Al:Fe molar ratio. Other samples with higher Al content (50 and 75% Al:Fe molar ratio) presented Al-oxyhydroxide segregation and lower As(V) adsorption. Since the reported investigations studied Fh with Al content from 22% to 75%, most of which were mixed with Al-rich phases, the effect of Al content, truly chemically substituted in Fh, remained unknown. The isomorphic substituted Al-for-Fe oxyhydroxides is commonly observed in soils and has been associated with high As loadings in the environment by our group (ANTÔNIO, DAPHNE C. *et al.*, 2021; FREITAS *et al.*, 2015) and, therefore, it became the focus of this investigation.

Despite the importance of AlFh in environmental systems, there are still many uncertainties, including the deficient characterization of Al incorporation and how the true chemical substitution will affect As adsorption. This work aimed to synthetize ferrihydrites isomorphically substituted with Al and study the role of Al on their morphological characteristics and arsenate adsorption features. An Al content of lower than 25% was used, intending to avoid the presence of segregated Al-rich phases. Arsenic uptake was studied at two different pH values (5 and 8), with the latter being near the point of zero charge (pH_{PZC}) of these materials so as to reduce the surface charge influence. The materials were characterized by X-ray diffraction, transmission electron microscopy, and selected area diffraction to investigate possible phase segregation and isomorphic substitution. The Fourier-transform infrared spectroscopy, Raman spectroscopy and X-ray photoelectron spectroscopy allowed an investigation on the surface groups. Based on the findings, a mechanism for the enhanced As(V) adsorption on AlFh is proposed.

3.2 Materials and methods

3.2.1 Synthesis of Al-Free and Al-bearing ferrihydrites

The 2-line ferrihydrites (Fh) were prepared following the method of Schwertmann and Cornell (2000) modified to include aluminum. Initial solutions (0.1 $mol.L^{-1}$ total of Al + Fe) in molar ratios of Al / (Fe + Al) 0, 0.05, 0.10, 0.15, 0.20 and 0.25 were prepared by mixing $Fe(NO_3)_3$ and $Al(NO_3)_3$ solutions. The solutions were neutralized to pH 7.0 ± 0.3 using 1 $mol.L^{-1}$ NaOH at 1.5 $mL.min^{-1}$ with vigorous stirring and at room temperature. The products were dialyzed against deionized water at 4 ^{o}C and kept at this temperature until being used. In all experiments 18 MΩ.cm Milli-Q water and reagent grade chemicals were used. Hereafter ferrihydrite samples will be referred to as AlFh-0, AlFh-5, AlFh-10, AlFh-15, AlFh-20 and AlFh-25, according to the Al / (Al + Fe) molar ratio of the initial solutions.

3.2.2 Oxisol samples

Tailings of As-sulfide concentrates from the hydrometallurgical processing plant of a gold mine in Minas Gerais, Brazil were stored for more than 10 years in three disposal facilities sealed with an enriched Fe and Al oxisol. These tailings were

excavated and reprocessed, and samples of the oxisol liners were recovered for analysis. The sample characterization and preparation for TEM analyses were described in Freitas et al. (2015).

3.2.3 Arsenic sorption experiments

The adsorption of As(V) was measured as a function of the reaction time at pH 5, ionic strength of 0.1 mol.L^{-1} $NaNO_3$, and 25 ^oC, in thermostatic magnetic stirrers for 200 h. At pH 5 all the samples have the highest adsorption capacity (MASUE; LOEPPERT; KRAMER, 2007). The pH values of the individual samples were adjusted during the experiments by adding 0.1 mol L^{-1} NaOH or 0.1 mol L^{-1} HNO_3. The Fh suspensions described in the previous section, AlFh-0 and AlFh-10 (0.28g), were placed in contact with arsenate solutions (400 mL, 1.4 m mol L^{-1}) prepared by dissolving disodium hydrogen arsenate of analytical grade ($Na_2HAsO_4.7H_2O$, Merck) in water (18 MΩ cm). Aliquots (10 mL) were removed from the dispersion during each adsorption and tested to As(V) content. These tests allowed evaluating the equilibrium time for the arsenic adsorption.

The samples of synthetic Fh suspension (AlFh-0, AlFh-5, AlFh-10, AlFh-15, and AlFh-20) were used to obtain the adsorption isotherms. The experiments were carried out in batches of 50 mL, with ionic strength of 0.1 mol L^{-1} $NaNO_3$, pH 5 and 8, containing 2.5 mg of AlFh and initial concentrations of As varying from 0.1 to 0.7 mM. The pH values of the individual samples were controlled by adding 0.1 mol L^{-1} NaOH or 0.1 mol L^{-1} HNO_3 daily. The flasks stayed 150 h on a platform shaker (200 revolutions per minute (rpm)) and 25 ^oC. The solids were collected from all experiments by centrifugation (4000 rpm for 10 min) and stored at 4 ^oC (to avoid phase transformation) until analysis, as well as the supernatant that was acidified by adding a droplet of 1 M HNO_3.

All experiments were performed in duplicate. The reported values correspond to the average of the obtained results.

3.2.4 Characterization of the adsorbent and quantification of arsenic in solution

The chemical composition of the AlFh samples was analyzed by ICP-OES (Perkin Palmer 7300). The solid samples were dissolved in 8% aqua regia to analyze As, Al

and Fe. For the quantification of As adsorbed to the AlFh samples, the dispersions resulting from the adsorption tests were centrifuged and the solid solubilized in 8% aqua regia. The arsenic was quantified also in the supernatants. The detection limit of the ICP-OES used is 1.3 µmol kg^{-1} for As, 3.5 µmol kg^{-1} for Fe and 7.5 µmol kg^{-1} for Al. The method's precision was guaranteed by an internal standard of Lu 0.6 µmol kg^{-1} (Ultra Scientific) with recoveries of 95-105%. For an improved accuracy of the measurements, calibration curves and standard solutions, with the same sample matrix, were used. For this purpose, it was used certified solutions of Al 10,000 µg mL^{-1} (Spex, 99.99%), Fe 10,000 µg mL^{-1} (Spex, 99.99%), and As 1,000 µg mL^{-1} (Spex, 99.99%). The coefficients of determination of the curves were, at least, 0.995 and the recoveries between 95 and 105%.

The chemical composition was also analyzed by TEM coupled with energy x-ray dispersive spectroscopy (EDS) at least in five points each sample. - The samples were also analyzed by high resolution TEM (HRTEM) and selected area - electron diffraction (SAD) using a LaB6-TEM Tecnai G2 20 SuperTWIN (FEI), operated at 200 kV, coupled with a Gatan Image Filter (GIF Quantum SE system). The SAD patterns were acquired by using elastic scattering only by filtering the zero-loss peak with 10 eV slit. For minimizing error all the SAD patterns were collected at the same day under the same microscope conditions (lenses strengths, apertures, camera length). For this purpose, each AlFh-X suspension was pipetted on a copper grid covered with an ultrathin (3-5 nm thick) carbon film (Cu-Lacey carbon, 400mesh, Ted-Pella). The grids were placed on Whatman® filter papers to remove excess water and allowed to dry at room temperature. The images were processed by the Software Digital Micrograph version 2.32. The SAD patterns were converted to rotational averages profiles and the peaks were calculated by the THF Peak Locator tool inside the package Difftools (MITCHELL, 2008). The parameters were hat width of 10, brim width of 10, and threshold of 0.01.

The specific surface area (SSA) was obtained by adsorption-desorption of N_2 using the Quantachrome equipment model Autosorb-1. Measurements were made on solids previously degassed at 40^{o}C / 72h. Higher degassing temperatures were avoided in order to prevent phase transformation. The SSA were obtained using the Brunauer-Emmett-Teller (BET) method in a relative pressure range of 0.005–0.1. The

pore size distribution was calculated using the density functional theory - DFT approach, using the "N_2 at 77K on silica Kernel (cylindr. Pore, NLDFT adsorption branch model)" of the Autorsob 1 version 1.54 program.

Fourier-transform infra-red spectroscopy-FTIR was performed in a Bruker Alpha spectrometer at a resolution of 4 cm^{-1} and 128 scans. These tests were conducted with an attenuated total reflectance (ATR) accessory, using a diamond crystal as the reflection element. The collected spectra were normalized using the band at 1625 cm^{-1} as reference.

Raman spectra were obtained with a LabRam-HR 800 (Horiba/Jobin Yvon) spectrograph equipped with an Olympus BX-41 microscope provided with lenses of 10, 50 and 100X, and helium laser of 632.8 nm. The optimum scanning method was found to be with laser power less than 0.04 mW, and, at least, 20 spectrum collections of 30s each.

X-ray diffraction-XRD was performed using a Philips (Panalytical PW1710) X-ray diffractometer, with Cu (K_α) radiation, tube voltage of 35kV and current of 50 mA. Powdered samples were loaded into XRD sample holders to create flat surfaces. Data was collected over the range of 10-90° 2θ with scan step size of 0.020° s^{-1}. The diffraction patterns were compared to the reference powder diffraction file (PDF) from Inorganic Crystal Structure Database- FIZ Karlsruhe (ICSD) for 2-3 nm ferrihydrites (ICSD-158477), proposed by Michel (MICHEL; EHM; ANTAO; *et al.*, 2007) and the PDF files for the other iron oxides. Differential plots were determined by subtracting the XRD patterns for the AlFh-0 from the Al-containing materials in order to assess changes in lattice parameters as a result of the aluminum insertion.

The X-ray photoelectron spectroscopy-XPS experiments were carried out on a Thermo Scientific (K-Alpha) spectrometer, using base pressure of 10^{-8} mbar, Al Kα (hv = 1486.6 eV) and 400 µm of spot size. All binding energies (BE) were referenced to the C (1s) peak at 285 eV. The peaks were deconvoluted by the software PeakFit 4.06, using Gaussian curves, and linear/Shirley baseline.

The isoelectric point (IEP) of the dispersed (in 0.01 M KCl) particles was estimated by interpolating the Zeta potential measured at different pH using a Zetasizer Nano-Zs

model ZEN3600. The samples were hydrated by keeping them in 0.01 M KCl solution for 24h before the measurements.

3.2.5 Sorption isotherms analysis

The amount of As(V) adsorbed by the AlFh at equilibrium is expressed as Γ (µmol m^{-2}) and is calculated as:

$$\Gamma = \frac{(C_0 - C_f) \times m_s}{m_{Fh} \times ASA} \quad (1)$$

where C_o and C_f are the As(V) initial and the final concentrations for each condition. The m_s is the mass of solution, the m_{Fh} is the mass of adsorbent, and ASA is the apparent surface area once the curves of the AlFh samples were characteristic of microporous materials (ROUQUEROL; LLEWELLYN; ROUQUEROL, 2007).

The adsorption isotherms were modelled using the Langmuir (2) and Freundlich (3) equation (FREUNDLICH, 1907; LANGMUIR, 1918; TRAN; YOU; *et al.*, 2017):

$$\Gamma = \frac{\Gamma_{max}[As]_{eq}K_L}{\left(1 + [As]_{eq}K_L\right)} \quad (2)$$

$$\Gamma = \Gamma_{max}[As]_{eq}^{\frac{1}{n_F}} \quad (3)$$

where Γ_{max} (µmol m^{-2}) is the maximum adsorption capacity, $[As]_{eq}$ (µmol kg^{-1}) the arsenic concentration after equilibrium time, K_L (kg µmol^{-1}) the effective Langmuir binding constant for arsenic at the pH investigated, and n_F is an empirical parameter of the Freundlich equation. They were least squares fit by using a Levenberge-Marquardt algorithm to minimize the quantity $\sum[As]_{eq} (\Gamma_{calc} - \Gamma)^2$. The goodness of fit parameter was estimated by the determination coefficient R^2. The errors are the standard deviation of the fit.

3.3 Results

3.3.1 Detection of Al-for-Fe substituted Ferrihydrites and Structural Modifications

Compositional analyses of the AlFh series by ICP-OES indicate that the Al / (Al+Fe)

molar ratios are approximately equal to the material synthesis' target values. The EDS results, obtained from multiple spots and particles from each sample, presented consistent elemental profiles, suggesting that aluminum is distributed homogeneously across the particles. The values are summarized in Table 3-1. The exception was the AlFh-25 sample, which showed the highest variation between the measured spots while presenting a lower Al content than that measured by ICP-OES. The difference is due to the segregation of Al-oxyhydroxides, as will be evidenced by the TEM/SAD analysis. These findings suggest that the samples with up to 20% Al did not segregate Al oxyhydroxides, and the expected Al:Fe molar ratio was achieved.

Table 3-1: The ASA_{BET} and Al content, in %mol Al/(Al+Fe), analyzed by ICP-OES and EDS of the AlFh samples

Target (%)	ICP-OES(%)	EDS(%)	$ASA_{BET}(m^2/g)$
0	0	-	312 ± 37
5	5.1 ± 0.7	5.2 ± 0.1	293 ± 34
10	9.5 ± 0.5	10.4 ± 0.3	306 ± 35
15	14.5 ± 0.6	14.3 ± 0.5	288 ± 30
20	19.0± 0.5	20.5 ± 0.2	287 ± 28
25	25 ± 1	21 ± 1	348 ± 36*

*The higher value was related to the presence of Al-oxyhydroxides in this sample.

The features of the N_2 adsorption curves on the AlFh samples are characteristic of microporous materials, as shown in Figure 3.1. Hence, the option was to measure the apparent surface area (ASA_{BET}). The areas were calculated in the range of relative pressures (P/P_0) from 0.005 to 0.1, following the linearity criterion of the BET plot, proposed by Rouquerol and co-workers (ROUQUEROL; LLEWELLYN; ROUQUEROL, 2007) and recommended by IUPAC (THOMMES *et al.*, 2015) for microporous materials. As shown in Table 3-1, most AlFh samples have an ASA of around 300 $m^2\ g^{-1}$, which is in good agreement with the literature (CISMASU *et al.*, 2013; DU *et al.*, 2018; EKSTROM *et al.*, 2010). The exception is the sample AlFh-25, which showed a slightly higher value, around 350 $m^2\ g^{-1}$, probably due to the presence of Al-oxyhydroxides. The microporosity pattern of the adsorption curve is associated with the interparticle porosity, likely caused by the drying procedure

(freeze-drying) prior to measuring the specific surface areas. The particle agglomeration during drying leads to the formation of ~1 and 2.5 nm pores. The interparticle pores and multilayers adsorption drive different N2 adsorbed volumes. Once the As(V) adsorption tests were made with wet ferrihydrites, the pores formed by drying process will not affect the arsenate uptake. Regarding the error associated with the measurements, no significant differences were found between the ASA of the other samples (AlFh-0 to AlFh-20), which are corroborated by their particle sizes (Figure 3.2). Since the particles do not show inside porosity and present similar pore volumes and distribution, their ASA_{BET} could be changed by different particle formats, densities, and sizes.

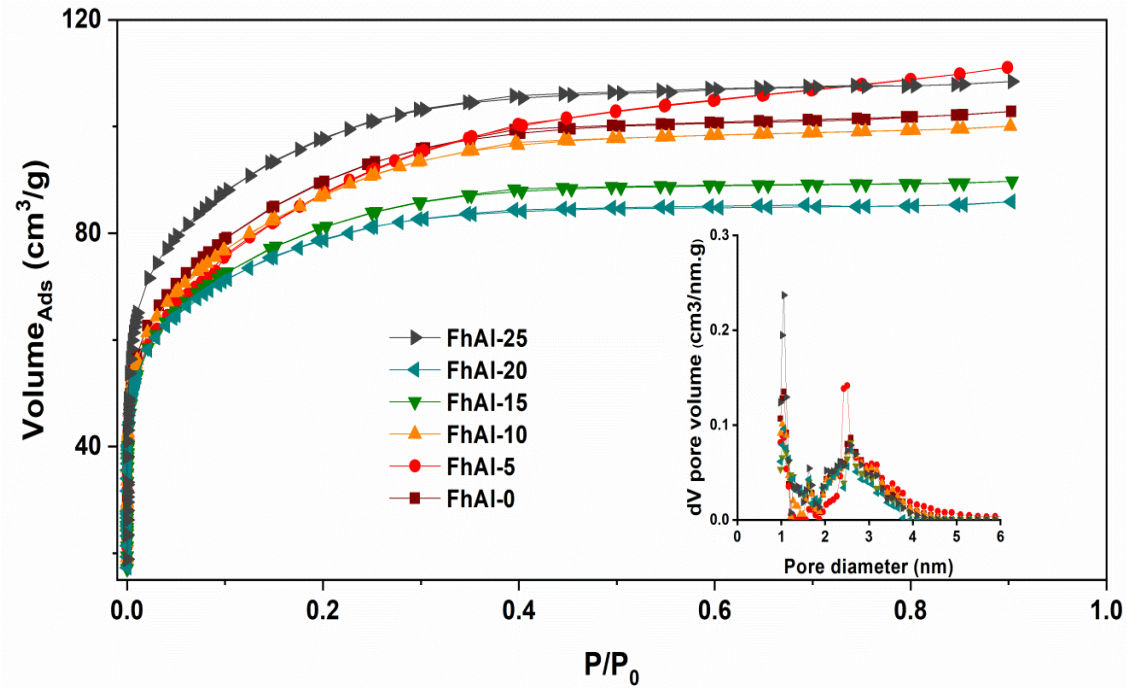

Figure 3.1: Nitrogen adsorption-desorption isotherm at 77 K of the AlFh samples. The inset shows the pore size distribution.

The qualitative HRTEM analyses shown in Figure 3.2 revealed that increasing Al content caused no significant variation in the general morphology and particle size, roughly estimated at 4 nm in all six samples. The theoretical density variation between the AlFh-0 and AlFh-20 samples was calculated considering the difference between the molar mass of Fe and Al, reaching up to 5%, which is less than the measurement's error. Therefore, without a substantial difference in particle sizes, it would be difficult to observe variation in their ASA_{BET}. The non-variation of SSA by introducing Al was also observed by others (CISMASU *et al.*, 2012; NAMAYANDEH;

KABENGI, 2019). The TEM images show that the particles have poorly defined edges and no distinct lattice fringes, regardless of the Al content, suggesting some degree of structural disorder, which was expected for materials with short- and intermediate-range ordering (CISMASU *et al.*, 2011). An exploratory search for particles with different formats or compositions by TEM was unable to detect any Al segregation, except for the sample AlFh-25, aged in water, 30 ^{o}C, for 130 days. Crystals of Al-oxyhydroxide with a bayerite structure were observed scarcely spread throughout. Therefore, the AlFh-25 sample was not considered for adsorption studies and will not be further investigated. Manceau and Gates (2013), in agreement with Pauling's distortion rule, proposed that Al-Al avoidance governed the saturation limit of Al substitution in the Fh structure and predicted this substitution to occur up to a 25% molar ratio. Previously, Masue and coworkers found the maximum of 20% for coprecipitated FhAl (MASUE; LOEPPERT; KRAMER, 2007), while Cismasu et al. (2012) observed Al-phase segregation from 15-30%, depending on the precipitation speed.

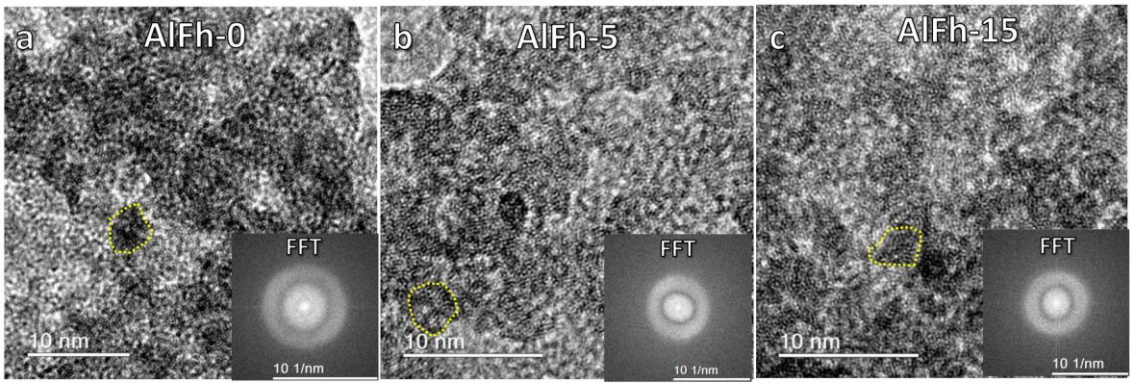

Figure 3.2: HRTEM images of selected AlFh-X samples, where X represents the Al molar ratio: 0% (a), 5% (b), and 15% (c) and its FFT in the insets.

Bulk XRD patterns indicate the low crystallinity of AlFh-0 sample (Figure 3.3), with broad peaks and d-spacings of about 0.26 and 0.15 nm, which are characteristic of 2-line ferrihydrite (JAMBOR; DUTRIZAC, 1998). Despite the increase in Al content, there was no crystalline Al oxyhydroxide phase (e.g., gibbsite or bayerite) detectable by this technique in the samples AlFh-5 to AlFh-20. Figure 3.3 also shows the difference among the patterns of Fh samples with and without Al. The slight depression at the 2-theta of around 35 degrees, showing a loss of intensity, is evidence for the decrease in crystallinity caused by Al. The reduction in XRD

intensity is in accordance with the findings from Cismasu and coworkers (2012). These authors observed a loss of crystallinity, the introduction of defects, and a reduced range of structure organization for fast and slow precipitated Al-substituted ferrihydrites (CISMASU *et al.*, 2012). The difference curves in Figure 3.3 also show a shift in the peaks at 35 degrees toward higher 2-theta values, with an increase in Al content, indicating a reduction in the lattice parameters, as observed by Jentzsch and Lee Penn (2006). The expected decrease in the lattice parameters on Fe oxyhydroxides is evidence of Al incorporation in Fe-oxyhydroxides. The smaller ionic radius of Al^{3+} compared with Fe^{3+} induces a contraction of the unit cell lattice parameters (CORNELL, R. M.; SCHWERTMANN, 2003; PINNEY; MORGAN, 2013b; VEGARD, 1921).

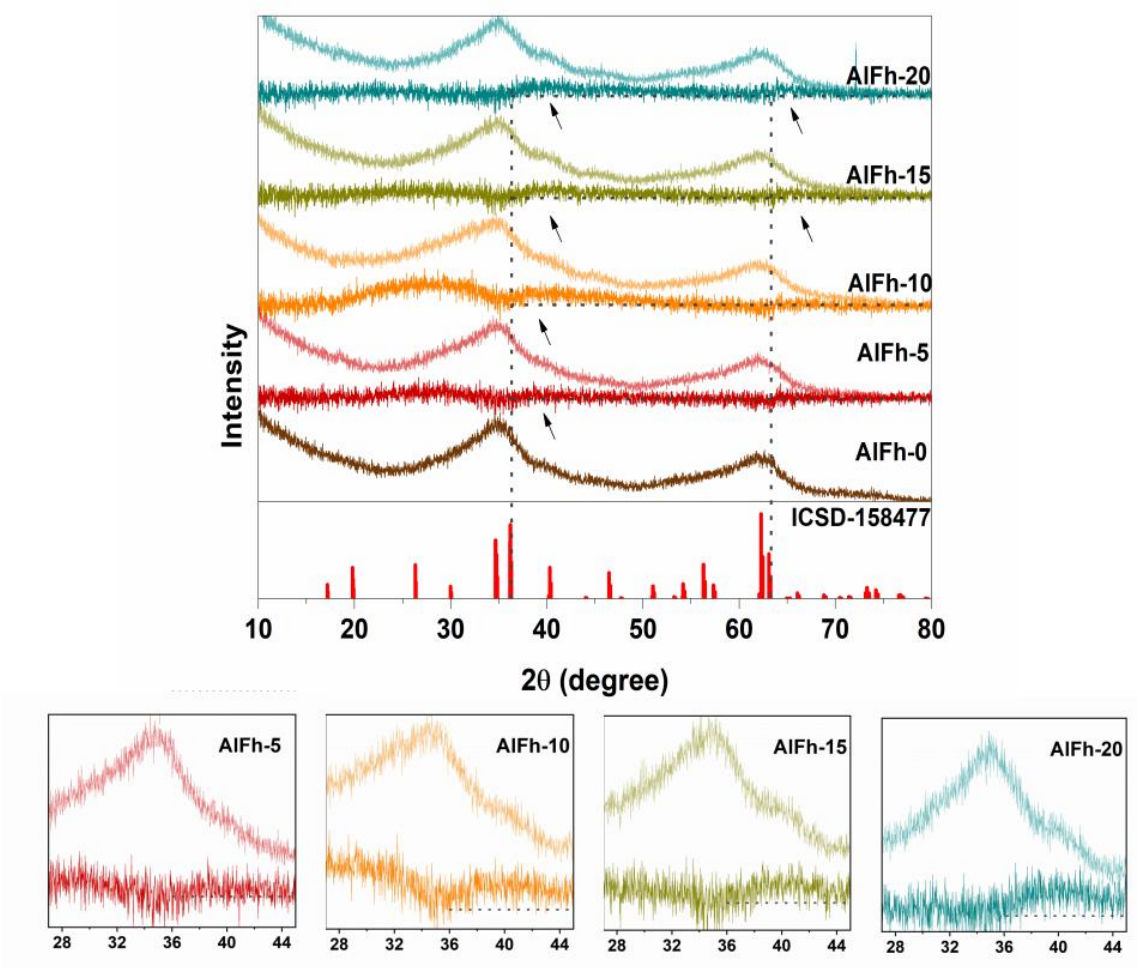

Figure 3.3: XRD patterns of the AlFh-0 and the difference plots determined by subtracting the 0% Al pattern from each Al-substituted pattern, and the reference pattern for 2-3 nm ferrihydrites (MICHEL; EHM; ANTAO; *et al.*, 2007), ICSD-158477.

The above results are supported by the selected area electron diffraction (SAD)

analysis (Figure 3.4). The electron diffraction pattern of sample AlFh-15, in Figure 3.4-a, shows two brighter and narrower rings, characteristics of nanocrystalline materials. The average rotational profiles for all samples were obtained from their respective SAD patterns. They feature a peak shift toward higher values in reciprocal space, which corresponds to shorter interplanar spacings (d_{hkl}). These parameters were used to find the d_{hkl} values (Table 3-2). The *a* and *c* lattice parameters were calculated considering that Fh has a hexagonal crystalline structure and interplanar spacings, identified by SAD, of approximately 0.26 and 0.15 nm, which were indexed as (103) and (006) reflections, respectively (Table 3-2). As shown by XRD shifts, the parameter *a*, calculated by SAD results, decreases as the Al content increases, ranging from 0.595 nm at FhAl-0 to 0.588 nm at FhAl-20, suggesting an Al-for-Fe isomorphic substitution. A similar trend was observed for parameter *c*. To the best of our knowledge, this is the first time that this evidence of Al incorporation in 2-line Fh is identified by SAD.

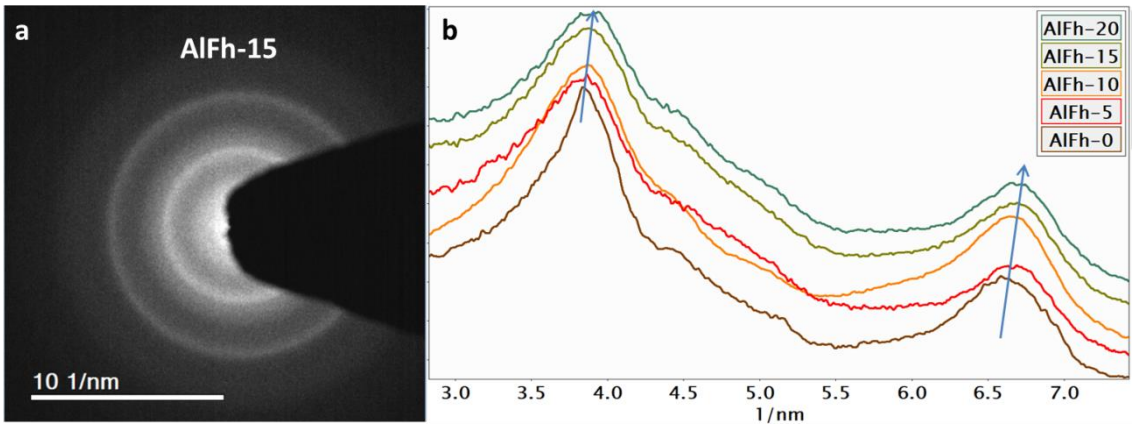

Figure 3.4: SAD pattern of AlFh-15 (a) and the SAD rotational average profile of the samples AlFh (b). The arrows show the peak shift toward higher values in the reciprocal space.

Table 3-2: Parameters obtained from rotational averages profiles extract of the SAD measurements

Sample	d_{103} (nm)	d_{006} (nm)	a (nm)	c (nm)
AlFh-0	0.2597	0.1503	0.5954	0.9017
AlFh-5	0.2589	0.1497	0.5953	0.8979
AlFh-10	0.2585	0.1494	0.5949	0.8965
AlFh-15	0.2576	0.1488	0.5934	0.8930
AlFh-20	0.2567	0.1486	0.5886	0.8915

The extent of cation substitution in crystalline solids is often described via an empirical relationship between unit cell parameters and composition, known as Vegard's rule (VEGARD, 1921). This rule states that an ideal mixing of Fe3+ with other trivalent cations, such as Al^{3+}, Cr^{3+}, and V^{3+}, would result in a linear relationship between the unit cell parameters of Fe-oxyhydroxides and their isostructural analogs. Such crystallographic analyses have been difficult to carry out for aluminous ferrihydrite, as a result of the poorly defined diffraction features of this nanophase and the disagreement on a nanoscale aluminous isostructural equivalent (MANCEAU, A.; GATES, 2013; MICHEL; EHM; ANTAO; *et al.*, 2007). One of the proposed theoretical isostructural equivalents for 2-line Fh is the Tohdite (Thd) ($5Al_2O_3.H_2O$) (Michel et al., 2007a, 2010). This Al-oxyhydroxide is considered to be an idealized structural equivalent for 2-line Fh because it is crystalline and defect-free (Yamaguchi et al., 1969), whereas Fh is nanoparticulate, poorly crystalline, and highly defective. To approximate the lattice parameters of a hypothetical defective Thd ($Thd_{disordered}$) as analogous to 2-line Fh, Cismasu and coworkers (CISMASU *et al.*, 2012) used the averaged differences in unit cell parameters between several pairs of Al- and Fe-oxyhydroxide structural analogs. The $Thd_{disordered}$ unit cell parameter of structurally equivalent Al- and Fe-oxyhydroxides was thus calculated to be 5.1% lower than Thd. We performed a similar treatment to our materials, and the Vegard-like relationship is shown in Figure 3.5. The parameter c is seen to follow this rule closely, but the parameter a deviates significantly. Cismasu et al. (2012) ascribed this behavior to the additional structure disorder introduced by Al incorporation (vacancies, defects). In the event of combined Al and vacancy defects, the dilatory nature of the excess hydroxyls within the cation vacancy defect counteracts the contraction induced by the Al (PINNEY; MORGAN, 2013a). This phenomenon has been observed in XRD as a deviation of the lattice parameters from the ideal Fe–Al Vegard relationship in experimental samples containing both Al and excess OH (WOLSKA; SZAJDA; PISZORA, 1994). According to Pinney and Morgan (2013b) the deviation from Vegard rule is an evidence of defective structure substitution for hydroxyls, and the decrease on the lattice parameters is inversely proportional to the quantity of defects filled by hydroxyls. Proton-compensated cation vacancy defects proved to cause lattice expansion in all calculated Fe and Al

materials. In fact, several studies have correlated excesses of hydroxyl content to the Al-for-Fe substitution on ferrihydrite (PINNEY; MORGAN, 2013b; RUAN *et al.*, 2002; RUAN; GILKES, 1995; WOLSKA; SZAJDA; PISZORA, 1994). The samples AlFh-10 and AlFh-15 presented the “a” parameter most distant from Vegard rule (Figure 3.5-b). Thus, based on the previous discussion, AlFh-10 and AlFh-15 should have the most defective proton-compensated structure by hydroxyls.

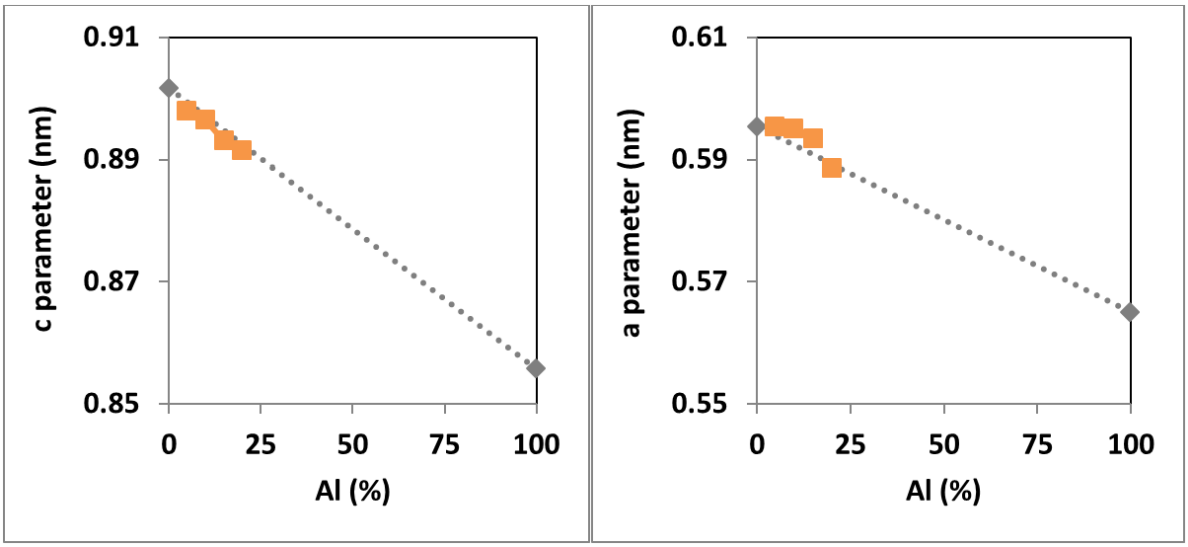

Figure 3.5: Vegard rule relationship for the *a* and *c* unit cell parameters of 2-line Ferrihydrite, obtained by SAD, and disordered tohdite (AlFh–$Thd_{disordered}$). The calculated *a* and *c* lattice parameters for the AlFh-5 to AlFh-20 series are plotted along the line that link AlFh-0 and $Thd_{disordered}$ cell parameters.

Figure 3.6 shows the FTIR of Fh before and after As(V) adsorption. The spectra of Fh without As(V), present the bands at ~3300, 1625, 1380, and 1330 cm^{-1}. A broad band around 3300 cm^{-1} is assigned to OH from the bulk, surface, and adsorbed water (CORNELL, R. M.; SCHWERTMANN, 2003). The Al introduction causes a shift on this band to higher wavenumbers, as also observed for goethite (RUAN *et al.*, 2002). This was attributed to Al-for-Fe substitution, which causes a shortening and strengthening of the hydrogen bond, leading to a shift in the hydroxyl deformation and water bending vibrations to larger wavenumbers. According to Cornell and Schwertmann (2003) the large width of this band is an indication of a disordered crystal structure. The band at 1625 cm-1 is usually assigned to adsorbed water while the others (i.e., at ~1330 and 1380 cm^{-1}) to Fe-O-H (CORNELL, R. M.; SCHWERTMANN, 2003; HAUSNER *et al.*, 2009; ROUT; MOHAPATRA; ANAND, 2012; SEEHRA *et al.*, 2004; TÜYSÜZ *et al.*, 2008). A broad band at 1380 cm^{-1} is

usually associated with Fe-O-H vibration mode (Tüysüz et al., 2008; Wang et al., 2015). The band was also reported in the products (Fh and hematite) of pyrite oxidation (CALDEIRA; CIMINELLI; OSSEO-ASARE, 2010). The interaction with adsorbing species or Fh substitution may shift the band position. Rout et al. (2012) studied the adsorption of a series of divalent cations with Fh synthesized in iron citrate solutions. The results showed that the band around 1380 cm^{-1} decreases its intensity and is shifted to lower wavenumbers, depending on the adsorbed metal. Seehra and co-workers (2004) ascribed a decrease in the intensity of the band 1365 cm^{-1}, characteristic Fe-O-H bending mode, to Si-doped Fh samples. The Al introduction also induces a shift on the band at ~1330 cm^{-1}, from 1329 to 1344 cm^{-1} for the samples from FhAl-0 to FhAl-20. Figure 3.6 also shows the emergence of a band at ~800 cm^{-1}, associated with As adsorption, and a significant reduction on the bands ~1380 and 1330 cm^{-1}. The shifts to higher frequencies observed by FTIR indicate shorter bond distance/stronger force constant. Those are the same bands whose intensity decreased following As adsorption, thus showing that the sites modified by Al introduction are involved in As adsorption. A small reduction on the band ~3300 cm^{-1} also substantiates the role of hydroxyl groups on arsenic adsorption.

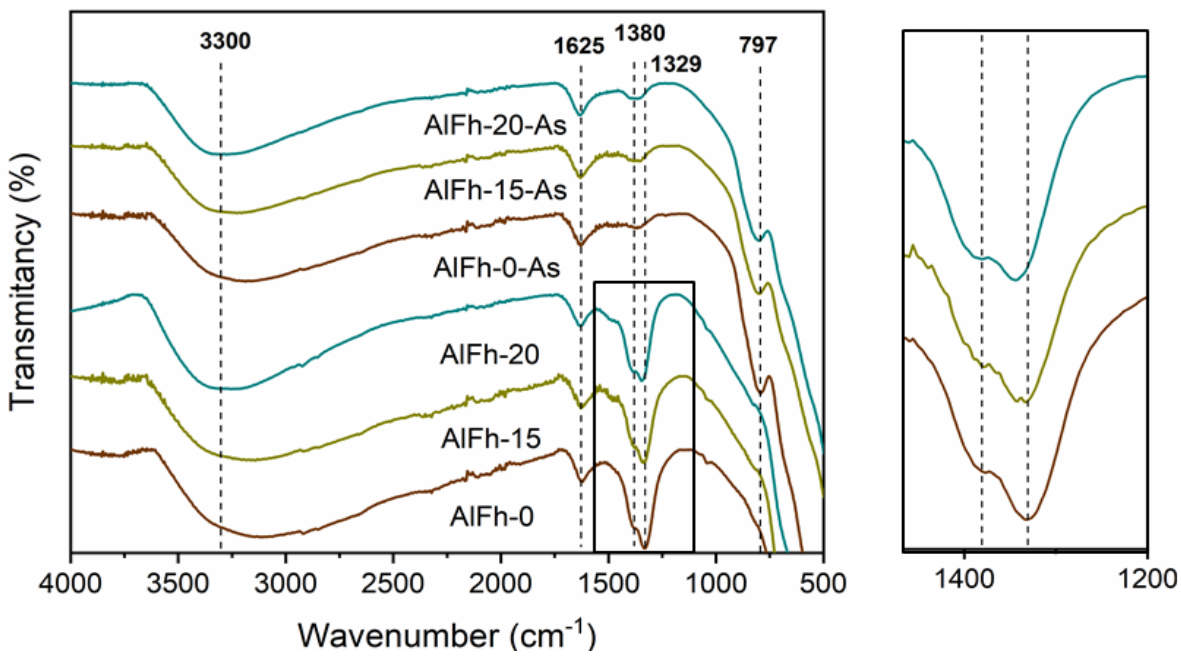

Figure 3.6: FTIR spectra of Fh before and after As(V) adsorption, normalized by the band at 1625 cm^{-1} .

Raman spectra of the ferrihydrites were obtained before and after the As(V) adsorption (Figure 3.7). The original samples show bands (~380, 515 and 710 cm^{-1}) characteristics of 2-line ferrihydrite (MAZZETTI; THISTLETHWAITE, 2002). After As(V) adsorption, a band appears at ~840 cm^{-1}, associated with arsenic adsorption by inner-sphere complexation (Müller et al., 2010).

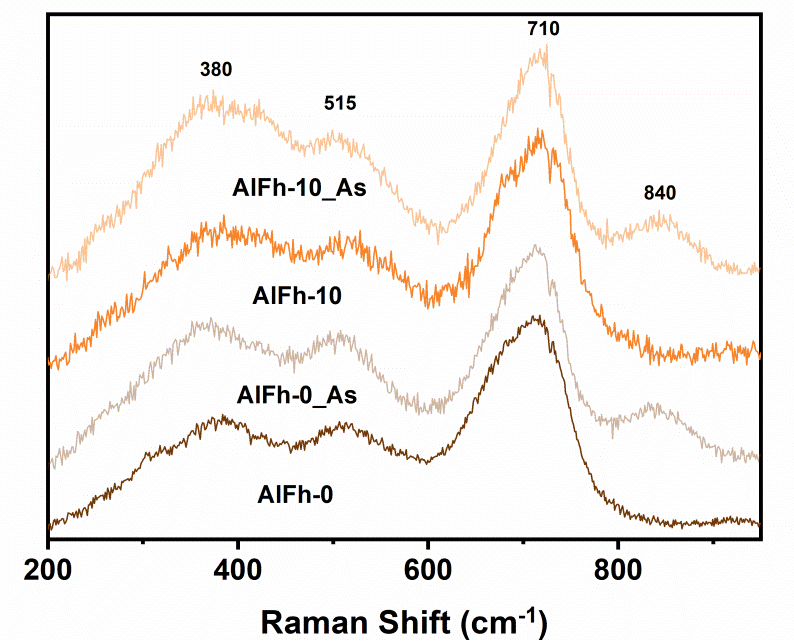

Figure 3.7: Raman spectra of AlFh-X before and after As(V) adsorption.

The XPS was employed to analyze the surface composition of the samples, and the results of O (1s) scans are shown in Figure 3.8. The high-resolution XPS O (1s) spectrum of ferrihydrites may be deconvoluted into three peaks at ~529, ~530.5 and ~532.5 eV. These were attributed to oxygen atoms directly bound to metal atoms (M–O), present in the surface hydroxyl sites (M–OH), and in the adsorbed water (H_2O), respectively (GLASAUER *et al.*, 2000; MALLET *et al.*, 2013). The XPS O (1s) scans of Al-substituted ferrihydrites clearly show that the relative amount of surface oxygen atoms in the M–OH sites increases as Al concentration increases. The (M-OH bindings) contribution increases (45%, 52%, 70%, 76%, and 77%) for the samples AlFh-0 to AlFh-20, respectively (Table A.3). These results are consistent with the deviation from the Vegard rule. The hypothesis that Al-substitution induces defects, thus increasing the surface hydroxyl sites, is demonstrated.

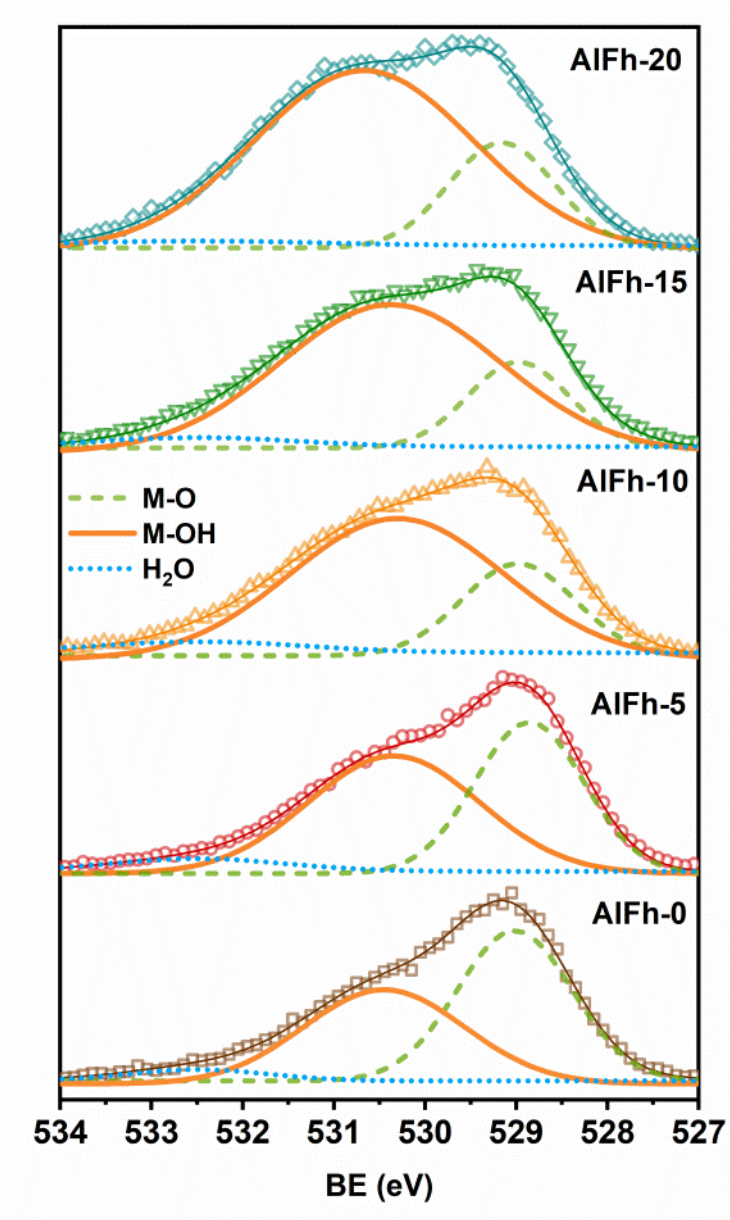

Figure 3.8: XPS O (1s) scan of the ferrihydrite samples (AlFh-X) with increasing aluminum content (X).

Arsenic adsorption is indicated by the variations observed in the region ~531 eV shown in Figure 3.9. The bindings As=O, As-OH, and Fe-OH, are too close to make it possible to discern their relative contribution (XUE *et al.*, 2019; ZHANG; LI; CHEN, 2010). The increased intensity in the region ~531, related to the non-complexed As-OH bindings of arsenates ions (LŮ *et al.*, 2013), is strong evidence of As adsorption (XUE *et al.*, 2019).

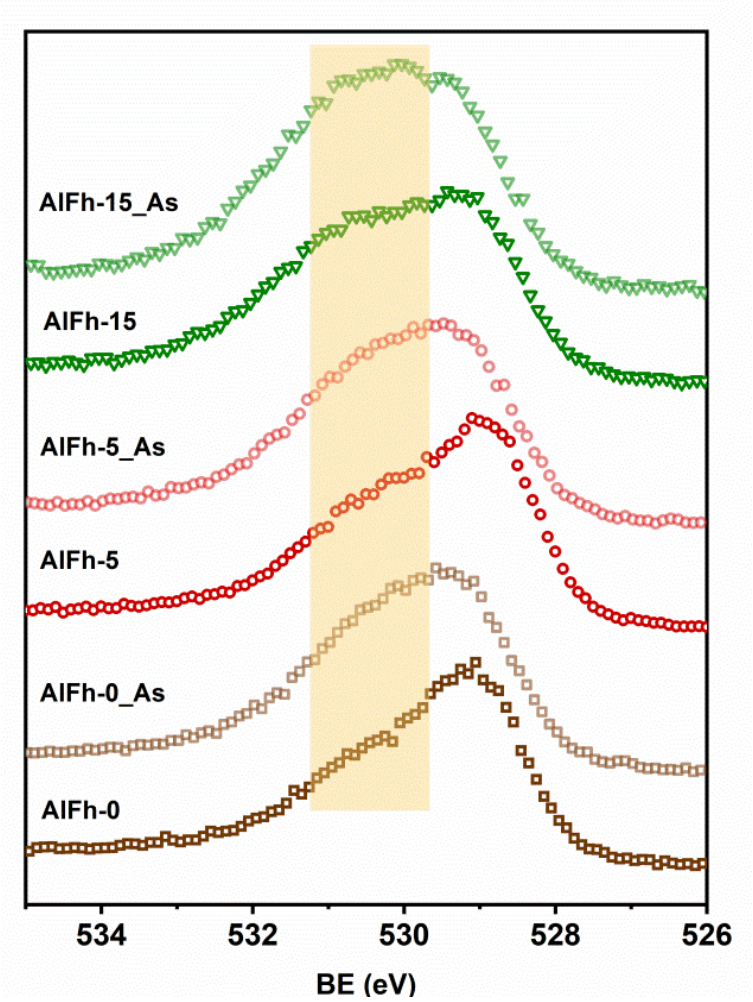

Figure 3.9: XPS O (1s) scan of AlFh-X highlighting the difference before and after As adsorption.

The XPS As (3d) scan of ferrihydrites containing Al was better fitted using two peaks (Figure A.1). The peak I, at ~44.5 eV, is characteristic of As(V) (ZHANG; LI; CHEN, 2010). The peak II, at ~46.5 eV, increased with Al, with relative intensities of 1%, 8%, and 15%, for samples AlFh-0, AlFh-5, and AlFh-15, respectively (Table A.4). Zhang et al. (2010) and Penke et al. (2016) related that shifts on BE to the presence of more protonated arsenate species (e.g., $H_2AsO_4^-$). The presence of protonated, less charged arsenates suggests monodentate complexation or weaker bonds. This hypothesis is also supported by decreasing the Langmuir constant (K_L) (section 3.2).

3.3.2 Effect of Al-for-Fe substitution in Ferrihydrites on Arsenic Adsorption

The sorption isotherms were studied for the AlFh series at 25 ^{0}C, and pH 5 and 8, as shown in Figure 3.10. The samples AlFh-0 and AlFh-10, representing Al-free and AlFh

samples, were selected for the kinetic tests carried out at pH 5, during 200 h. The results are shown in the inset of Figure 3.10. Differences in the initial As(V) adsorption rates are not evident, and for both samples, approximately 70% of the total adsorbed arsenate was taken in the first hour (table A.1 in the appendix A). The adsorption rates then decreased differently for each sample, and the equilibrium was achieved after about 100 h for AlFh-10, and 50 h for AlFh-0. The time selected for determining the adsorption isotherms was 150 h. The formation of ferric arsenate is favored at pH values lower than 5 (JIA, Y. *et al.*, 2007; PANTUZZO, F.L.; CIMINELLI; BRITO, 2008). Poorly crystalline ferric arsenate was not identified by SAD analysis of AlFh.

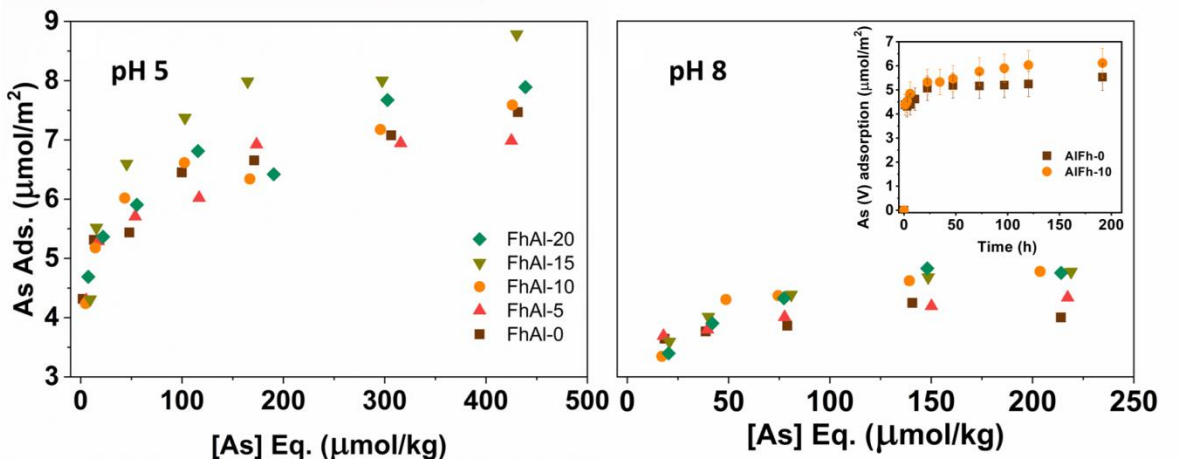

Figure 3.10: Isotherms for As(V) sorption on AlFh ferrihydrites in pH 5 and 8, 25°C. The points are the average of duplicate experiments. The inset shows the As(V) adsorption on AlFh-0 and AlFh-10 evaluated during 200 h, pH 5, $[As]_0$ = 100 mg kg^{-1}.

The amount adsorbed at pH 5 was approximately 50% higher than those at pH 8. The highest adsorption at lower pH is typically found for As(V) adsorption on iron oxyhydroxides. Masue et al. (2007) studied As(V) adsorption on Al-for-Fe substituted Fh (0, 20, 50, and 100% mol Al) under different pH conditions. The authors observed the maximum adsorption around pH 5 for the Al-oxyhydroxide and pH < 6.5 for the other samples. As mentioned previously, in such conditions, there may be partial segregation of Al phases. Only samples without detectable Al oxyhydroxide particles were employed in the present work.

At pH 5 Figure 3.10 shows that, when increasing the Al:Fe ratio in the ferrihydrite sorbent, the fraction of adsorbed arsenate increases until 15% Al. The curves were fitted to Freundlich and Langmuir equations (not shown). The Langmuir model was

deemed more suitable to describe our results based on the determination coefficients obtained for each.

The results of Γ_{max} and K_L can be seen in Table A.2 and Figure 3.11. This fit confirms the increase in adsorption capacity up to 15% Al described above. According to the Langmuir fit, the adsorption capacity at pH 5 increased from 6.7 to 8.6 µmol.m^{-2} (samples AlFh-0 to AlFh-15) and then decreased to 7.4 µmol.m^{-2} (AlFh-20). The samples tested at pH 8 also showed an increasing As(V) uptake up to 15% in Al - considering the error associated with the fit (represented in Figure 3.11-b by the error bars) and the small adsorption of these samples. Although the effect of Al remains at pH 8, which is more favourable to the adsorption of As(III), these results cannot directly imply a greater adsorption of As(III). Previous work (Masue-Slowey et al., 2011) showed that the reduction of adsorbed As (V) to As(III) leads to a greater release of As in Fh containing Al, thus suggesting that the effect of Al demonstrated in this work, for As(V), may not extend to As (III), which needs further investigation.

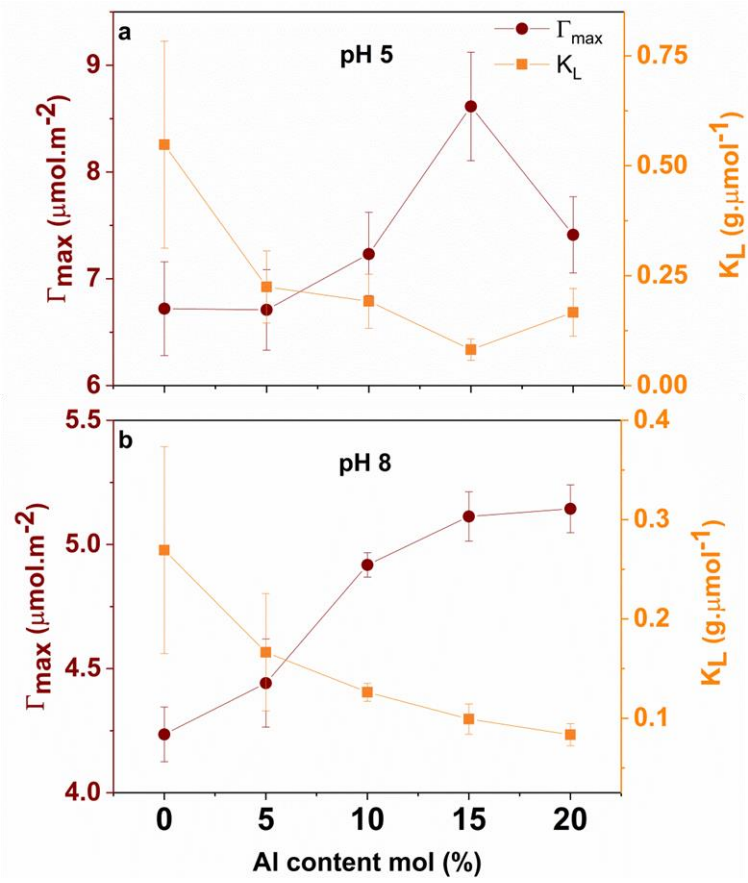

Figure 3.11: Maxima adsorption capacity (Γmax) and constant (K_L) for arsenate adsorption onto AlFh samples at 25°C according to the nonlinear fit to the Langmuir equation.

Tufo and collaborators (2016), who studied the adsorption of As(V) on goethite, partially substituted with Al at pH 5.5, showed an increasing maximum As(V) adsorption capacity with 3.78% Al substitution and further reduction for higher Al content (7.61%). Silva and coworkers also observed an increase, followed by a decrease in As(V) adsorption on Al-goethite for 13%, 20%, and 23% Al (SILVA *et al.*, 2010). As for Fh, the results are contradictory (ADRA *et al.*, 2016; MASUE; LOEPPERT; KRAMER, 2007). Adra and coworkers observed an increased As(V) maximum adsorption capacity with a 22% AlFh sample, whereas Masue et al. (2007) observed no variation between samples without Al and with a 20% Al content. Arsenic adsorption on Fe oxyhydroxides has been extensively investigated. For ferrihydrites, the maximum As uptake was found to vary from 3.4 (Masue et al., 2007) to 248 mg g^{-1} (XUE *et al.*, 2019), most of which were below 100 mg g^{-1}. The present work found 193 mg g^{-1} maximum As uptake in the best-studied conditions.

The Langmuir constant (K_L) values, as shown in Table A.2 and Figure 3.11, decrease with increasing aluminum content in Fh, except for the sample AlFh-20 at pH 5. Similar behavior was reported previously by various investigators, regardless of the different Al content, where the maximum adsorption was observed (ADRA *et al.*, 2016; MASUE; LOEPPERT; KRAMER, 2007; SILVA *et al.*, 2010; TUFO; AFONSO; SILEO, 2016). These decreasing values indicate lower adsorption energy between the arsenate and the sorbent surface. Previous investigations have reported increased arsenate release from soils with Al content in a sequence of leaching tests (LADEIRA, ANA C.Q.; CIMINELLI, 2004). Similar results were found in coprecipitated Al-substituted iron oxyhydroxides, where more As(V), and especially As(III), were desorbed by phosphate with an increase in Al:Fe molar ratio (MASUE; LOEPPERT; KRAMER, 2007).

3.4 Discussion

The lower As(V) adsorption above neutral pH is often attributed to the reduction of positively charged surface species, where the Coulombic contribution to the adsorption of an anion on a less protonated oxide surface is reduced (WILKIE; HERING, 1996). Similar reasoning has been used to explain arsenate's higher adsorption when increasing Al content in ferrihydrite (ADRA *et al.*, 2016; CISMASU *et al.*, 2013; MASUE; LOEPPERT; KRAMER, 2007). Figure A.2 shows the

electrophoretic mobility of the studied samples as a function of pH. The IEP values were 7.3, 8.2, 8.3, 8.7 and 8.8 for the samples AlFh-0 to AlFh-20, respectively. The Al insertion increases the isoelectric point (IEP), according to previous reports (Cismasu et al., 2013; Ye et al., 2020). It is well established that As(V) adsorption on iron and aluminum oxyhydroxides involves inner-sphere complexation (Dantas et al., 2011; Ladeira et al., 2001; Sherman and Randall, 2003). Therefore, the surface charge is not expected to have a major role. Moreover, for both pH levels, the As uptake increased approximately 28%. Since the pH 8 is near the pH_{PZC} and the effect of Al-for-Fe substitution on adsorption is still, the hypothesis that Al increases the As uptake by increasing surface charge is weakened.

Namayandeh and Kabengi (2019) studied the sulfate complexation on AlFh surfaces. The authors proposed that enhancing the percentage of Al increased not only positive surface sites, but also the number of singly coordinated surface groups due to defects in the structure of Fh. The increase of Pb^{2+} adsorption on Al-hematite was ascribed to increased hydroxyl groups induced by Al-substitution defects (LIANG *et al.*, 2019). The singly coordinated surface groups, controlled by the surface structure, may influence Fh reactivity (Hiemstra, 2013; Hiemstra and Van Riemsdijk, 2009), and hydroxyl groups are directly related to the As(V) adsorption, as shown by FTIR results. Our analysis using the Vegard rule for the characterization of Fh indicates an excess of hydroxyls (see section 3.3.1) for the AlFh-10 and AlFh-15 samples. Similar results were found by XPS O (1s) scans. The excess may explain their higher arsenate adsorption capacity. We claim that the Al introduction on Fh induces more iron oxyhydroxide sites available for arsenic adsorption, which increases the As uptake. An additional combined effect due to a more positively charged surface, also associated with Al in Fh, cannot be discarded.

Regarding the strength of the adsorption interaction, the Langmuir equation also shows a decrease in K_L values with increasing Al content, which means a reduction in adsorption energy, which agrees with the previously reported ease of desorption (MASUE; LOEPPERT; KRAMER, 2007). According to Hiemstra and Zhao (2016), singly coordinated groups present at the corners of the Fe1 octahedra in Fh form monodentate complexes. When present in pairs at two different octahedra, double corner complexes can be formed (i.e., binuclear bidentate surface complexes of arsenate $\equiv(FeO)_2AsO_2$). Aluminum is found in octahedral coordination with oxygen in

an Fh structure (CISMASU *et al.*, 2012). Arsenate commonly adsorbs more on the Fe than Al oxyhydroxides (LI, F.; GENG; CAO, 2015).

It is possible that Al introduction increases singly coordinated surface groups and favors monodentate complex formation. The XPS As (3d) scans of AlFh-x after As(V) adsorption shows a slight increase on higher BE region, which may indicate the presence of monodentate or weaker bonds, as described before (section 2.3.1). This singly-coordinated surface groups may imply a weaker bond and explain the lower K_L values with increasing Al reported by this and previous works (ADRA *et al.*, 2016; MASUE; LOEPPERT; KRAMER, 2007). However, to provide more evidence to favor monodentate complexation, further studies are needed. Arsenic adsorption is proposed to occur in two processes—a fast and a slow one. The amount of As adsorbed was related to the rapid process (Luengo *et al.*, 2007). Grossl *et al.* (1997) and Soldoozy *et al.* (2020) suggest that fast adsorption is predominantly electrostatic or monodentate. The slow process would involve the conversion to bidentate complexes. Since the FTIR analyses were made after 150 h of adsorption, it would represent the latter condition.

3.5 Environmental implications for arsenic uptake by AlFh

The results from the present investigation are consistent with the observed positive effect of Al within the Fe-(hydr)oxides on As concentration in soil (Antônio, 2021; Freitas et al., 2015; Yang and Donahoe, 2007), and help to explain the As distribution in the environment. Table 3-3 shows EDS analysis from hematite (H) crystals found in oxisol samples exposed to As sources. The soil was used, for ten years, as liners in tanks for the disposal of As-sulfide concentrates from the hydrometallurgical processing plant of a gold ore (FREITAS *et al.*, 2015). This contact led to enriched As concentrations relative to the typical, non-exposed oxisol. Arsenic-bearing Al-goethite and Al-hematite were identified by SAD and EDS analyses, but Al-hematite was the predominant As-bearing phase in all the oxisol liners. On average, a larger amount of As was found in Al-goethite relative to Al-hematite, though the largest As content (3.23 wt%) was found for Al-hematite. The presence of up to 1.8 wt% As (V) in hematite nanocrystals synthesized from ferrihydrite has been reported (Bolanz et al., 2013). However, the arsenic incorporation in naturally-formed hematite was first documented by our group (FREITAS *et al.*, 2015). The results from Table 3-3 show a

clear and linear (y = 0.38x - 0.81, R^2 = 0.968) increase of As content (wt%) in these oxisol liners, with an increase in the Al/(Al+Fe) molar ratio. A linear increase was also identified for non-exposed oxisol samples (Antônio et al., 2020). A good correlation was found between the aqua regia soluble Al and the As (wt%) in the soil samples (y = 0.79x + 0.01, R^2 = 0.970). In summary, the increase of As concentrations with Al content in iron oxyhydroxides is observed for synthetic (up to 15% Al) and natural samples. This increase is related to the hydroxyls' insertion on structural defects created by the Al isomorphic substitution. The results reported here on Al substituted ferrihydrites advance the understanding of the role of Al on As adsorption. Such knowledge is important in the context of the fate and fixation of As in the environment, and in the selection of materials for As immobilization.

Table 3-3: Arsenic and Al content found in hematite (H) crystals from EDS analysis of the oxisol samples, and the molar ratios As/(As+Fe) and Al/(Al+Fe) calculated from EDS data

Sample	H1	H2	H3	H4	H5
As (%wt)	0.9	1.0	1.5	1.8	3.2
Al/(Al+Fe) (% mol)	4.0	4.9	6.5	7.3	10.2

3.6 Conclusion

An original rationale is proposed to explain critical effects associated with As uptake by Al-for-Fe substituted ferrihydrites. The effect of increasing Al in ferrihydrites, truly Al-for-Fe substituted, on As adsorption were studied. The challenging Al-for-Fe chemical substitution was undoubtedly demonstrated for the first time, to the best of our knowledge, by selected area electron diffraction (SAD). This study observed the reduction of the interplanar spacings from 0.5954 to 0.5886 nm (unit cell parameter *a*) and from 0.9017 to 0.8915 nm (unit cell parameter *c*), when Al content was increased from 0% to 20% mol Al. The unit cell parameter a, calculated from the SAD results, proved to deviate from the Vegard rule. The deviations were associated with the insertion of hydroxyls on the Fh structural defects. The increase of OH with Al-substitution is clearly demonstrated by XPS O (1s) scans. The peak at ~531 eV, related to M-OH bindings, increase from 45% to 77% for the samples without Al and AlFh-20. The Al isomorphic substitution was found to impact As adsorption, where

the maximum adsorption capacity increased up to 28% with 15 mol% Al content. The As uptake is corroborated by the emergence of the 797 cm-1 and 840 cm-1 bands at the FTIR and Raman spectra, respectively, and the increased intensity in the region ~531 (XPS O (1s)). The Langmuir binding constants decreased from -0.55 to 0.17, at pH 5, and 0.27 to 0.08, at pH 8, for 0% to 20% mol Al, respectively - indicating a weaker bond between arsenic and the solid surface. Thus, the work proposes a novel rationale to explain the increase of As(V) uptake by AlFh, ascribed to the insertion of hydroxyls on the Fh structural defects created by Al isomorphic substitution. Accordingly, the FTIR band ~1330 cm^{-1} ascribed to the Fe-O-H bond was shifted to higher wavenumbers by Al insertion and significantly decreased after As adsorption. These findings help understand aluminum's role in arsenic adsorption on Al-for-Fe substituted Fh, and its fate in the environment. They may also help in designing strategies for arsenic fixation.

4. MECHANISM OF AMOXICILLIN ADSORPTION BY FERRIHYDRITES: EXPERIMENTAL AND COMPUTATIONAL APPROACHES [2]

Highlights

Ferrihydrite (Fh) shows superior capacity for amoxicillin-AMX uptake (75 mg g-1)

The Al-for-Fe substitution increases surface OH and decreases AMX adsorption

Bidentate-binuclear complexation is the main AMX adsorption mechanism on Fh

Inner-sphere complexation characterizes strong sorption, less mobile adsorbate

Strong sorption on soils can minimize superficial and groundwater contamination

Graphical abstract

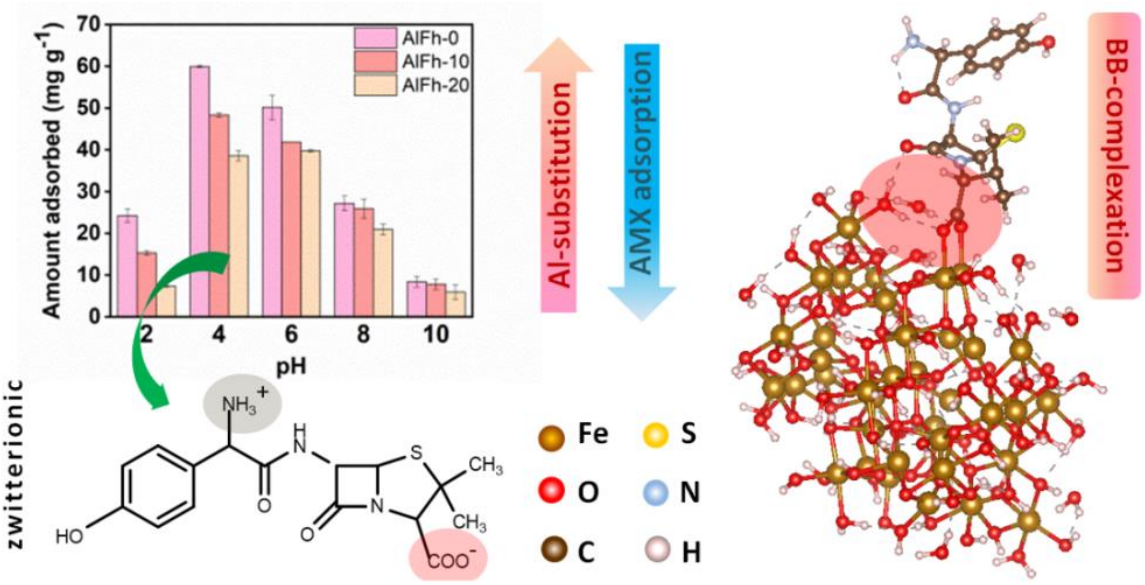

[2] Souza, T.G.F., Olusegun, S.J., Galvao, B.R.L., Da Silva, J.L.F., Mohallem, N.D.S., Ciminelli, V.S.T., *submitted for publication to a journal in June, 29th, 2022*

Abstract

The fixation of amoxicillin (AMX) by soils is a strategy to minimize the contamination of plants and groundwater by this antibiotic. Ferrihydrite (Fh) is a mineral largely found in the soil, and capable of removing emerging contaminants, such as AMX. To better understand the role of this mineral on AMX retention, nanoparticles containing 0, 10, and 20 mol% of Al, a common substitutive in Fh, were synthesized. Ferrihydrites showed AMX adsorption capacity superior (75 mg g-1) to other common soil constituents. The optimum pH for the AMX adsorption by the studied materials (Fh-0%Al, Fh-10%Al, and Fh-20%Al) was pH 4. This condition favors electrostatic attraction (AMX-carboxyl/Fh), but experiments demonstrated that is not the main mechanism of adsorption. Raman and Fourier transform infrared spectroscopies combined with theoretical approach using the density functional tight-binding method showed the bidentate binuclear complexation of the AMX - COO- group with the Fh particle as the main adsorption mechanism. The Al substitution decreases AMX uptake. The effect was attributed to the increase of surface OH, thus avoiding CH3 interaction with the Fh surface. The interaction mechanism suggests that a strong AMX fixation on Fh-rich natural soil will occur, preventing water contamination and allowing for further biotic degradation.

Keywords: Al-substituted ferrihydrites, amoxicillin, adsorption, mechanism, computational simulations.

Environmental implication:

This work explores several aspects of amoxicillin (AMX) adsorption, an emergent contaminant. The findings help to understand aluminum’s role in AMX adsorption on Al-for-Fe substituted ferrihydrite (Fh), a mineral commonly found in soils. The results support the potential use of Fh in AMX remediation and sheds light on AMX fate in the environment. The elucidation of the strong interaction mechanism (bidentate binuclear complexation of the AMX via COO- group) corroborates the hypotheses that AMX fixation takes place on Fh-rich natural soil, which likely helps to prevent groundwater contamination, and provides the longer retention time required for further biotic degradation.

4.1 Introduction

Antibiotics were firstly produced less than 100 years ago and, since then, they have become indispensable tools for a healthier and longer life. The contamination by these drugs, even at low concentrations, has been shown to affect the aquatic organisms and causes metabolic and reproductive disorders (BOJARSKI; KOT; WITESKA, 2020). More so, it may be transferred through the food chain by accumulating in plant tissues (DANNER et al., 2019; LI, W. C., 2014; MACKUĽAK et al., 2019); and cause intoxications and chronic diseases (YE, J. et al., 2019). The presence of antibiotics in the environment may develop antibiotic-resistant bacteria, death, or growth inhibition of important bacteria in the ecosystem (COSTANZO; MURBY; BATES, 2005). It is important to know that, increasing antibiotic resistance has become one of the major issues in public health.

The sources of antibiotics in the environment include wastewaters from hospitals, pharmaceutical industries, research centers, households, irrigation, agricultural activities (which consume these drugs for livestock and poultry farming), and the excretion (either unchanged or due to the incomplete metabolization of this class of drug in the body) (GRENNI; ANCONA; BARRA CARACCIOLO, 2018; KÜMMERER, 2009). For example, it was calculated that over 80% of amoxicillin is excreted after 2 h of ingestion (AKSU DEMIREZEN; YILDIZ; DEMIREZEN YILMAZ, 2019), and up to 79% of cephalosporin and 74% of penicillin are emitted into sewage (KÜMMERER, 2009). Amoxicillin is most commonly used in human and veterinary medicine around the world. Conventional wastewater treatment technologies do not efficiently remove the contaminant, which may result in the presence of trace amounts in drinking water and water bodies (SODHI; KUMAR; SINGH, 2021). The wastewater, which is commonly considered the major source of antibiotics to agricultural soil, is used to irrigate soils. Others are animal manures and biosolids, used as fertilizers. All these practices, which drive to multiple economic and environmental benefits, now face the disadvantage of carrying emergent contaminants (PAN; CHU, 2017). The use of advanced techniques to remove antibiotics has limited application especially in rural areas, where agricultural activities are more intensive. To better control the mobilization of antibiotics to the environment, it is important to understand the soils characteristics that favor the antibiotic’s fixation and the mechanism involved. A

recent investigation on AMX uptake by agricultural soils shows that the abundance of non-crystalline minerals of Fe and Al, organic matter, and pH are the most determining factors in the process (CELA-DABLANCA; BARREIRO; LÓPEZ; et al., 2022; CELA-DABLANCA; BARREIRO; RODRÍGUEZ-LÓPEZ; et al., 2022).

The adsorption mechanism of β-lactam antibiotics on mineral surfaces (e. g., clay minerals) remains poorly investigated (KLEIN et al., 2021; PUTRA et al., 2009; TRI; NGUYEN; TRUNG, 2020). Ferrihydrite is an abundant nanocrystalline mineral (often misinterpreted as a non-crystallline phase) in soils. Due to its high density of reactive surface sites and high specific surface area, Fh plays a crucial role in the transport and fate of many environmental contaminants and nutrients (FAIVRE, 2016). Comprehending AMX uptake by this ubiquitous mineral found in soil and riverbeds is relevant considering its role on the fate of this drug in the environment.

Ferrihydrite rarely exists as a pure phase in natural systems. The impurities associated with Fh may affect its properties, such as, adsorption capacity (CISMASU et al., 2014; HARVEY; RHUE, 2008; JOHNSTON; CHRYSOCHOOU, 2016; SOUZA et al., 2021). The isomorphic substitution in naturally occurring Fh is mainly by Al, Si, and Mg (CORNELL, R. M.; SCHWERTMANN, 2003) and has been shown to alter the removal of aqueous contaminants, such as chromium (NI et al., 2016), arsenic (ADRA et al., 2016; SOUZA et al., 2021), and phosphorus (LIU, Y.; HESTERBERG, 2011). In our previous investigation, it was demonstrated an increase in arsenate adsorption by increasing the Al amount in the Fh. Such adsorption increase was associated with the insertion of surface defects by the Al substitution and, consequently, to the increase of surface OH (SOUZA et al., 2021). As AMX adsorption was suggested to be improved by the increasing of surface OH (PINTO et al., 2016), and the presence of noncrystalline compounds of Fe and Al (CELA-DABLANCA; BARREIRO; RODRÍGUEZ-LÓPEZ; et al., 2022), these hypotheses will be examined with synthesized Al-Fh. The AMX adsorption on Fh has not been previously reported, to the best of the authors' knowledge. Furthermore, Fh-based sorbents are relatively simple to produce. Despite Fh (pure or Al-substituted) attractive features, the adsorption capacity, and mechanisms of interaction with AMX remain to be investigated.

For the above reasons, the objectives of this work are to assess AMX's removal from

aqueous solution by using synthesized Fh and Al-substituted Fh and investigate its interaction mechanisms. The influence of pH, ionic strength, and specific surface area, on AMX's adsorption by Fh is examined. The interaction of AMX with Fh and Al-Fh is studied in detail using Raman spectroscopy, Fourier-transformed infrared spectroscopy (FTIR), and molecular modeling simulations.

4.2 Materials and methods

4.2.1 Synthesis of adsorbents

The Fh sorbents were synthesized through the Schwertmann and Cornell (2000) method, modified to incorporate aluminum, as previously reported by Souza et al (SOUZA *et al.*, 2021). Briefly, the Al and Fe nitrate solutions, with the initial concentration of 0.1 mol L^{-1}, were precipitated by adding 1 mol L^{-1} of NaOH solution, at 1.5 mL min^{-1}, until pH 7.0 ± 0.3. The solutions contained Al / (Fe + Al) molar ratios of 0, 0.10, and 0.20, and the Fh samples obtained will be named as Fh-0%Al, Fh-10%Al, and Fh-20%Al according to the Al-containing of the initial solutions. The precipitates were washed at 4 °C and freeze-dried. After adsorption, samples Fh-0%Al and Fh-10%Al were calcined at 500 ^{o}C/ 2h. The calcined samples (Fh-0%Al-500 and Fh-10%Al-500) were also used for amoxicillin adsorption.

4.2.2 Characterization of the adsorbent

The Fh samples were analyzed using an ICP-OES (Perkin Palmer 7300) to assess chemical composition. By the method used the detection limit for Fe was 3.5 µmol kg^{-1}, and 7.5 µmol kg^{-1} for Al. A solution of Lu 0.6 µmol kg^{-1} (Ultra Scientific) was used as an internal standard to guarantee the method's precision (95-105% recoveries accepted). Calibration curves with the same sample matrix and certified solutions from Spex (99.99%) of Fe 10,000 µg mL^{-1}, Al 10,000 µg mL^{-1}, and As 1,000 µg mL^{-1}, were used to improve the accuracy of chemical analyses. The results were accepted when recoveries were between 95 and 105% and coefficients of determination of the curves were, at least, 0.995. The solid were digested in 8 v/v% aqua regia.

High resolution TEM images (HRTEM) were obtained at 200 kV in a FEI- LaB6-TEM (Tecnai G2-20-SuperTWIN), with Image Filter (Gatan-Quantum SE), and processed at the Digital Micrograph Software (version 2.32). The Fourier-transform infrared

spectroscopy (FTIR) was conducted in attenuated total reflectance (ATR) mode in a Bruker Alpha spectrometer. The Raman spectra were a collection of, at least, 10 spectra scanned for 60 s each, performed at a Horiba LabRam-HR 800 with a 632.8 nm helium laser, operated at a power less than 0.04 mW. The diffractograms were obtained in a Panalytical (PW1710) X-ray diffractometer, between 10–80° 2θ, scanning at 0.020° s^{-1} step size, and with Cu (Kα) radiation. The reference patterns were from FIZ Karlsruhe library: Inorganic Crystal Structure Database (ICSD). In order to identify lattice parameters reduction due to Al-for-Fe isomorphic substitution, the Al-containing XRD were subtracted of Fh-0%Al and called difference curve. A Zetasizer Nano-Zs (ZEN3600) was used to measure the Zeta potential of the particles, at different pH, previously dispersed in 0.01M KCl. The N_2 adsorption-desorption isotherms were performed in a Quantachrome (Autosorb-1). The isotherms allow the inference of specific surface area (SSA) and pore size distribution, the last calculated by using the Kernel “N2 at 77 K on silica (cylindr. Pore, NLDFT)” from Autorsob 1 (1.54) software.

4.2.3 Adsorption study

The adsorption study was carried out at room temperature. The effect of solution pH was investigated by measuring 15 mL of 100 mg L^{-1} of amoxicillin and added to 50 mL beakers that contained 10 mg of the respective adsorbents (Fh-0%Al, Fh-10%Al, and Fh-20%Al). The pH of each AMX solution, in each beaker, was adjusted 2, 4, 6, 8, and 10, by adding dropwise HCl and NaOH solution. The pH used for subsequent studies was defined as the one with the maximum amount of AMX adsorbed. Therefore, the effect of ionic strength was carried out at optimum pH (pH 4), by varying the concentration of $NaNO_3$ (20, 40, 60, 80, and 100 mg L^{-1}). A concentration study was done within the range 0f 20 – 200 mg L^{-1} of AMX. The amount of AMX that was adsorbed under each study was calculated after 24 h by measuring the absorbance of the unadsorbed AMX in the solution at λmax 240 nm. The amount (q) adsorbed (mg g^{-1}) was calculated using equation 1.

$$q = \frac{(C_o - C_e)V}{m} \qquad 1$$

C_o and C_e in the equation stand for the initial and final concentration (mg L^{-1}) of the antibiotic solutions, respectively, m is the mass of the adsorbent (g) and V is the

solution volume.

4.2.4 Computational methods

The model structure used to simulate the ferrihydrite nanoparticle was taken from Kubicki et al. (KUBICKI *et al.*, 2018), having a $Fe_{38}O_{112}H_{110}$ charge-neutral structure and was built based on an experimentally determined structure. The AMX molecule was placed on the surface of this particle at several sites considering several possible conformations. The calculations were performed within the density functional tight-binding (DFTB) method, including the self-consistent charge approach (SCC-DFTB)(ELSTNER *et al.*, 1998). The parameters come from the *mio* (NIEHAUS; ELSTNER; *et al.*, 2001; NIEHAUS; SUHAI; *et al.*, 2001) and *trans-3d* (ZHENG *et al.*, 2007) sets while the Fe-S interaction parameters were obtained from Lourenço et al. (2016, 2020). Solvent effects were included approximately with the polarizable continuum model (LI, H.; JENSEN, 2004), and long range interactions were treated with UFF-type dispersion correction (RAPPE *et al.*, 1992). All calculations were carried out using the GAMESS-US package (SCHMIDT *et al.*, 1993).

4.3 Results and discussion

4.3.1 Adsorbent characterization

The synthesized Fh-0%Al, Fh-10%Al, and Fh-20%Al materials were analyzed. The target Al contents were achieved, as shown in the chemical analyses. The Al / (Al+Fe) molar ratios based on ICP-OES results were 0, 10.4, and 21 mol% for the samples Fh-0%Al, Fh-10%Al, and Fh-20%Al, respectively. The TEM images show, regardless of the Al content, particles smaller than 5 nm (Figure **4**.**1**). The particles have no distinct lattice fringes and exhibit poorly defined edges, which indicates structural disorder as expected for materials with short- and intermediate-range ordering (CISMASU *et al.*, 2011). TEM images did not show different compositions or particle formats, suggesting no Al segregation. The theoretical limit for Al substitution in the Fh structure is up to 25% molar ratio (MANCEAU, A.; GATES, 2013). Previous works observed phase segregation for Al molar ratio higher than 20% (MASUE; LOEPPERT; KRAMER, 2007) or ranging from 15 to 30%, according to the

precipitation rate (CISMASU *et al.*, 2012).

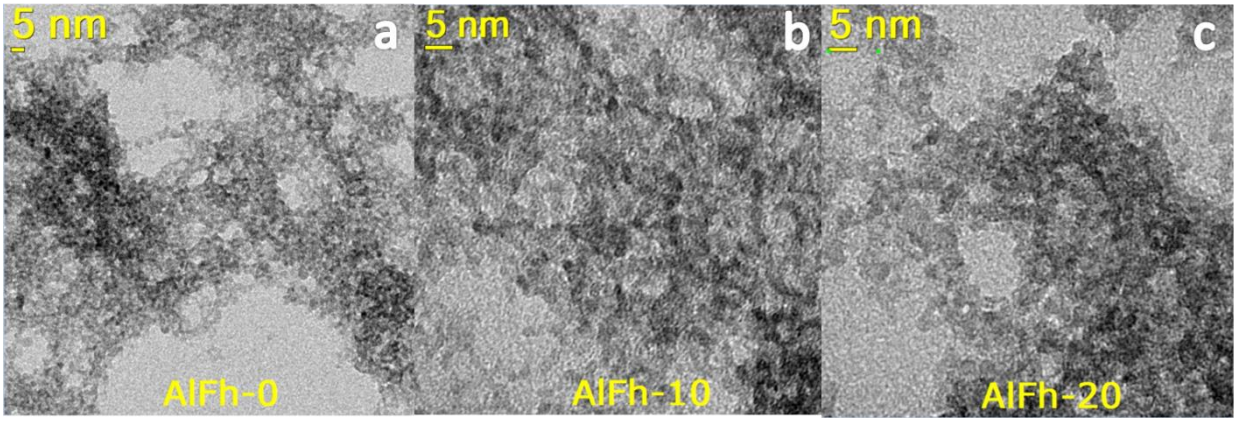

Figure 4.1: TEM of samples AlFh-0 (a), AlFh-10 (b), and AlFh-20 (b) before amoxicillin adsorption.

Figure 4.2 shows the N_2 adsorption-desorption isotherms on the AlFh samples before amoxicillin adsorption. The isotherms are characteristics of materials with broad pore size distributions including wider micropores and possibly narrow mesopores. For this type of isotherm, the monolayer-multilayer adsorption process and micropore filling are difficult to separate. Then, in these cases, the surface area measured is called apparent surface area (ASABET). The criteria for choosing the relative pressures (P/P_0) range used to measure the ASA followed the conditions recommended by Rouquerol et al. (ROUQUEROL; LLEWELLYN; ROUQUEROL, 2007) and IUPAC (THOMMES *et al.*, 2015). The surface areas and pore volume are presented in Table 4-1. It was not found significant differences between the ASABET of the samples Fh-0%Al and Fh-10%Al (~400 m^2 g^{-1}), which agrees with the literature, regarding measurement errors (CISMASU *et al.*, 2013; DU *et al.*, 2018). The Fh-20%Al surface area was slightly higher (440 m^2 g^{-1}) than others, probably due to its higher pore volume and size, but the numbers were within the expected

values for Fh (CISMASU *et al.*, 2013; DU *et al.*, 2018).

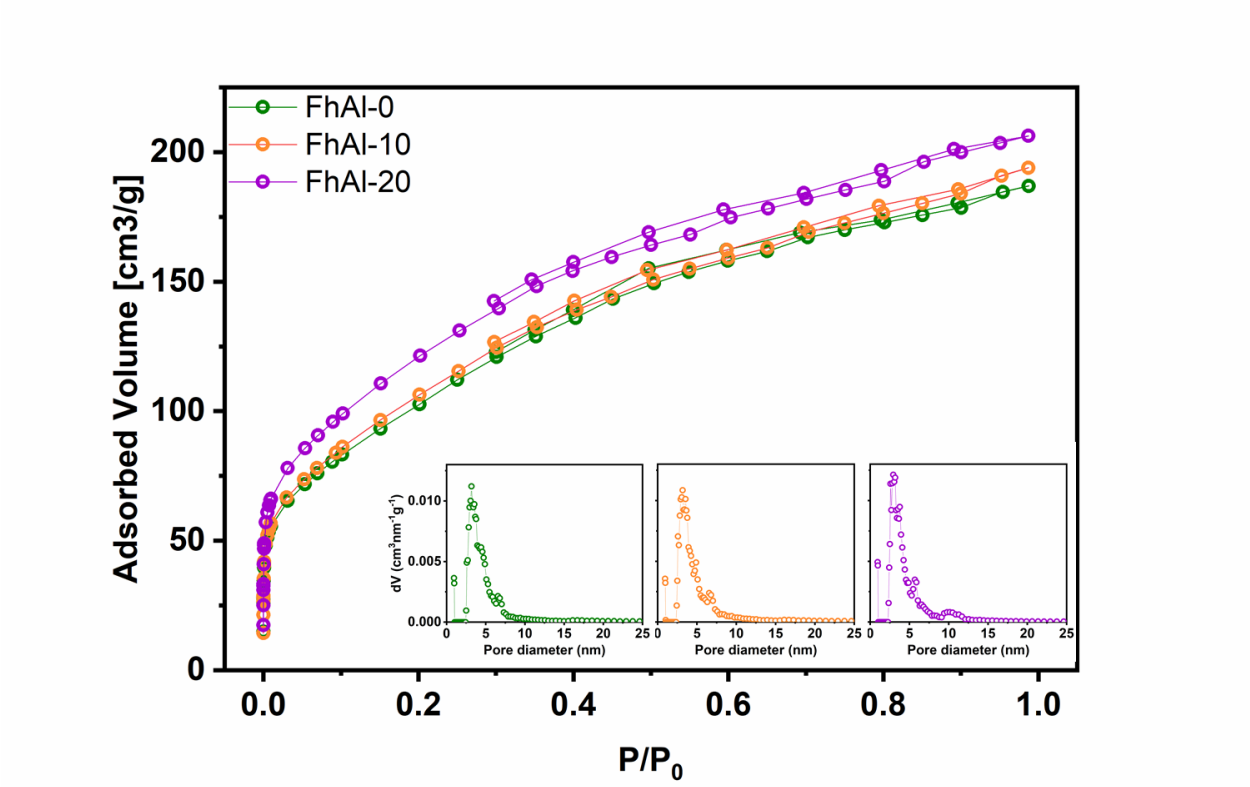

Figure 4.2: Isotherms of N_2 adsorption.

Table 4-1: The ASA_{BET}, pore volume, and mean pore diameter of the AlFh samples

Sample	$ASA_{BET}(m^2/g)$	Pore volume (cm^3/g)	Pore size median (nm)
AlFh-0	386 ± 28	0.278	3.2
AlFh-10	395 ± 32	0.288	3.2
AlFh-20	448 ± 32	0.310	2.9

Figure 4.3 presents the XRD of AlFh samples. The diffractograms are characteristics of 2-line Fh due to its broad peaks and d-spacings of about 2.6 and 1.5 Å (JAMBOR; DUTRIZAC, 1998). Despite increasing Al content, there is no piece of evidence for the formation of crystalline Al-oxyhydroxides (e.g., bayerite or gibbsite), which would indicate Al-phases segregation. Associated with that, there is a little shift of the peaks around 35 degrees toward higher 2-theta values, by increasing Al content. The shift is highlighted by subtracting Al free Fh from the Al-containing diffractograms, the

difference plots in Figure 3, as previously observed by others (JENTZSCH; PENN, 2006; SOUZA *et al.*, 2021). The shifts suggest Al-for-Fe isomorphic substitution by the reduction of the lattice parameters, which drives a contraction of the unit cell lattice parameters due to the smaller ionic radius of Al^{3+} compared with Fe^{3+} (PINNEY; MORGAN, 2013b, a).

The isomorphic substitution by Al impacts the isoelectric point (pH_{IEP}) of Fh, by increasing it (YE, C. *et al.*, 2020). Our measurements showed a slight pH_{IEP} increase (i.e., 7.3, 8.3, and 8.8) for the samples Fh-0%Al, Fh-10%Al, and Fh-20%Al, respectively.

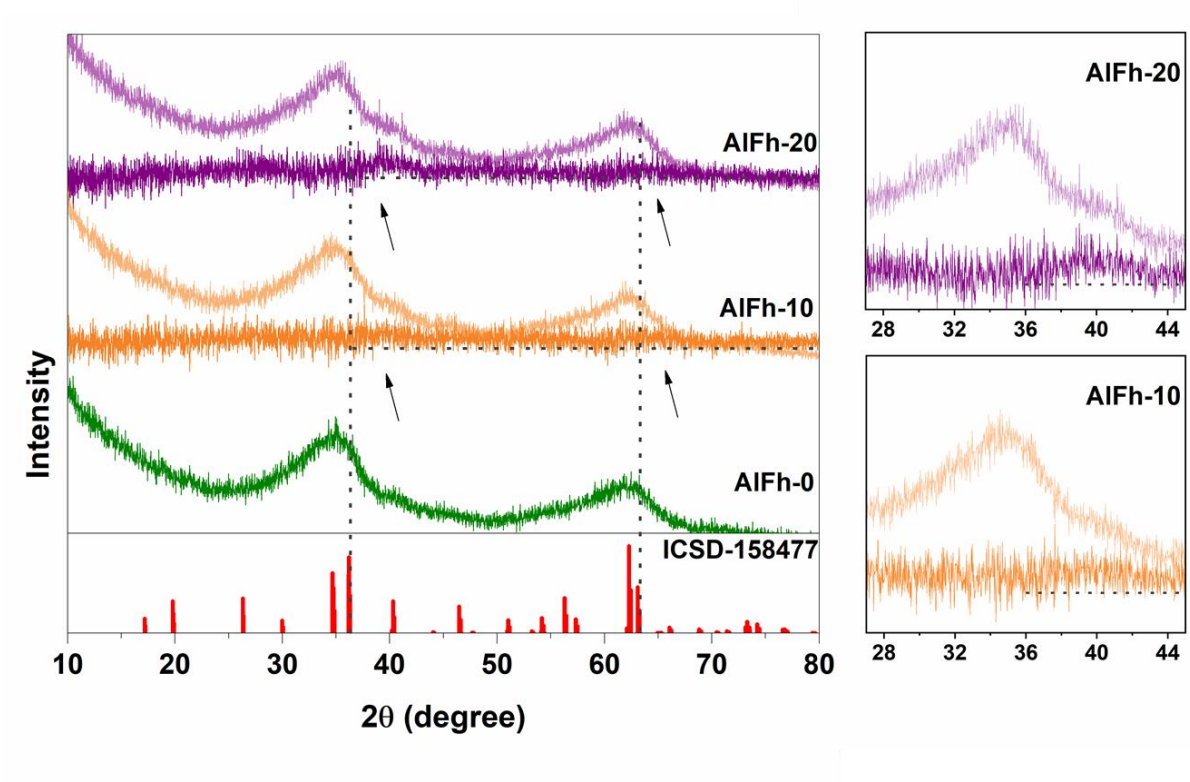

Figure 4.3: Diffractograms of AlFh samples, the difference curves, determined by subtracting the Al free Fh pattern from Al-containing, and the reference pattern for Fh with 2–3 nm (MICHEL; EHM; LIU; *et al.*, 2007), ICSD#158477

4.3.2 Effect of pH and ionic strength on the adsorption of amoxicillin

Amoxicillin is a molecule (Figure 4.4-b) containing a β-Lactam ring associated with phenol, amino, and carboxylic groups. These three functional groups tend to deprotonate and protonate under different pH conditions (Figure 4.4-c and d)

(GODDARD *et al.*, 1996). The carboxyl group deprotonates at pH 2.68 (pKa_1), the amino group at pH 7.49 (pKa_2), and the phenol group at pH 9.63 (pKa_3). The Fh-0%Al, Fh-10%Al Fh-20%Al samples will be positively charged at pH < 7.3, 8.3 or 8.8, respectively. Figure 4.4a shows the effect of pH on the adsorption of AMX on Fh-0%Al, Fh-10%Al, and Fh-20%Al. As it can be seen, the adsorption of AMX increases from pH 2 to 4 and decreases gradually at pH 6, 8, and 10. The lowest amount of AMX was adsorbed by the three samples at pH 10, while the highest amount was adsorbed at pH 4. In general, Fh-0%Al performed better than Fh-10%Al and Fh-20%Al, while Fh-10%Al performed better than Fh-20%Al, implying that the presence of Al inhibits the adsorption of AMX. The pattern in the AMX adsorption with the increase in the solution pH may be due to the different ionization potential of AMX interacting with the surface charge of Fh-0%Al, Fh-10%Al, and Fh-20%. As the phenol group remains uncharged within the studied pH interval it was not considered in this discussion. At pH 2, the amine functional group (NH_3^+) of AMX is protonated (Figure 4.4-c), which causes electrostatic repulsion with the positively charged sorbents; the carboxylic group is uncharged. Between pH 4-7 both the amine and carboxylic acid functional groups are charged (protonated NH_3^+ and deprotonated COO^-), in other words, AMX is in its zwitterionic form (Figure 4.4-c) (LIU, L. *et al.*, 2020). Therefore, the adsorption within this pH range may be favored by electrostatic interactions between the positively charged Fh samples and the negatively charged carboxylic group. At pH greater than 8, the carboxylic group is deprotonated and both the Fh surface and COO^- group are negatively charged, thus resulting in electrostatic repulsion and an expected decrease in the amount adsorbed at basic pH conditions. The highest uptake was observed at pH 4 - 59.9, 48.3, and 38.5 mg g^{-1} for Fh-0%Al, Fh-10%Al, and Fh-20%Al respectively. The results suggest a contribution of electrostatic interaction in the AMX uptake by Fh.

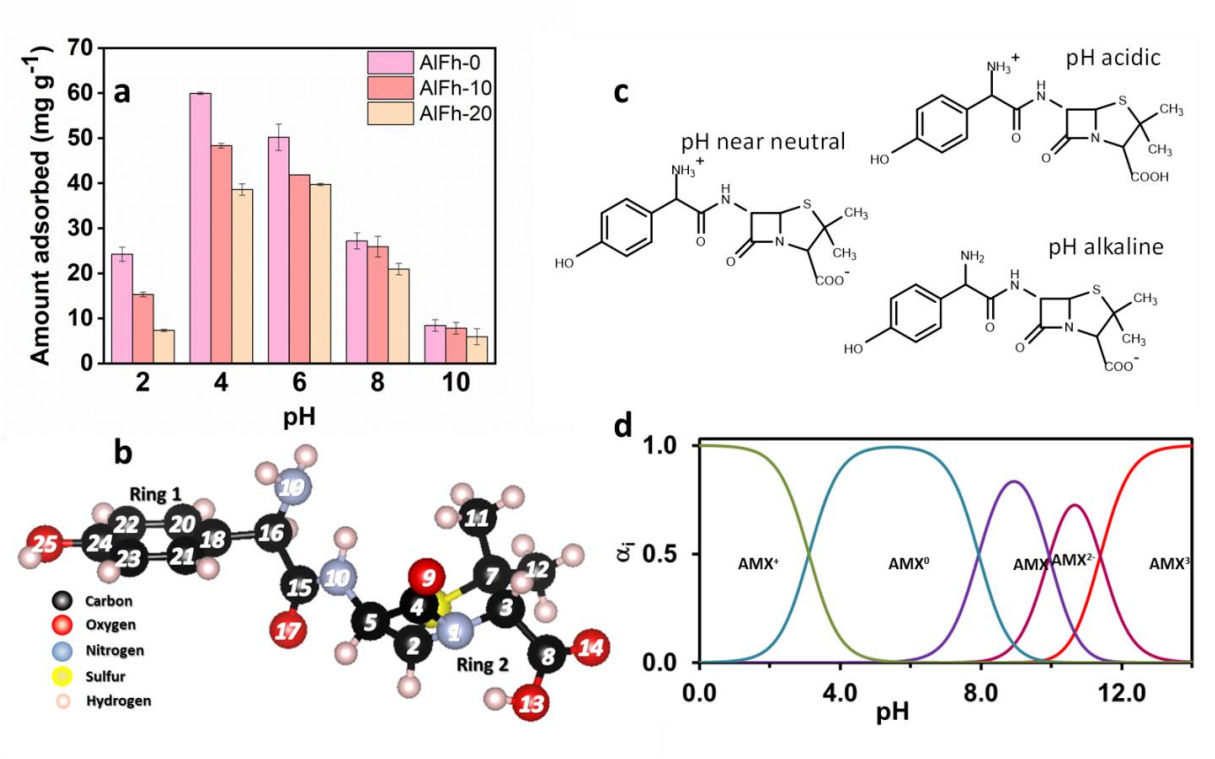

Figure 4.4: The effect of pH on the adsorption of AMX using FhAl (a), model of AMX molecule (b) and AMX speciation (c) and (d).

One approach to confirm the influence of electrostatic interaction in the adsorption process is by investigating the trend of the amount adsorbed as ionic strength increases using an indifferent electrolyte – usually monovalent ions with no specific affinity by the sorbent's surface sites. An increase in the ionic strength can reduce adsorption when the process is predominantly controlled by electrostatic interactions. Therefore, the effect of increasing $NaNO_3$ concentration within the range of 0-100 mg L^{-1}, at pH 4, on AMX adsorption by both Fh-0%Al and Fh-10%Al was investigated. The results shown in Figure 4.5 show no significant difference in the amount of AMX adsorbed when ionic strength increases. In the absence of $NaNO_3$, 57 mg g^{-1} of AMX was adsorbed by Fh-0%Al whereas the adsorbed amount was reduced to 48 mg g^{-1} when 100 mg L^{-1} of $NaNO_3$ was added. In the case of Fh-10%Al, the amount of AMX that was adsorbed decreased from 40 to 38 mg g^{-1} in the presence of 100 mg L^{-1} of $NaNO_3$. Therefore, one may conclude of electrostatic interaction is not the dominant mechanism in the adsorption of AMX by the studied materials.

Spectroscopy methods and theoretical modelling will help to identify the surface groups and the mechanism involved in AMX uptake by Fh.

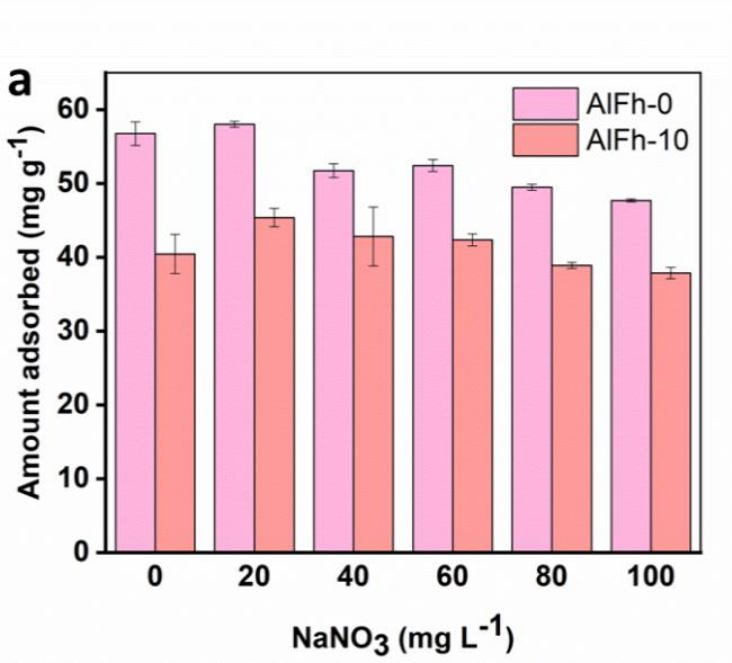

Figure 4.5: The effect of ionic strength on the adsorption of AMX by Fh-0%Al and Fh-10%Al at pH 4, room temperature, 20 mg of Fh, and 30 mL of 100 mg L^{-1} AMX solution.

4.3.3 Adsorption capacity and adsorption isotherm

Adsorption isotherms are helpful tools in modelling adsorption in solid-aqueous interfaces. Among the commonly used equations are Langmuir, Freundlich, and Liu with their respectively non-linear form listed in the appendix B, and their curve-fit plots shown on Figure 4.6. The values of their respective adjusted coefficient of determination ($R^2_{adjusted}$) and the standard deviation (which is calculated from the square root of reduced Chi-squared help to appropriately determine the model that is more suitable for the adsorption process (LIMA; ADEBAYO; FERNANDO, 2015; TRAN; YOU; *et al.*, 2017). Based on this, the itemized parameters of the three isotherms indicate that the Liu isotherm model is the best isotherm to describe the behavior of AMX on both Fh-0%Al and Fh-10%Al. This isotherm (Liu), a combination of Langmuir and Freundlich equations, assumes that the active sites of adsorbent (i.e., Fh-0%Al and Fh-10%Al in our case) do not possess the same energy, as expected in mineral interfaces. The maximum adsorption values obtained by adjusting the Liu isotherm are accepted as the sorption capacity of Fh-0%Al and Fh-10%Al for the removal of AMX (Table 4-2). These values are superior to maximum uptakes previously reported for mineral samples and iron oxyhydroxides: iron oxyhydroxide/Al2O3 composite (42 mg g-1) (PINTO; LANZA; LAGO, 2019), iron

oxide supported on MCM 41 (25 mg g-1) (SALVIANO et al., 2018), phosphate rock (23.3 mg g-1) (BOUYARMANE et al., 2015), bentonite (33-45 mg g-1) (BUDYANTO et al., 2008), alumina supported Fe oxide (35 mg g-1) (PINTO et al., 2016), among others..

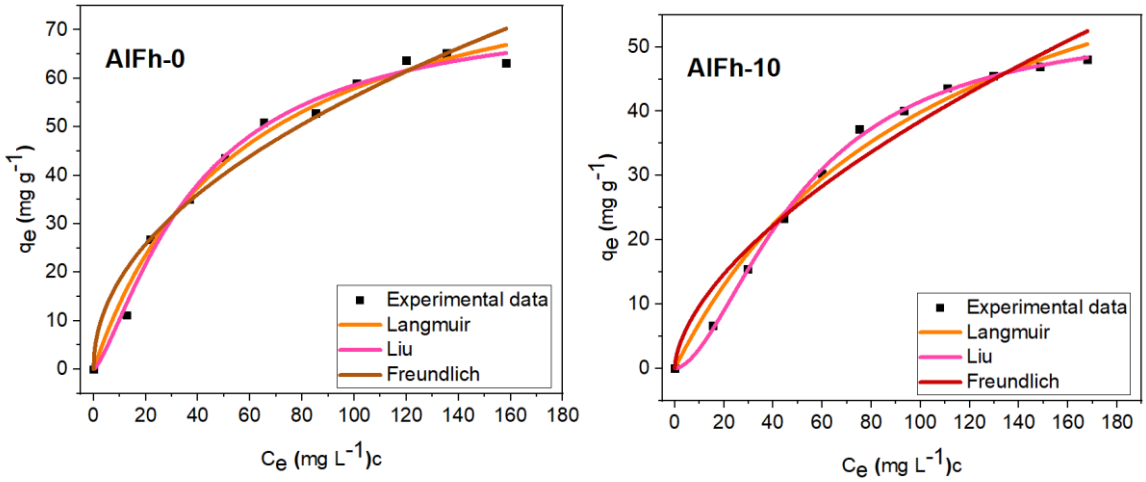

Figure 4.6: Adsorption isotherms for the removal of AMX by Fh-0%Al and Fh-10%Al, room temperature, pH4, 50 mg of Fh, and 75 mL of AMX solution.

Table 4-2: Langmuir, Liu and Freundlich isotherms parameters for the adsorption AMX at room temperature, pH 4

	AMX	
	Fh-0%Al	Fh-10%Al
Langmuir		
$\mathbf{q_{max}}$ (mg g^{-1})	91	82
$\mathbf{K_L}$ (L mg^{-1})	0.017	0.009
$\mathbf{R^2_{adjusted}}$	0.987	0.983
SD (mg g^{-1})	2.57	2.19
Liu		
$\mathbf{q_{max}}$ (mg g^{-1})	75	54
$\mathbf{K_g}$ (L mg^{-1})	0.025	0.019
$\mathbf{n_L}$	1.37	1.72
$\mathbf{R^2_{adjusted}}$	0.990	0.998
SD (mg g^{-1})	2.16	0.58
Freundlich		
$\mathbf{K_F}$ (mg g^{-1} (mg $L^{-1})^{-1/nF}$	6.05	2.44
$\mathbf{n_F}$	2.06	1.67
$\mathbf{R^2_{adjusted}}$	0.967	0.956
SD (mg g^{-1})	4.56	3.53
$\mathbf{q_{max}}$ (mg g^{-1})	91	82

4.3.4 Groups involved in AMX uptake by FH

The identification of the groups involved in the AMX adsorption by ferrihydrite was carried out by Raman and FTIR spectroscopy. Figure 4.7 shows the Raman spectra of the adsorbate and sorbent before and after contact. The pristine Fh samples show very broad lines at ~350, 510, and 710 cm^{-1} associated with 2-line Fh (MAZZETTI; THISTLETHWAITE, 2002). The amoxicillin spectrum, on the other hand, is characterized by well-defined peaks.

The most intense peak at 851 cm^{-1} is associated with ring 2 breathing and bending mode of $N19H_2$ + CH + ring 2 CH. Other lines (801, 838, 870, 1616, and 1681 cm^{-1}) are also associated with ring 2 and amino group deformations (BEBU *et al.*, 2011; CALBOREAN *et al.*, 2007). Besides being related to the bending modes of ring 2 and the amino group, the line at 1172 cm^{-1}, is also due to O25H bending mode. The line at 1011cm^{-1} is due to CH_3 bending or C4, C5 stretching and ring 1 breathing. The line at 1193, 1258, and 1282 cm^{-1} related to OH deformation of COOH. The line at 1282 cm^{-1} is also associated with ring 1 in plane deformations as well as 1312 cm^{-1}. The line at 1594 cm^{-1} is associated with O25H bending mode. Finally, the stretching of C=O from COOH is at 1771 cm^{-1}. It can be noticed that after amoxicillin adsorption, the lines associated with ring 2 breathing or bending modes and the COOH group disappeared. The lines at 1011, 1164, 1288, ~1312, and 1595 cm^{-1} remained and a new one appeared at 1500 cm^{-1}, indicating possible interactions between AMX and Fh by the ring 2 and COOH group.

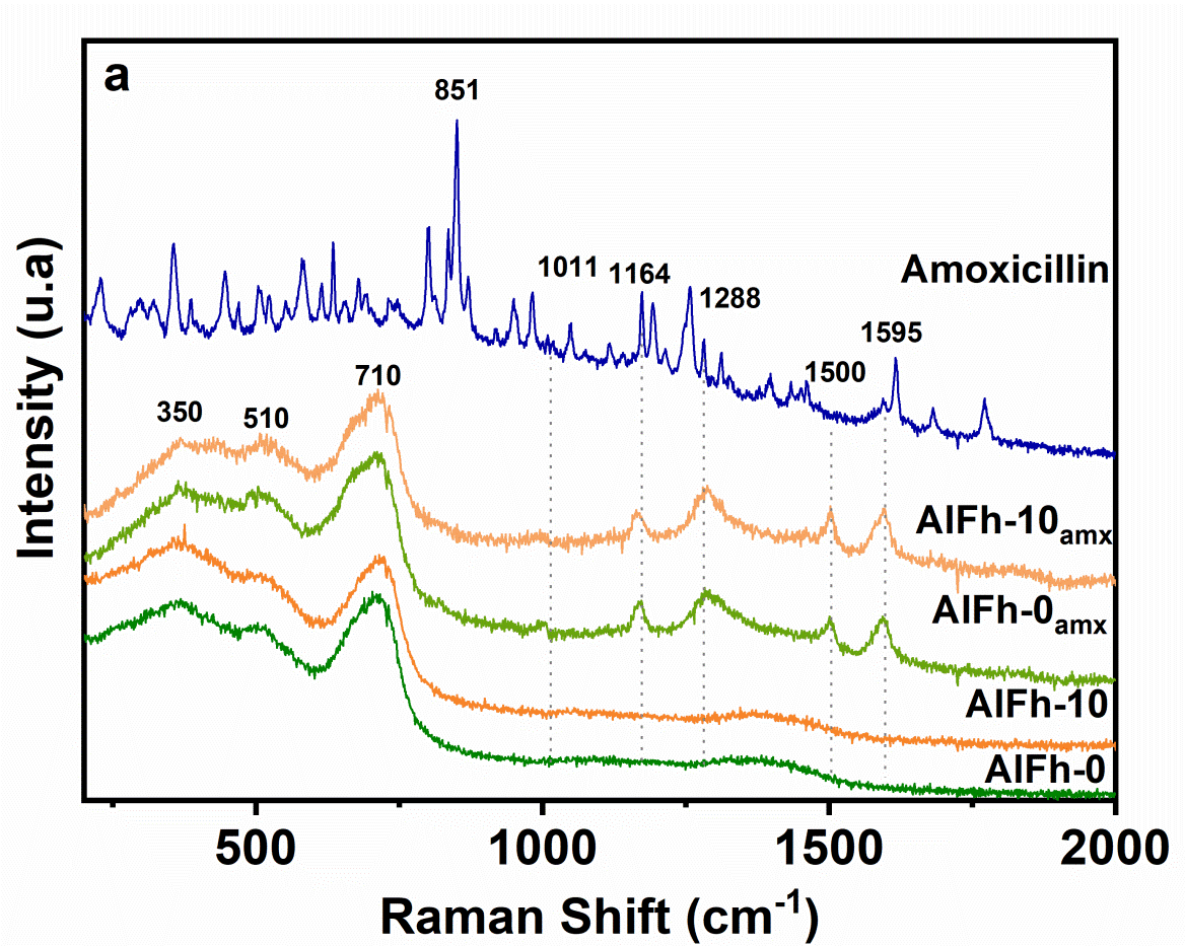

Figure 4.7: Raman Spectra from ferrihydrites before amoxicillin adsorption.

The FTIR spectra are shown in figure 4.8. Before adsorption, Fh shows bands at ~3300, 1625, 1465, 1380, and 1330 cm^{-1}. The large band around 3300 cm^{-1}, is assigned to surface, bulk, and adsorbed water hydroxyls, being the width related to the crystal structure's disorder (CORNELL, ROCHELLE M.; SCHWERTMANN, 2003). The adsorbed water is also associated with the band at 1625 cm^{-1}. The one at 1465 cm^{-1} is associated with the presence of carbonate (from exposure to the atmosphere), while those at ~1330 and 1380 cm^{-1} are attributed to Fe-O-H (Cornell and Schwertmann, 2003; Hausner et al., 2009; Seehra et al., 2004; Souza et al., 2021; Tüysüz et al., 2008; Wang et al., 2015). Figure 4.8 also presents the FTIR of AMX sodium salt. The peak around 3300 cm^{-1} is associated with phenol OH, water OH, amine, and amide NH stretches and the one at 2967 cm^{-1} to the group CH_3 (BRITTAIN, 1994; PEZOTI *et al.*, 2016). The bands at 1762 cm^{-1} were associated with β-lactam CO (BRITTAIN, 1994) and 1513 cm^{-1} to benzene C=C rings stretch

(BRITTAIN, 1994; XIE *et al.*, 2016). The one at 1399 cm^{-1} is likely related to phenol or CH_3 (BEBU *et al.*, 2011; BRITTAIN, 1994). Finally, the peaks at 1595 and 1244 cm^{-1} may be assigned to the asymmetric and symmetric stretches of COO^-, respectively, meaning that the difference between these two peaks (Δ_{COO}) is 351 cm^{-1} (BRITTAIN, 1994; NAKAMOTO, 2009). These band assignments are in concordance with the calculated spectrum of zwitterionic AMX (results not shown).

After adsorption, the intensities of the FTIR bands at 1330 and 3300 cm^{-1}, assigned to OH, are reduced, indicating AMX interaction with the Fe-O-H surface groups. The Fe-O-H surface groups' interaction with antibiotics has been reported by Pinto and coworkers (PINTO *et al.*, 2016) suggesting AMX complexation with the solid surface. This reduction was also proposed to be due to hydrogen bond interaction between adsorbed molecules and the adsorbent (TRAN; WANG; *et al.*, 2017). The peak at 1625 cm^{-1} which is related to adsorbed water, is also reduced after adsorption of AMX, which may indicate water replacement by AMX molecules. Ferrihydrites is capable of forming hydrogen bond through the hydroxyl surface groups (BOILY; SONG, 2020). The bands associated with CH_3, β-lactam CO, benzene C=C rings, and asymmetric COO^- on pure AMX were present after adsorption and undergo a redshift. The exception is for sample Fh-10%Al, where the band at 2967 cm^{-1}, related to CH_3, was not modified. On the other hand, the symmetric COO^- undergoes a blueshift, reducing the difference between the asymmetric and symmetric stretches, Δ_{COO}, from 351 to 333 cm^{-1} after AMX adsorption. The reduction of this delta may indicate a chemisorption interaction (NAKAMOTO, 2009), which will be discussed in the next section.

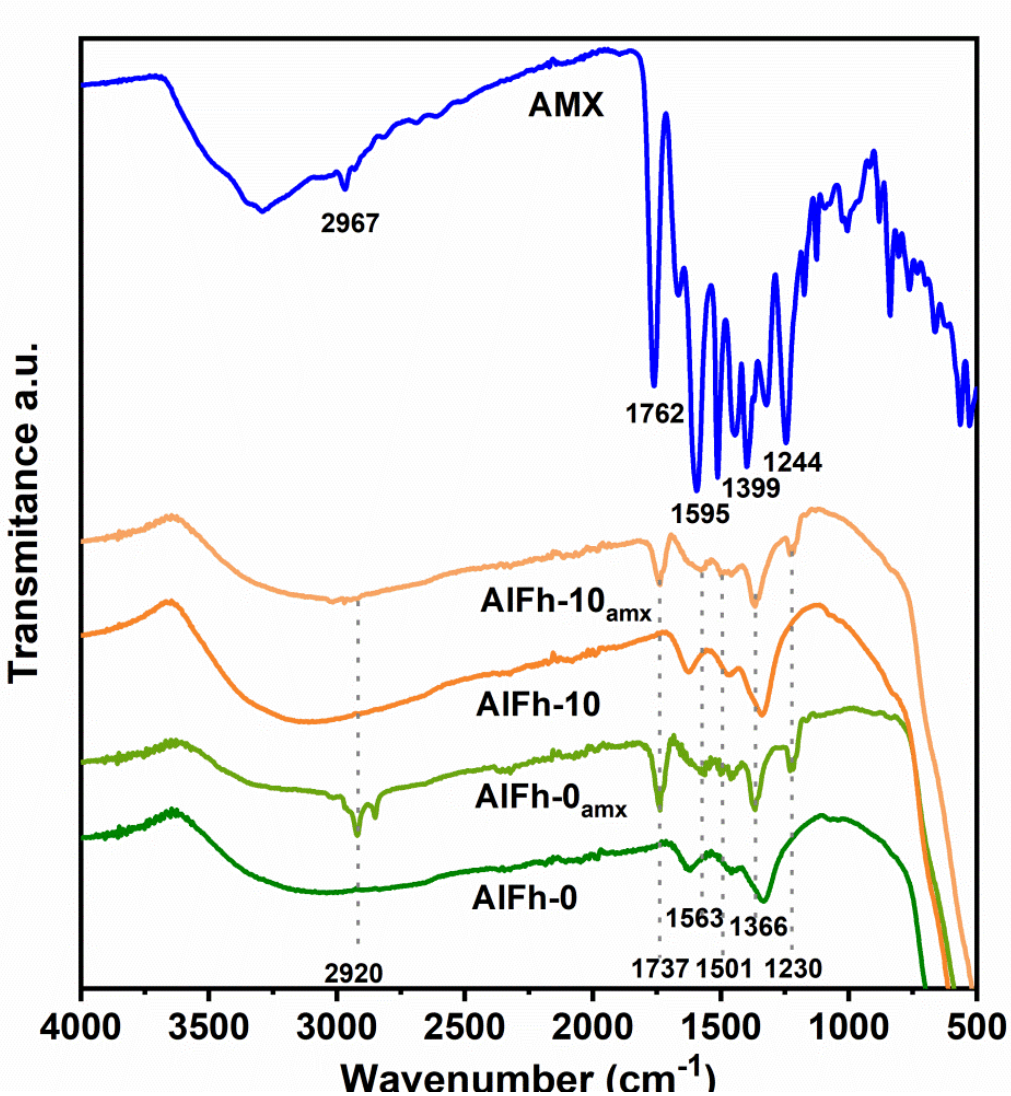

Figure 4.8: FTIR spectra from AMX and Fh before and after amoxicillin adsorption showing the peak shifts after AMX adsorption.

4.3.5 Computational results and mechanisms of AMX adsorption by Fh

After analyzing the experimental results of the materials before and after adsorption, a computational study was performed, in order to better elucidate the adsorption mechanisms and to provide further rationale for the experimental data from an atomistic point of view. The model particle is shown in Figure 4.9, where it can be seen that most of the exposed oxygen atoms are hydrogenated as Fe-OH and Fe-OH_2 groups. Bridging oxygen groups such as Fe-O-Fe also exist, but these are less exposed, and thus less prone for interaction.

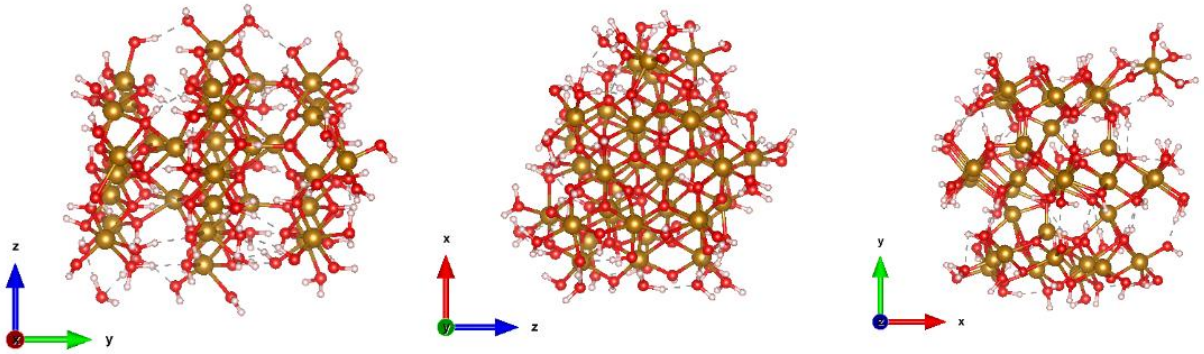

Figure 4.9: Model particle obtained from Kubicki et al. (2018) from three different perspectives.

Firstly, for an exploratory part, 110 configurations have been generated by randomly placing the AMX molecule around the Fh particles using the algorithm developed by Zibordi-Besse and coworkers (ZIBORDI-BESSE *et al.*, 2016). Geometry optimization was performed on each of these configurations at the DFTB level. The results are given in Figure B.1 of the supporting information, and overall, the DFTB calculations predict reasonable geometries for both particle and molecule, except for one C-S larger than the other, which was deemed as not crucial for the present discussion. Although the results covered a wide range of different sites of the particle, interacting with different functional groups of the molecule, no displacement of the OH_2 or OH groups of the particle was obtained in this way, and thus only physisorbed configurations were achieved. Such configurations are insufficient to explain the experimental results, pointing to chemisorption (surface complexation).

As a second step, it was simulated a mechanism in which the incoming AMX molecule adsorbs by replacing a surface H_2O group with a carboxyl, ketone, or phenol group of the molecule. In each of these cases, several possible molecular conformations were sampled and optimized and the results are given in the graphical form in Figure B.2. It was found that the most energetically favored configuration had a monodentate COO-Fe arrangement. At this most stable configuration, we have performed a vibrational analysis to predict the wavenumbers of all possible vibrational modes. The symmetric and asymmetric COO stretches of the adsorption complex were predicted to lie at 1022 and 1414cm^{-1}, respectively, amounting to a Δ_{COO} of 392 cm^{-1}. Compared to the calculated free zwitterionic AMX (Δ_{COO} of 232 cm^{-1}), the monodentate configuration shows a substantial increase in Δ_{COO} which contradicts the experimental results of a small reduction in this value after adsorption.

Therefore, this monodentate COO-Fe interaction is not likely the main adsorption mechanism.

Another possibility would be a binuclear bidentate configuration, in which the difference between symmetric and asymmetric COO stretches may be expected to deviate less from the isolated AMX case. However, most of the Fe-Fe distances available in the particle are too large to allow a proper attachment of this kind. Nevertheless, two such cases are available but would imply a mechanism in which the AMX molecule replaces two OH groups from their Fe-OH position simultaneously. Although this would correspond to a more energetically difficult approach, the zeta-potential analysis indicates that, at the most favorable pH, the surface should be positively charged, absorbing H^+ from the solution and providing more $Fe\text{-}OH_2$ groups than present in our model particle. This protonation would make it easier for the molecule to substitute the surface groups and bind to two adjacent Fe atoms.

After placing the molecule at the two possible binuclear bidentate configurations of the model particle (replacing the corresponding OH groups previously bound at the irons of the site) we have performed further geometry relaxations and performed the vibrational analysis. The two chemically adsorbed configurations are shown in Figure 4.10, and their Δ_{COO} values are 253 and 228 cm^{-1}. These configurations show a strongly chemisorption character. When compared to the calculated free zwitterionic AMX (Δ_{COO} of 232 cm^{-1}), the second configuration (Figure 4.10-b) is energetically more stable than the first (Figure 4.10-a) and shows a small reduction of Δ_{COO} value, compatible with the experimental data. The theoretical results are in agreement with the interaction modes postulated by Nakamoto (NAKAMOTO, 2009) in which a large increase in Δ_{COO} after adsorption indicates a monodentate adsorption mechanism. In turn, slightly small Δ_{COO} changes after adsorption mean a binuclear bidentate configuration. Therefore, our results indicate that the binuclear bidentate configuration should be the main mechanism for AMX-Fh adsorption.

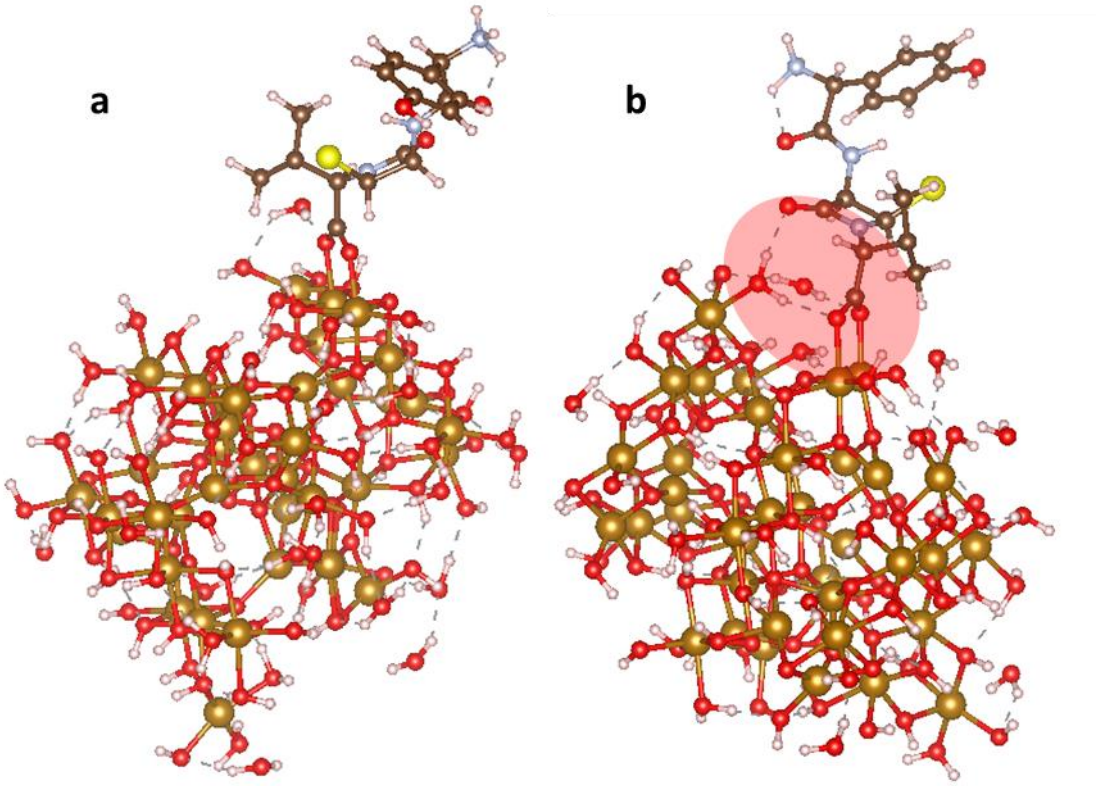

Figure 4.10: Computational predictions of binuclear bidentated adsorbed configurations. The red area highlight the interactions formed.

Comparing the experimental spectra of adsorbed and non-adsorbed AMX, a few other shifts can be observed, which we attribute to non-chemical interactions between the different groups of the molecule to other parts of the particle. One such example is illustrated in Figure 4.10-b (the most energetically stable configuration) predicted by the theoretical calculations, in which a CO group of the molecule participates in a hydrogen bond with a coordination H_2O of the particle. The shift of the carbonyl band observed in the experimental FTIR (from 1762 to 1737 cm^{-1}) is also observed in the theoretical calculations (from 1773 to 1728 cm^{-1}). One may also notice that the shift of the band at 2967 cm^{-1} attributed to the CH_3 group stretching is present in Fh-0%Al, but not in Fh-10%Al. However, in the configurations tested computationally, interactions between the CH_3 group and the model particle were not observed. Interestingly, our previous work (SOUZA *et al.*, 2021), with the same material, showed that the Al introduction increases the quantity of OH on the Fh surface. The high resolution XPS O (1s) spectra show that the oxygen atoms present on the surface may be directly bound to the metal atoms (M–O sites), hydroxyl (M–OH sites), or surface water (H_2O sites). It was shown that the relative amount of

oxygen atoms, from the surface, in the M–OH sites increases with Al content (45%, 70%, and 77%) for the samples Fh-0%Al, Fh-10%Al, and Fh-20%Al, respectively.

Since the particle model used in the present work has the entire surface coordinated with OH or H_2O, further tests were performed where coordinated water was removed (to expose a Fe site) followed by further geometry relaxations with an AMX binding via methyl group, and vibrational analysis (Figure B.3). The calculations show a shift, for the CH_3 asymmetric stretching, when comparing the calculated free zwitterionic AMX (3024 cm^{-1}) with the one bonded to the model particle via methyl group (2929 cm^{-1}). A new band at 2310 cm^{-1} due to the stretching of the CH directly interacting with Fe also was observed. Therefore, the interaction of the CH_3 group with Fe-O-Fe sites, without coordinated OH or H_2O, may explain the experimental FTIR shift observed in Al free Fh (from 2967 to 2920 cm^{-1}) but not in the 10% containing Fh (Fh-10%Al). The reduction in possibilities of interaction between AMX and Fh particles may be the reason why Fh-10%Al presents lower AMX adsorption capacity.

To better understand to role of surface OH on the adsorption mechanism, a thermal treatment of the AMX- loaded Fh-0%Al and Fh-10%Al samples was carried out at 500 °C for 2 h (table B1). After calcination the N2 adsorption-desorption isotherms of samples Fh-0%Al and Fh-10%Al became a type IV (Figure B4a), according to the IUPAC classification. The presence of hysteresis, due to the capillary condensation, is characteristic of mesoporous materials (THOMMES et al., 2015). The SSABET decreased from, around, 400 m^2 g^{-1} to 40 and 72 m^2 g^{-1} for Fh-0%Al and Fh-10%Al, respectively (table B1). Even the pristine materials were very similar in terms of surface area and porosity, Al prevents the SSA_{BET} reduction, and after calcination, the materials differ a lot from each other. The Al introduction led to an SSA_{BET} almost twice of Al-free Fh and to the formation of smaller pores (14 nm for Al-free and 9 nm for Fh-10%Al). The pore volume also increased for sample Fh-10%Al (0.165 cm3 g-1) compared with Fh-0%Al (0.130 cm^3 g^{-1}). The Raman spectra from AlFh samples (Figure B4-b) show that the calcination promotes the phase transformation of Fh to hematite, as characterized by the lines at 228, 294, 412, 612, and 1320 cm^{-1} (MÜLLER et al., 2010). No lines related to the presence of AMX were identified, thus indicating that the thermal treatment removes the antibiotic.

One can observe a significant reduction (from 56 to 7 mg g^{-1} for the sample Fh-0%Al)

in terms of adsorption capacity per gram of adsorbent, which was ascribed to a decrease in the SSA_{BET}. It is noticeable that the adsorption capacity of AMX on Fh-0%Al, by surface area, before and after calcination, shows a small increase (0.14 to 0.18 mg m^{-2}, respectively). Therefore, the phase transformation to hematite and the consequent reduction of surface OH did not imply the decrease of AMX adsorption capacity, evidencing that this decrease is due to the reduction of SSA_{BET}, and the AMX adsorption is not the surface OH, as claimed before. Once hematite is also abundant in the soils, this result is also important to understand the possible role of Fe-oxyhydroxides in AMX remediation.

4.4 Conclusion

In a comprehensive study of amoxicillin-AMX adsorption on Al-ferrihydrite, a common soil constituent (i) the high uptake capacity of ferrihydrite for AMX removal was identified, (ii) aluminum's role on AMX adsorption was better understood, and (iii) the mechanisms involved in the process of AMX uptake were clarified. The AMX, once in contact with a soil containing Fh, will not be easily removed by the increase in the electrolyte concentration. A strong sorption interaction leads to a less mobile adsorbate, and less potential groundwater contamination concomitantly to longer retention times allowing for natural degradation.

The synthesized nanoparticles – smaller than 5 nm and with apparent surface area (ASA_{BET}) of about 400 m^2 g^{-1} – showed broad XRD peaks (d-spacings of 2.6 and 1.5 Å) characteristics of 2-line Fh. The shifts of the XRD peaks, around 35 degrees, confirm the Al-for-Fe isomorphic substitution. The best pH for AMX adsorption on Fh with or without Al was found to be 4, a condition where the sorbent and the adsorbate (due to deprotonate carboxylate group) have opposite charges. But the lack of a significant effect of ionic strength, up to 100 mg L^{-1} of $NaNO_3$, indicates that AMX adsorption cannot be primarily attributed to electrostatic attraction.

Raman and FTIR spectra combined with theoretical molecular modeling by DFTB support the complexation of COO- with the Fe in a bidentate binuclear configuration as the main mechanism of AMX adsorption by Fh. This conclusion is based on the differences between the symmetric and asymmetric COO- stretching (ΔCOO), before (ΔCOO = 351 cm^{-1}) and after adsorption (ΔCOO = 333 cm^{-1}), and theoretical

calculations that identified the most energetically favorable configuration.

The Al-for-Fe substitution reduces the adsorption capacity (from 75 to 54 mg g^{-1}), which may be related to the increase of surface OH, due to the Al substitution, avoiding AMX CH_3 interaction with the surface. This interaction, demonstrated by the FTIR shift (from 2967 to 2920 cm^{-1} before and after adsorption respectively), was present in the Fh free of Al, but not in the Fh-10%Al sample. A FTIR shift from 3024 to 2929 cm^{-1} is also predicted by the theoretical calculations, when the interaction between CH_3 and Fe from the surface is present.

The thermal treatment of Fh reduces the ASA_{BET} (from ~400 to 40 and 70 m^2 g^{-1} for the samples AlFh-0 and AlFh-10, respectively). However, there was no reduction in the adsorption capacity by area after calcination, which transformed the particles into hematite, as shown by the Raman spectra. The hematite particle is known to have less OH on surface, therefore, the reduction of OH on surface did not imply in the decrease of AMX adsorption capacity.

This strong interaction Fh-AMX is of interest if one considers AMX- contaminated soils, as it may prevent the antibiotic to be carried to groundwater before degradation. Finally, it should be highlighted the synthesized Fh showed superior adsorption capacity (i.e., up to 75 mg g^{-1}) compared to most materials previously tested for AMX removal, according to the literature.

5. INFLUENCE OF ALUMINUM ON THE PHASE TRANSFORMATION AND AS(V) FIXATION BY FERRIHYDRITE NANOPARTICLES

Highlights

Aluminium and As delay Ferrihydrite phase transformation.

The Al-for-Fe substitution on Ferrihydrite inhibits goethite formation.

The presence of Al changes the hematite growth mechanism.

Al-substitution directs growth mechanism, even when As is present.

Increasing Al in Fh increases the As release from Ferrihydrite.

After aging, increasing Al decreases As release from Ferrihydrite.

The Al-containing Fe-oxyhydroxides promotes As fixation in soils.

Graphical abstract

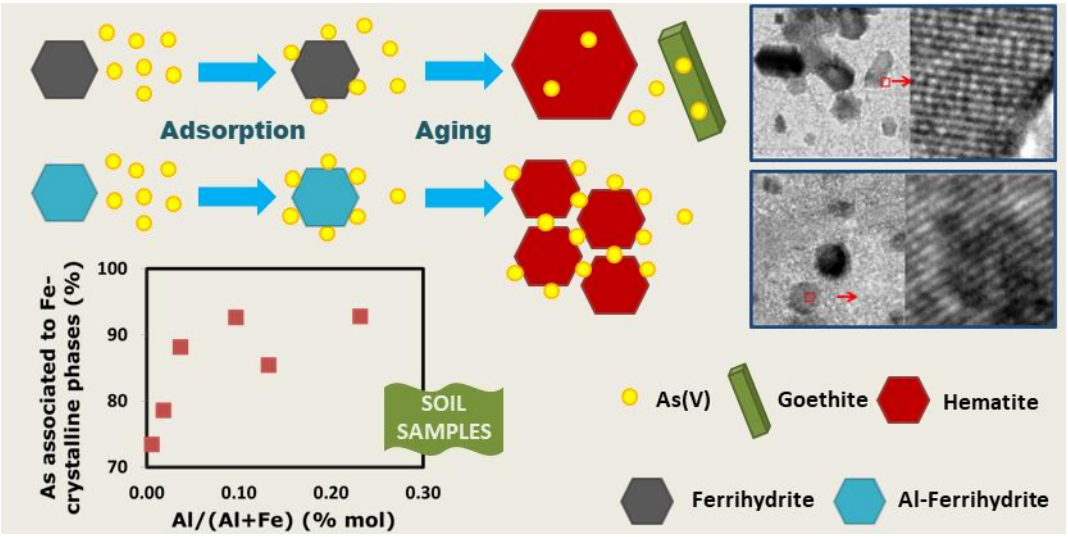

5.1 Introduction

The ferrihydrites (Fh) are metastable nanosized minerals, very abundant in the soils (FAIVRE, 2016). This iron oxyhydroxide has been studied due to its capacity for pollutants' removal, its role in their transport, and possible fixation by phase transformation into more stable minerals (LI, B. *et al.*, 2021; LIANG *et al.*, 2019; LIU, J. *et al.*, 2019; LU *et al.*, 2019; NAMAYANDEH; KABENGI, 2019; YANG, Z. *et al.*, 2021a). Seldom found as a pure mineral, iron replacement on Fh, mainly by Al, Si, and Mg, may affect the contaminants removal or fixation (Cismasu et al., 2014; R. M. Cornell and Schwertmann, 2003; Johnston and Chrysochoou, 2016; Masue-Slowey et al., 2011; Ye et al., 2020).

Understanding the role of Al in the As uptake by Fe oxyhydroxides containing Al is crucial for the development of remediation technologies for the immobilization of As in such mixed phases, considering the frequent Al-Fe association in the environment. Greater As uptake by Oxisols rich in Al and Fe was demonstrated by Ladeira et al. (LADEIRA, ANA C.Q.; CIMINELLI, 2004; LADEIRA, ANA CLÁUDIA Q.; CIMINELLI; NEPOMUCENO, 2005). The soils were selected as a chemical barrier in tailings dams in a gold mine in Paracatu, state of Minas Gerais, Brazil. The work of Duarte et al. (2016) and Freitas et al. (2015) on the same Fe–Al-oxisols exposed over 10 years to a sulfide concentrate in tailings impoundments found more than 60% As immobilized in Al-Fe-mesocrystals, suggesting an entrapment of the metalloid in the oxyhydroxides structures. The immobilization of As in soils containing Al-Fe oxyhydroxides is also supported by the low As-bioaccessibility (ANTÔNIO, DAPHNE C. *et al.*, 2021; CIMINELLI *et al.*, 2018). The effect of increasing Al in ferrihydrites, truly Al-for-Fe substituted up to 15 mol% Al, for example, was demonstrated to increase in almost 30% arsenate adsorption (SOUZA *et al.*, 2021). However, the impact of Al insertion on the stability of the As-containing products and its behaviour with aging remains to be investigated, and soil observations suggest a positive impact of Al in long-term As fixation.

Seeking to better understand the mechanism of As fixation on iron oxyhydroxides, As-Fe or As-Fe-Al coprecipitations were studied (Pantuzzo and Ciminelli, 2010; Shi et al., 2018; Violante et al., 2009; Wang et al., 2015). The authors reported a delay in phase transformation of the Al-Fe and As-Al-Fe coprecipitates. Wang et al. (2015) show the stabilization of coprecipitated As-containing Fh, with the increase of the As/Fe molar ratio (from 0 to 0.5). The arsenic inhibited Fh phase transformation towards hematite. Retaining as a result of phase transformation was also reported by studying arsenite (XIU *et al.*, 2018) and arsenate (Yang et al., 2021) adsorption on Fh. The stability of As-adsorbed Fh was related to As surface complexes and pH (closer to pH_{zpc}) inhibiting mineral dissolution. The influence of As (Bolanz et al., 2013; Das et al., 2014; Wang et al., 2015) and Al (LI, W. *et al.*, 2016; WANG, W. *et al.*, 2022) alone have been investigated. However, the combined effects of aging Al-for-Fe substituted Fh and exposure to environments containing As, in phase transformations, as well as in the remobilization of As to the environment, remain unknown. Furthermore, the detailed aging/recrystallization mechanisms that occur after the initial adsorption/co-precipitation of As and the role of Al in these processes remain to be understood The mechanism of As fixation in these bimetallic oxyhydroxides and its fate during the transformation of As-host phases is also to be explained. In this context, the main objective of this work is to comprehend the role of Al in phase transformation and As remobilization from Al-containing iron oxyhydroxides.

5.2 Materials and methods

5.2.1 Synthesis and characterization of Al-Free and Al-bearing ferrihydrites

The 2-line ferrihydrites (Fh), containing or not Al, were prepared and characterized as previously described in section 2.2. The results of characterization before aging or adsorption experiments is described in detail in should be consulted at section 2.3.1. Hereafter the samples will be called FhAl-X%, where X represents the molar Al contain target during synthesis.

5.2.2 Soil samples

The soil sampling was undertaken in June-July of 2014, Paracatu, northwest of

Minas Gerais state. The city hosts one of the largest open-pit gold mines of the world and the metal is found in association with arsenopyrite (FeAsS). The samples were collected in areas that represent the background of the region (i.e., with no evidence of anthropogenic activities) following the State Environmental Agency-FEAM protocol (FEAM, 2013), and in agreement with international practice (USEPA, 1992), as previously reported (Ciminelli et al, 2018). The surface soil samples (0-20 cm) were transferred to clean polypropylene bags, identified and stored at room temperature (~ 25 °C) until further processing. The bulk samples were oven-dried at 40 °C for 12 hours until they reached a constant weight, then disaggregated and subdivided, and sieved. The fraction < 2 mm was used (CONAMA, 2013; USEPA, 2007). The analyses were undertaken according to the procedure adopted by the State Program Solos de Minas following the State Environmental Agency-FEAM protocol (FEAM, 2013) , and in agreement with international practice (USEPA, 1992).

5.2.3 Arsenic sorption and aging experiments

An AlFh suspension, containing 50 mg of Fh, was added to As(V) solutions to reach a 100 mL suspension with final concentrations of about 3.4, 100 or 200 mg kg^{-1} of As(V), and 0.01 mol L^{-1} NaCl. The adsorption of As(V) was performed at pH 5 – that represents a near circumneutral and favorable condition for As uptake - and constant temperature of 25 °C, on a platform shaker (200 revolutions per minute-rpm) for 24 h. The pH values of the individual samples were adjusted during the experiments by adding 0.1 mol L^{-1} NaOH or 0.1 mol L^{-1} HNO_3. The amount of As(V) adsorbed by AlFh after 24 h is expressed as Γ (µmol m^{-2}) and is calculated as:

$$\Gamma = \frac{(C_0 - C_f) \times m_s}{m_{Fh}} (1)$$

where C_o and C_f are the As(V) initial and the final concentrations for each condition. The m_s is the mass of solution, the m_{Fh} the mass of adsorbent.

Ferrihydrites suspensions were placed in closed polyethylene bottles. The bottles were kept in a water bath, at 30 °C, for aging until 580 days. The samples FhAl-0% and FhAl-10% were also aged in the presence of 0.01 M of NaCl. Other group of suspensions, containing or not As, were put in covered polyethylene bottles and

submitted to 70 °C in a thermostatic bath for a period up to 90 days. The suspensions were collected periodically from the bottles and the solids separated by centrifugation (4000 rpm for 10 min). A fraction of the samples was submitted to arsenic sequential extraction experiments and the other was freeze dried for future characterizations. The supernatants were acidified by adding a droplet of 1 M HNO_3 and stored at 4 °C until analysis.

5.2.4 Arsenic sequential extraction tests

The sequential extraction protocol (SEP) followed the procedure developed by Pantuzzo and Ciminelli (2010) for the soil samples, and with minor modifications for synthetic samples. Differently from soil samples, which pass through the 7 steps (described in table C.1 in the appendix), the FhAl samples and their aging products were not submitted to the steps with water and solution with pH 5 extractions, since the solids were taken directly from the adsorption experiment, in water solution at pH 5, to the SEP. The residual fraction, which was observed only in the soil samples, not in the synthetic ones, was submitted to microwave digestion in a closed vessel. Arsenic, Fe, and Al were quantified in each step.

5.2.5 Characterization after adsorption or aging and quantification of arsenic in solution

The chemical composition of the Fh samples was analysed by ICP-OES (Perkin Palmer 7300). The solid samples were dissolved in 8% aqua regia to analyse As, Al and Fe. The arsenic was also quantified in the supernatants and liquors. The detection limit of the ICP-OES used is 1.3 µmol kg^{-1} for As, 3.5 µmol kg^{-1} for Fe and 7.5 µmol kg^{-1} for Al. The method's precision was guaranteed by an internal standard of Lu 0.6 µmol kg^{-1} (Ultra Scientific) with recoveries of 95-105%. For an improved accuracy of the measurements, calibration curves and standard solutions, with the same sample matrix, were used. For this purpose, it was used certified solutions of Al 10,000 µg mL^{-1} (Spex, 99.99%), Fe 10,000 µg mL^{-1} (Spex, 99.99%), and As 1,000 µg mL^{-1} (Spex, 99.99%). The coefficients of determination of the curves were, at least, 0.995 and the recoveries between 95 and 105%.

Powdered samples were submitted to X-ray diffraction by using a Philips (Panalytical

PW1710) X-ray diffractometer, with Cu (Kα) radiation, tube voltage of 35kV and current of 50 mA. Data was collected over the range of 10-90° 2θ, with scan step size of 0.020° s-1, and time collection of 2s at each step. The diffraction patterns were compared to the reference powder diffraction file (PDF), from Inorganic Crystal Structure Database- FIZ Karlsruhe (ICSD), of 2-3 nm ferrihydrites, $Fe_5O_8H.4H_2O$ (ICSD-158477), proposed by Michel (MICHEL; EHM; ANTAO; *et al.*, 2007), goethite, α-FeO(OH) (ICSD-9002158), hematite, Fe_2O_3 (ICSD-40152), lepidocrocite, γ-FeO(OH) (ICSD-93948), and ferroxyte, δ–FeO(OH) (ICSD-291515).

Raman spectra were obtained with a LabRam-HR 800 (Horiba/Jobin Yvon) spectrograph equipped with an Olympus BX-41 microscope provided with lenses of 10, 50 and 100X, and helium laser of 632.8 nm. The optimum scanning method was found to be with laser power less than 0.04 mW, and, at least, 10 spectrum collections of 60 s each.

The chemical composition was also analyzed by TEM coupled with energy x-ray dispersive spectroscopy (EDS) at least in five points each sample. - The samples were also analyzed by high resolution TEM (HRTEM) and selected area - electron diffraction (SAD) using a LaB6-TEM Tecnai G2 20 SuperTWIN (FEI), operated at 200 kV, coupled with a Gatan Image Filter (GIF Quantum SE system). The SAD patterns were acquired by using elastic scattering only by filtering the zero-loss peak with 10 eV slit. For minimizing error all the SAD patterns were collected at the same day under the same microscope conditions (lenses strengths, apertures, camera length). For this purpose, each AlFh-X suspension was pipetted on a copper grid covered with an ultrathin (3-5 nm thick) carbon film (Cu-Lacey carbon, 400mesh, Ted-Pella). The grids were placed on Whatman® filter papers to remove excess water and allowed to dry at room temperature. The images were processed by the Software Digital Micrograph version 2.32. The SAD patterns were converted to rotational averages profiles and the peaks were calculated by the THF Peak Locator tool inside the package Difftools (MITCHELL, 2008). The parameters were hat width of 10, brim width of 10, and threshold of 0.01.

5.3 Results and discussion

5.3.1 The effect of Al on the Fh aging process and phase transformation

As described in section 2.3.1, there is no substantial difference in particle size and apparent surface area (ASA_{BET}) among the synthetized Fh, except for the ASA_{BET} of sample FhAl-25%. This finding was related to a possible segregation of Al oxyhydroxides and confirmed after 130 days of aging. The previous results also show the Al-for-Fe isomorphic substitution of the synthetized Fh for all the other samples.

The onset of FhAl-0% phase transformation was observed after 30 days of aging at 30 °C (Figure 5.1). The lower magnification TEM images (Figure 5.1-a and b) show the predominance of ferrihydrites particles and regions of greater contrast associated with different crystallographic orientations. The HRTEM of the areas inside de yellow circles, in combination with the fast Fourier transformed (FFT), showed the interplanar distances associated with the presence of hematite ($d_{10\text{-}2}$ = 3.61 Å) and goethite (d_{011} = 2.54 Å). No piece of phase transformation was observed for the other FhAl samples, showing that the Al presence affect the kinetics of the phase transformation.

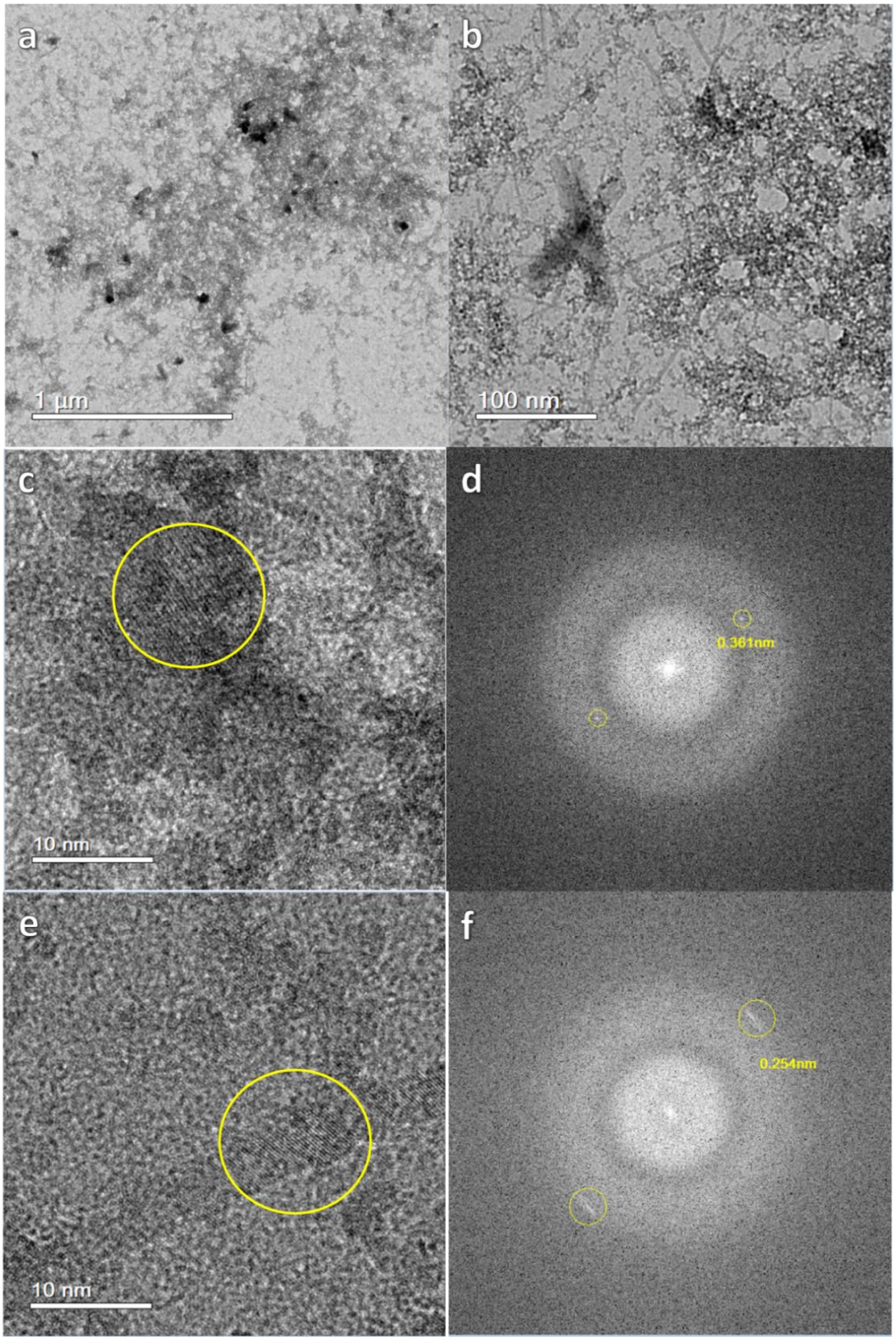

Figure 5.1: TEM from FhAl-0% sample aged for 30 days. Lower magnification images showing the majority of ferrihydrites (a), and goethite acicular crystals (b), HRTEM of hematite crystals in formation(c), goethite crystal (e), and its FFT showing the interplanar distances (d and f, respectively).

The increase in time for FhAl phase transformation is clearly demonstrated by the XRD of Fh suspensions, kept at 30 °C for 580 days (Figure 5.2). Even after the long time elapsed beyond FhAl-0% started phase transformation (30 days), no sign of hematite or goethite is observed in samples containing 15% mol Al (or more). The XRD of sample FhAl-25% has a peak associated with the presence of gibbsite due to the Al-oxyhydroxide segregation, as described before. Figure 5.2-a also shows that the Al in Fh fully restrains goethite formation. In the absence of Al, goethite appears as the main product of Fh phase transformation. In contrast, no indication for goethite is found in the samples containing Al, regardless the Al content.

NaCl is considered an indifferent electrolyte - a monovalent ion with low attachment to an adsorbent surface - commonly used in adsorption studies to maintain ionic strength during the experiments. As this work aims to investigate the phase transformation after As(V) adsorption, the influence of NaCl in the phase transformation was also evaluated. The diffraction patterns of the samples aged at 30 °C for 580 days (Figure 5.2-b) show that the NaCl presence did not inhibited phase transformation. However, the ratio between the peaks intensities at 33 and 35.5 2-theta degree of sample FhAl-10%, associated with the planes (104) (110), respectively, has changed in the presence of NaCl. This indicates that NaCl induces preferred planes of growth. Comparing the XRD of the sample FhAl-0% with and without NaCl is possible to notice changes in the ratio between the peaks intensities, indicating again preferred planes of growth, or even that NaCl favors the formation of hematite, due to the decrease of the intensity of the peaks related to goethite and the increase of the ones associated with hematite.

Figure 5.3 shows the Raman spectra of Fh samples before and after 150 days of aging. The 2-line Fh is characterized by the lines at Raman shift ~350, 510 and 710 cm^{-1}(MAZZETTI; THISTLETHWAITE, 2002), as shown in Figure 5.3-a. After 150 days, the Raman spectrum of FhAl-0% (Figure 5.3-b) indicates that Fh transforms into a mixture of goethite and hematite, once the most intense line is a combination of a goethite line at 387 cm^{-1}, and hematite line at 410 cm^{-1}. The goethite formation is completely prevented in the sample FhAl-5% after 150 days, as expected by the previous XRD patterns after longer ageing time (Figure 5.2). TEM images and SAD of samples with 10% mol Al aged for 130 days corroborate the formation of hematite

(Figure 5.4-a and Figure C.1, respectively), It was not possible to identify the acicular and twinned shapes, associated with goethite in FhAl-10%-130d sample. Goethite was observed in the Al-free samples after 30 (Figure 5.1-b) and 130 days (Figure C.1 e C.2). The hematite find in the FhAl-10% TEM images are the high contrast agglomerated particles.

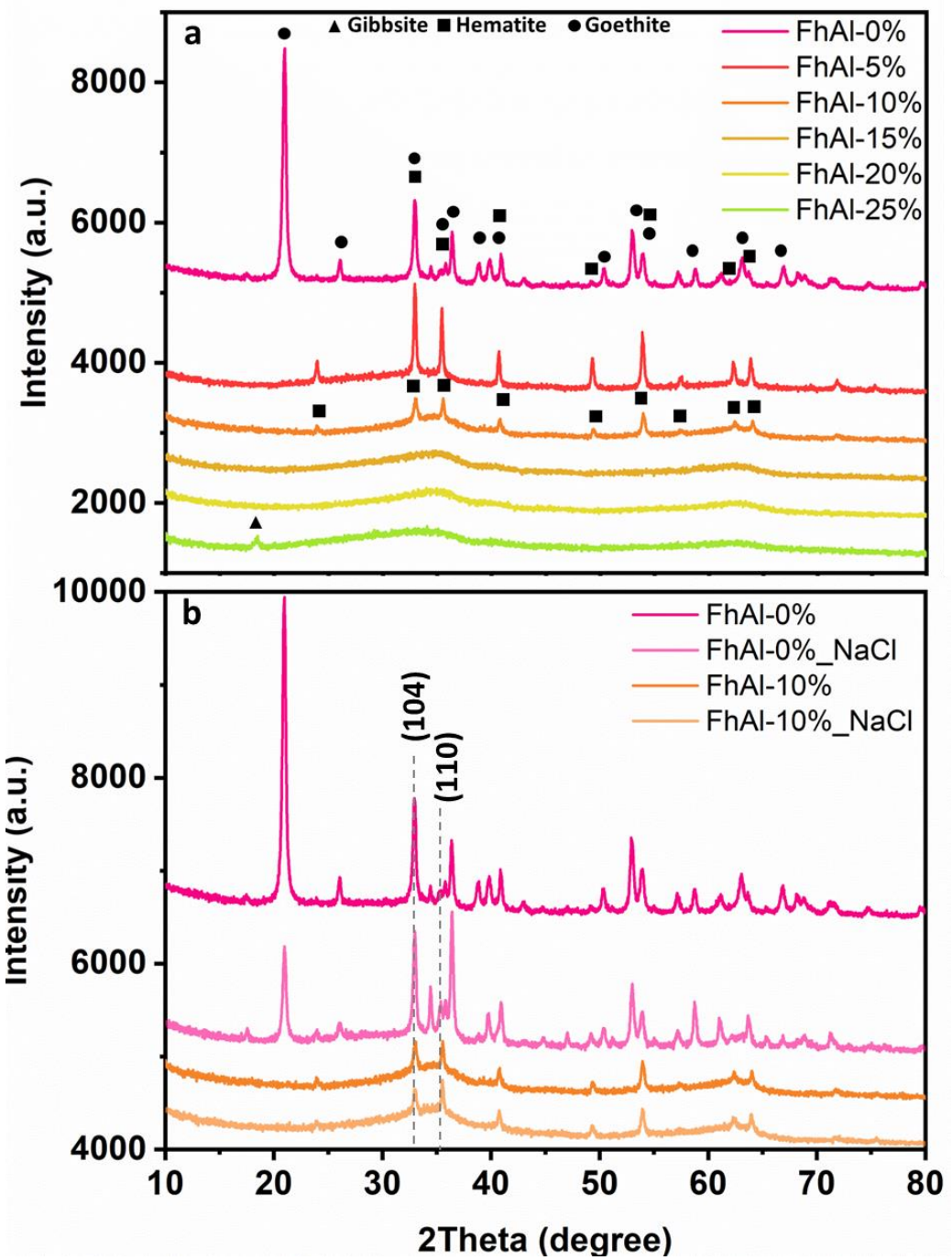

Figure 5.2: XRD of Fh aged during 580 days at 30 °C of samples FhAl (a) and the comparison between the FhAl-0% and FhAl-10% with and without NaCl 0.01 mol L^{-1}.

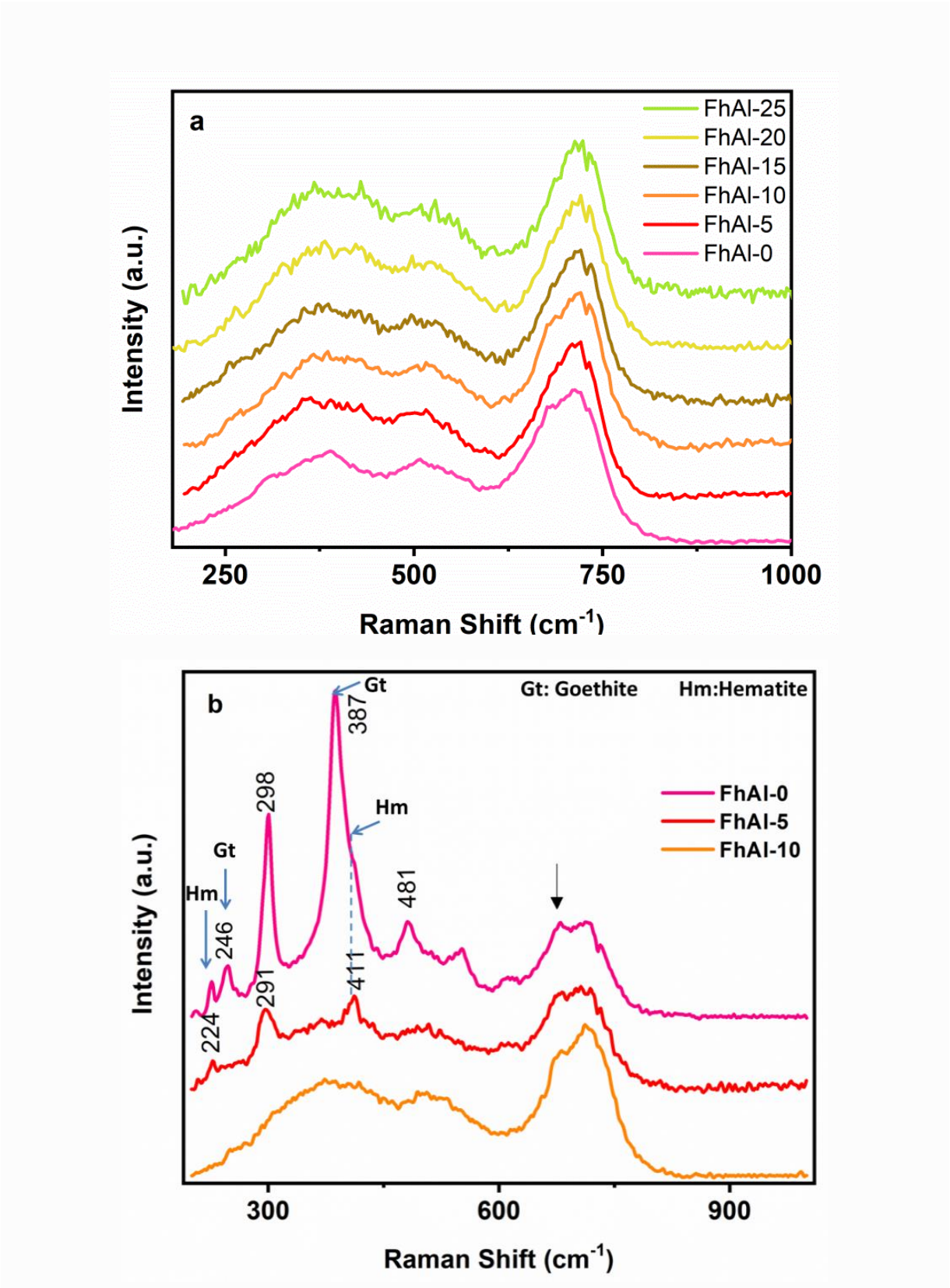

Figure 5.3: Raman spectra of Fh samples before (a) and after 150 days of aging at 30 °C (b).

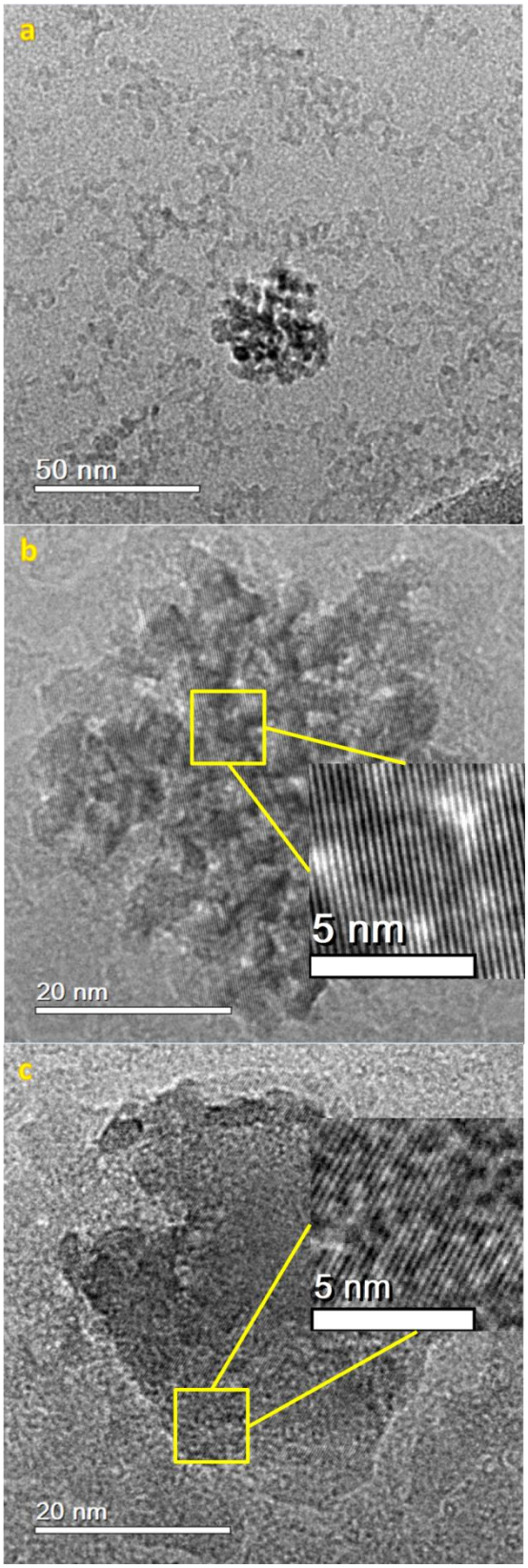

Figure 5.4: TEM image (a) and HRTEM of the sample FhAl-10% aged for 130 days at 30 °C showing the hematite mesocrystal (b). HRTEM of the sample FhAl-0% aged for 130 days at 30 °C showing relatively euhedral hematite crystal (c).

The formation of goethites from Fh in aqueous phase, is known to involve Fh dissolution and recrystallization, while hematite is formed through reshuffle within the Fh aggregates and internal dehydroxylation (FISCHER; SCHWERTMANN, 1975; KHALIL *et al.*, 2014; SCHWERTMANN, UDO; FRIEDL; STANJEK, 1999). Therefore, the inhibition of goethite formation is possibly related to the low availability of ferric ions in solution. In the case of the experiments described here, this low concentration may be associated with the decreased solubility of Fh containing Al or the solution pH. The Al-for-Fe substitution on Fh has been demonstrated to reduce the solubility of Fh. The suppression of goethites formation by aged Al-containing Fh is also reported by Schwertmann et al. (2000). The authors attribute this behaviour to the decrease in the solubility of Al-containing Fh and, consequently, its higher stability, also reported by (EKSTROM *et al.*, 2010; HANSEL *et al.*, 2011; MASUE-SLOWEY; LOEPPERT; FENDORF, 2011) in aging or reductive experiments.

The pH variation in during aging of FhAl samples at 70 °C, exposed or not to As(V) are shown in Figure 4.5. The initial pH was set at 5.3 ± 0.2. At the end of the experiment, all pH values decreased. However, for the Fh-Al samples pH dropped less and proportionally to the Al content (e.g., pH 5.3 to 4.7, 3.8 and 2.4 for the samples FhAl-0%, FhAl-10%, and FhAl-20%, respectively). As the iron oxyhydroxides solubility decreases with increasing pH up to circumneutral conditions, the relatively higher pH of Al-containing Fh will reduce the ferric ions availability for goethite formation, which can justify the inhibition of goethite after Fh-Al aging.

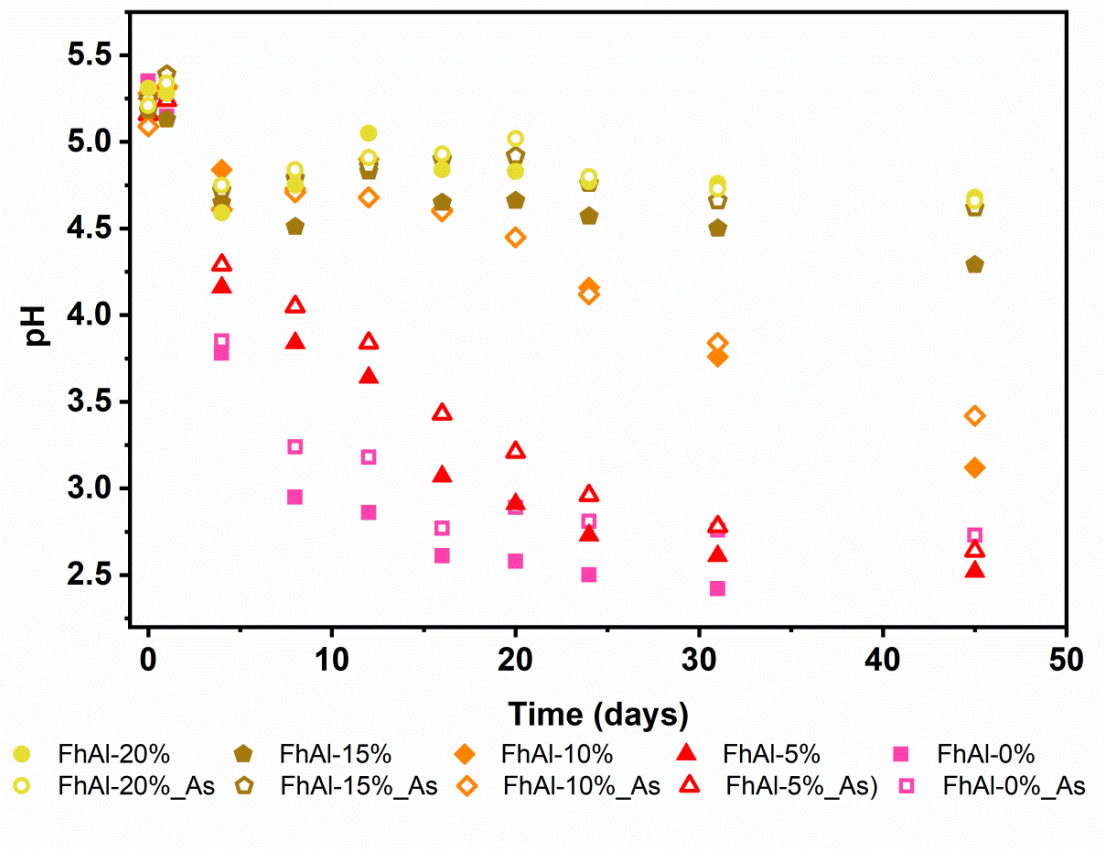

Figure 5.5: Variation of pH of FhAl suspensions with the time of aging at 70 °C and $[As]_0$ = 100 mg kg^{-1}.

5.3.2 The effect of Al on the mechanism involved in Fh phase transformation, and reactivity

After a fast primary nucleation of the particles, the growth mechanisms are mainly, or some variation of, the classic model known as Ostwald Ripening (OR) and the more recently, described by the aggregation of crystallography aligned nanoparticles, Oriented Attachment (OA). The former is largely used to explain the formation of complex nanostructures, such as hollows, MOF, or flower-like shapes (CHAI *et al.*, 2022; CHUN ZENG, 2007; LIU, YUAN *et al.*, 2019; LOU; ARCHER; YANG, 2008). In the OR mechanism, the smaller particles solubilizes and the monomers deposit over the bigger particles. It is a mechanism driven by the reduction of the chemical potential of a particle by its increase in size (MCMAHON *et al.*, 2009; PENN, 2004). On the other hand, the OA mechanism is a special case of aggregation, where nanocrystals with common crystallographic orientation attached to each other, drive the formation of mesocrystals, monocristals, twins, and intergrowths (CHEN, J. S. *et al.*, 2011; DE YOREO *et al.*, 2015; PENN, 2004). The mesocrystals are

superstructures formed by crystallography aligned nanoparticles (NIEDERBERGER; CÖLFEN, 2006). Molecules adsorbed onto the mesocrystals surface may stabilized or merge the structures into a monocrystal (DE YOREO *et al.*, 2015). Even when OA dominates the crystallization process, the concomitant occurrence of Ostwald ripening mechanism should be considered (DE YOREO *et al.*, 2015). According to Jia and Gao (2008), the formation of crystals with well-defined edges and faces and less internal defects, may be interpreted as a result of OR main growth process. These features are observed in sample FhAl-0% (Figure 5.4-c).

The contribution of each mechanism will change with the increase of the particle size (FAIVRE, 2016), the OR being favored for the smaller particle sizes . It happens because the solubility of small particles is higher than that of larger particles (PENN, 2004). As the Al-substitution decreases Fh solubility, one may expect it will favor the OA relatively to the OR mechanism, explaining the mesocrystals found in sample FhAl-0% (Figure 5.4-b).

The temperature of the experiment will also affect the mechanism of crystal growth. Soltis and coworkers (2016) found that the consumption of primary particles of 2-line Fh in an oxalate medium increases with temperature. Therefore, the increase in temperature may favor the OR mechanism. Differently from several works (KHALIL *et al.*, 2014; LI, W. *et al.*, 2016; SOLTIS *et al.*, 2016; WANG, W. *et al.*, 2022), which use increased temperature to accelerate the experiments, the results presented in Figure 5.4 and the Figure 5.6 were obtained at almost environmental temperature (30 °C), being so, more representative of the environmental phenomena. In fact, Al-hematites and FhAl mesocrystals were identified in oxisol samples from Morro do Ouro mine in Paracatu, northwestern Minas Gerais state, Brazil (FREITAS *et al.*, 2015).

The HRTEM images (Figure 5.4-a and b) and SAD (Figure C.1-d) of sample FhAl-10% demonstrate that the high contrast agglomerated particles are hematite mesocrystals formed by the oriented attachment of Fh nanoparticles. Conversely, in the FhAl-0% HRTEM (Figure 5.4-c), no individual oriented particle is observed, suggesting a growing mechanism mainly by Oswald Ripening mechanism. Therefore, the presence of Al in Fh was shown to increase the time for phase transformation, affect the products of this transformation (e.g., retaining goethite formation in favor of hematite), and the mechanism involved (e.g., OA preferentially to OR), which finally

leads to the oriented aggregates of hematite nanoparticles.

The phase transformation of Fh into hematite, in aqueous media, occurs by internal rearrangement and dehydration within the ferrihydrite aggregates (SCHWERTMANN, U; MURAD, 1983). Therefore, OH and H_2O at the Fh surface may affect the particle aggregation and Fh-into-hematite transformation. In our previous work, the Al-for-Fe substitution was demonstrated to increase surface OH (SOUZA *et al.*, 2021), then the retarded Fh transformation of the samples containing Al may be related to the increased surface OH of these samples.

Figure 5.6 shows the Fh particles containing Al after 430 days of aging.

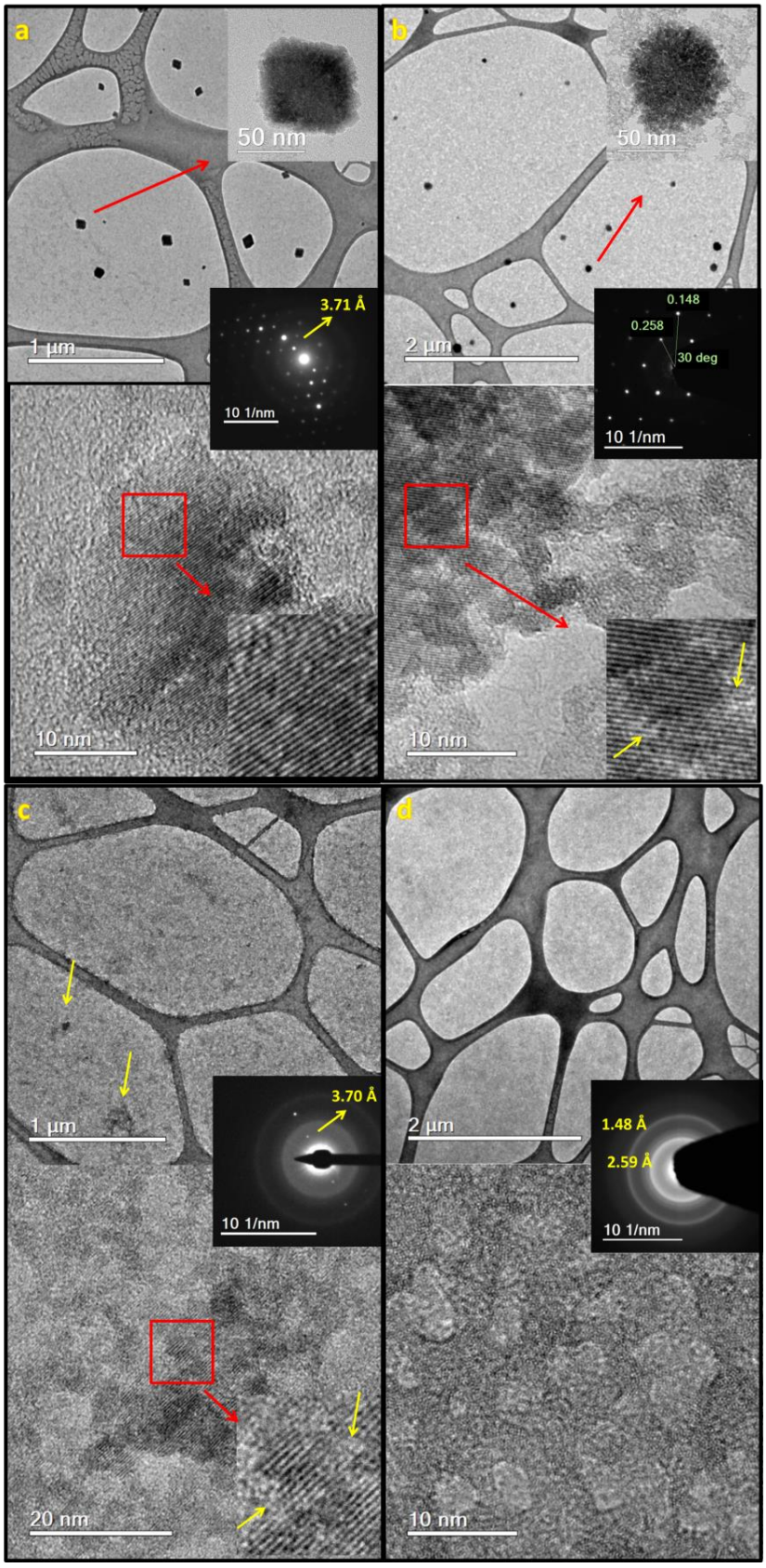

Figure 5.6: Low magnification, high-resolution TEM images and the SAD patterns from the samples FhAl-5% (a), FhAl-10% (b), FhAl-15% (c), and FhAl-20% (d) after 430 days of aging.

In this figure, the effect of Al on retarding Fh-into-hematite transformation is also clear. The low magnification images of the samples FhAl-5% and FhAl-10% (Figure 5.6-a and b) show several high-contrast particles and their SAD patterns (inset) confirm they are hematite. The sample FhAl-15% (Figure 5.6-c) shows very incipient hematite particles in the high-contrast aggregates. The sample FhAl-20% show no evidence of phase transformation (Figure 5.6-d), even after 430 days, since there is no different contrast in the image and the lattices fringe show a very low range of organization. The SAD confirms the presence of Fh only. The low magnification images from the samples FhAl-5%, FhAl-10%, and its insets (Figure 5.6- a and b), also clearly show the change in particle shape, according to the Al content. The FhAl-5% show a rhombohedral shape, whereas FhAl-10% are disc-like particles. These conclusions are also supported by the XDR patterns of the FhAl samples after 570 days of aging (Figure 5.2). The peak intensity ratios of the (104) and (110) planes for samples FhAl-5% and FhAl-10% indicate the platter format of the latter (LI, W. *et al.*, 2016).

The rhombohedral hematite particles have exposed eight equivalent {012} facets, while the plate hematite particles were composed of two symmetric {001} facets on the basal surfaces and six equivalent {102} facets on the side surfaces (WANG, W. *et al.*, 2022). Each facet of an iron-oxyhydroxide will present different quantities of OH, as well as the type of coordination between the OH and the Fe (i.e., numbers of –FeOH, $–Fe_2OH$, and $–Fe_3OH$ sites per nm^2) (BARRÓN; TORRENT, 1996). Ferrihydrites, without Al substitution, have a surface dominated by singly-coordinated surface groups (6.0 ± 0.5 nm^2) (HIEMSTRA; VAN RIEMSDIJK, 2009). The type of OH coordination and the quantity of OH on the Fh surface will affect the surface reactivity, consequently, the crystal growth. Therefore, the influence of the Al-content in Fh on hematite's particle shape may be ascribed to a preferential increase in the surface OH in some facets and the type of OH coordination that Al introduction drives in the facets. One can also infer that Al introduction will affect reactivity (i.e., the capacity of adsorption and retention of contaminants) of Fh and the resulting hematite produced by aging.

5.3.3 The effect of As(V) on the aging process and phase transformation

The ferrihydrites were submitted to an adsorption experiment under $[As]_0$ = 200 mg

kg^{-1}, 0.01 M of NaCl, and pH 5.3 ± 0.2. After adsorption, the suspensions were submitted to a long-term aging at 30 °C. The presence of As(V) was shown to strongly affect the time necessary for the phase transformation of Fh. For the Al-free samples, goethite and hematite can be observed after 30 days of aging (Figure 5.1). When Fh is aged in a solution with an initial concentration of 200 mg kg^{-1} As(V) no phase transformation was identified along 570 days. Figure 5.7 shows just the Fh (a), with low ordering structure (b), corroborated by its SAD pattern (c) corresponding to Fh one, without any evidence of hematite or goethite formation (30 and 210 days aging TEM images are available in the appendix, Figure C.3). The As(V) adsorption on Fh was shown to occur by binuclear bidentate complexation (ADRA *et al.*, 2016; WAYCHUNAS, G. A. *et al.*, 1993; WAYCHUNAS, GLENN A.; DAVIS; FULLER, 1995). These arsenate complexes may inhibit dehydroxylation, which favours the phase transformation by charge imbalance and structural disorders (Wang et al., 2015; Zhao et al., 1994). According to Wang et al. (2015), the transformation process may request higher temperatures in the presence of As due to the formation of Fe-O-As surface coverage.

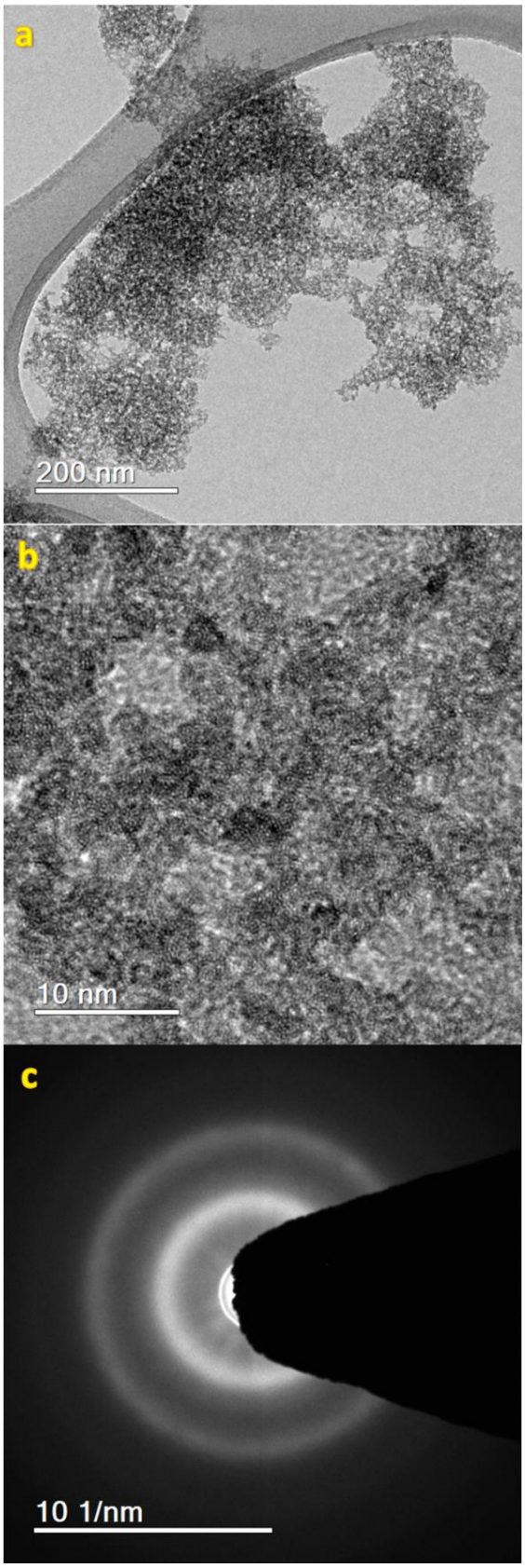

Figure 5.7: TEM (a) and HRTEM (b) images of FhAl-0% aged for 570 days, at 30 °C and $[As]_0$ = 200 mg kg^{-1}, and the SAD pattern (c) showing Fh.

To accelerate phase transformations, a set of adsorption experiments (initial As(V) concentrations, $[As]_0$, of 3.4, 100, and 200 mg kg^{-1} followed by aging at 70 °C (initial pH of 5.3 ± 0.2 and constant ionic strength 0.01 mol L^{-1} NaCl) was performed. The samples are named accordingly: FhAl-0%-0/70, FhAl-0%-3/70, FhAl-5%-3/70, FhAl-10%-3/70. The TEM images of samples with no exposure to As and after As adsorption (3.4 mg $kg^{-1}[As]_0$), and 9, and 14 days of aging are shown in Figure 5.8.

At the lowest level (3.4 mg $kg^{-1}[As]_0$), there was no As effect on the particle's features and the mechanism of particle growth. In the Al-free Fh samples one can observe the hexagonal, rhombohedral, and needle-like particle formats typical of hematite and goethite, regardless the absence (Figure 5.8-a) and presence (Figure 5.8-c) of As. These formats were also observed in the samples aged at room temperature (Al and As Free Fh). The crystals show well-defined edges without mesocrystals. By increasing the Al-content in the presence of As, again, no change in the particle's shape was observed for samples FhAl-5%-3/70 and FhAl-10%-3/70 (Figure 5.8-c and d, respectively) when compared to the same particles aged wihout As (FhAl-5%-Figure 5.6-a and FhAl-10%-Figure 5.6-b).

As arsenic concentration increases ($[As]_0$ = 100 mg kg^{-1}), goethite was still formed after 20 days (FhAl-0%-100/70), compared to 4 days aging for the FhAl-0%-3/70 sample (Figure C.4). Only the samples exposed to $[As]_0$ = 200 mg kg^{-1} did not show signals of phase transformation along the 90 days of experiments. The presence of As does not impact the mechanism of phase transformation and particle growth as Al. Bolanz and coworkers (2013), who aged Al-free Fh at pH 7, 70 °C, under different $[As]_0$. The authors found that phase transformation to a mixture of goethite, hematite, and ferrihydrite was unchanged by increasing $[As]_0$. In summary, though As increases the onset time to phase transformation, but the mechanism of transformation is mostly dictated by the Al-substitution.

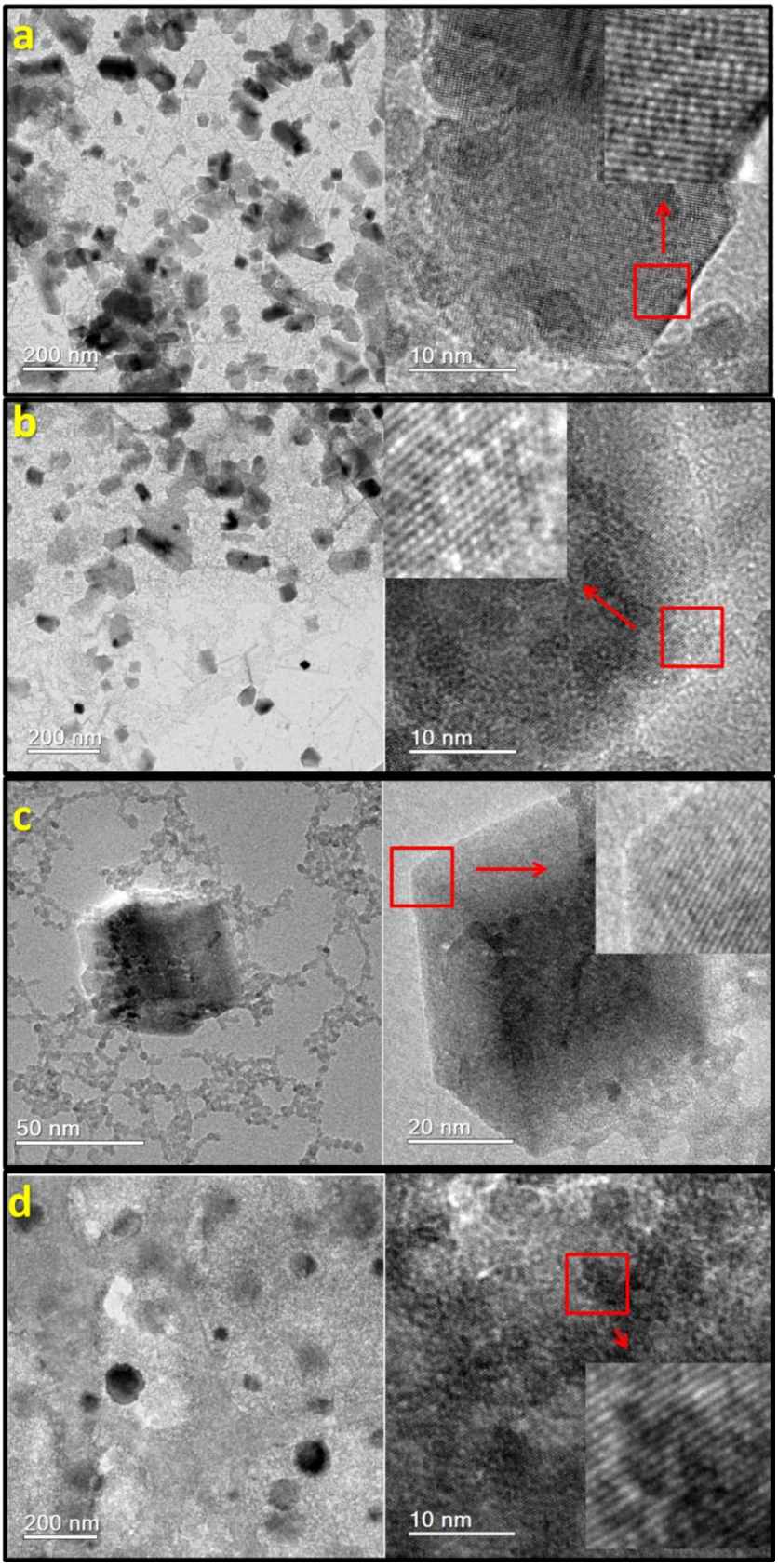

Figure 5.8: TEM and HRTEM images from the samples aged for 9 days, at 70 °C, without As FhAl-0% (a) and containing $[As]_0$ = 3.4 mg kg^{-1} FhAl-0% (b), and FhAl-5% (c). FhAl-10% (d) aged for 14 days, at 70 °C, containing $[As]_0$ = 3.4 mg kg^{-1}.

5.3.4 The effect Al-containing on As remobilization before and following aging

During the aging experiments in the presence of As, the supernatants of the samples were collected and tested for the presence of As, Fe, and Al. The As concentration dropped from 3.4 mg kg^{-1} to below 0.005 mg kg^{-1} and from $[As]_0$ = 100 mg kg^{-1} to 0.05 mg kg^{-1} (Figure 5.9). The results also indicate a stabilization of As concentration in the supernatants. Contrary to what was expected, the phase transformation did not imply in As liberation to the suspension. Thus, the As was likely incorporated into the new iron oxyhydroxide phases.

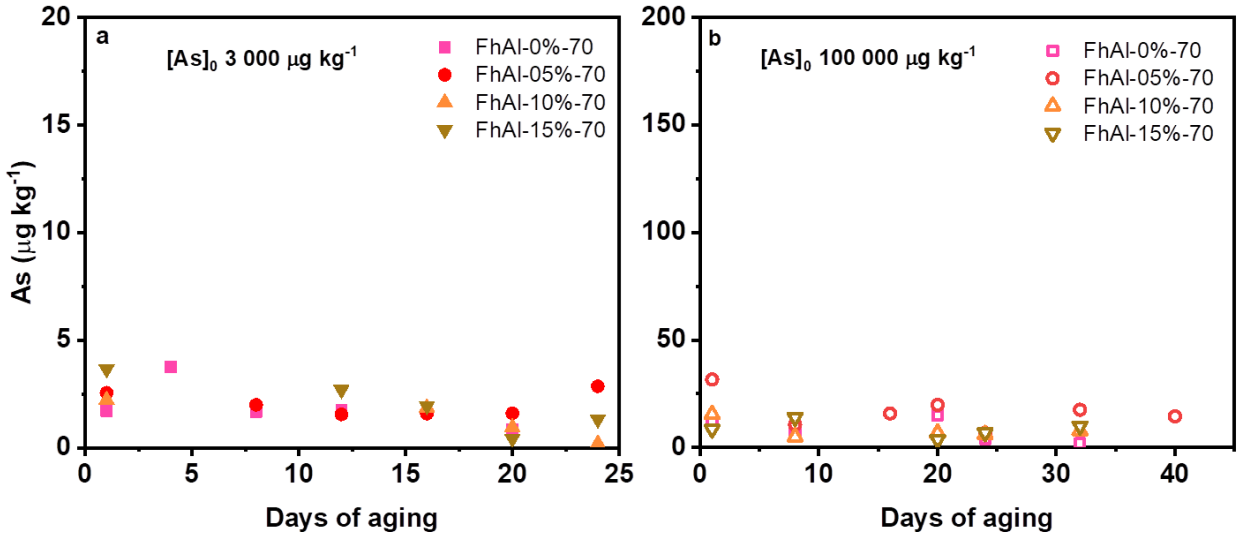

Figure 5.9: Arsenic present in the supernatant during Fh aging, at 70 °C.

A protocol for sequential extractions (SEP) of As (Pantuzzo and Ciminelli, 2010) was applied to the Fh just after adsorption and after approximately 30% of phase transformation. This protocol helps to understand the potential mobility of As, as well as the nature and strength of As binding to the FhAl and its aging products. Figure 5.10 shows the As and Fe partitioning in the FhAl samples after adsorption at 25 °C, $[As]_0$ of 3 or 100 mg kg^{-1}, pH 5.3 ± 0.2, and 0.01 mol L^{-1} NaCl. No As is released at the first step of SEP, which would remove the readily soluble As. There was also no As or Fe associated with the crystalline iron oxide and hydroxide phases, once the aging process did not start. The As was distributed between As-strongly adsorbed and associated with Fh. The SEP step to remove strongly adsorbed As is quite selective as iron was released only during Fh solubilization. The samples from adsorption with $[As]_0$ = 100 mg kg^{-1} (FhAl-x%-100) has less As associated with Fh

than samples with $[As]_0$ = 3 mg kg^{-1} (FhAl-x%-3). Between 30 to 60% of arsenate is released with Fh solubilization prior to ageing. The decrease in the As associated with Fh solubilization, from the samples with $[As]_0$ = 100 mg kg^{-1}, suggests a mass (or time) limitation of As incorporation by Fh.

Figure 5.10 also shows the effect of Al in the As mobility in fresh Fh samples (not aged). The increase in the Al-content in Fh increases the strongly adsorbed fraction relatively to the As associated with the iron oxyhydroxide. These results support the findings reported in section 2.2.5, that is the increase in the Al in the FhAl increases As uptake, but reduces the Langmuir constant (K_L), indicating a weakening of the As-FhAl interaction.

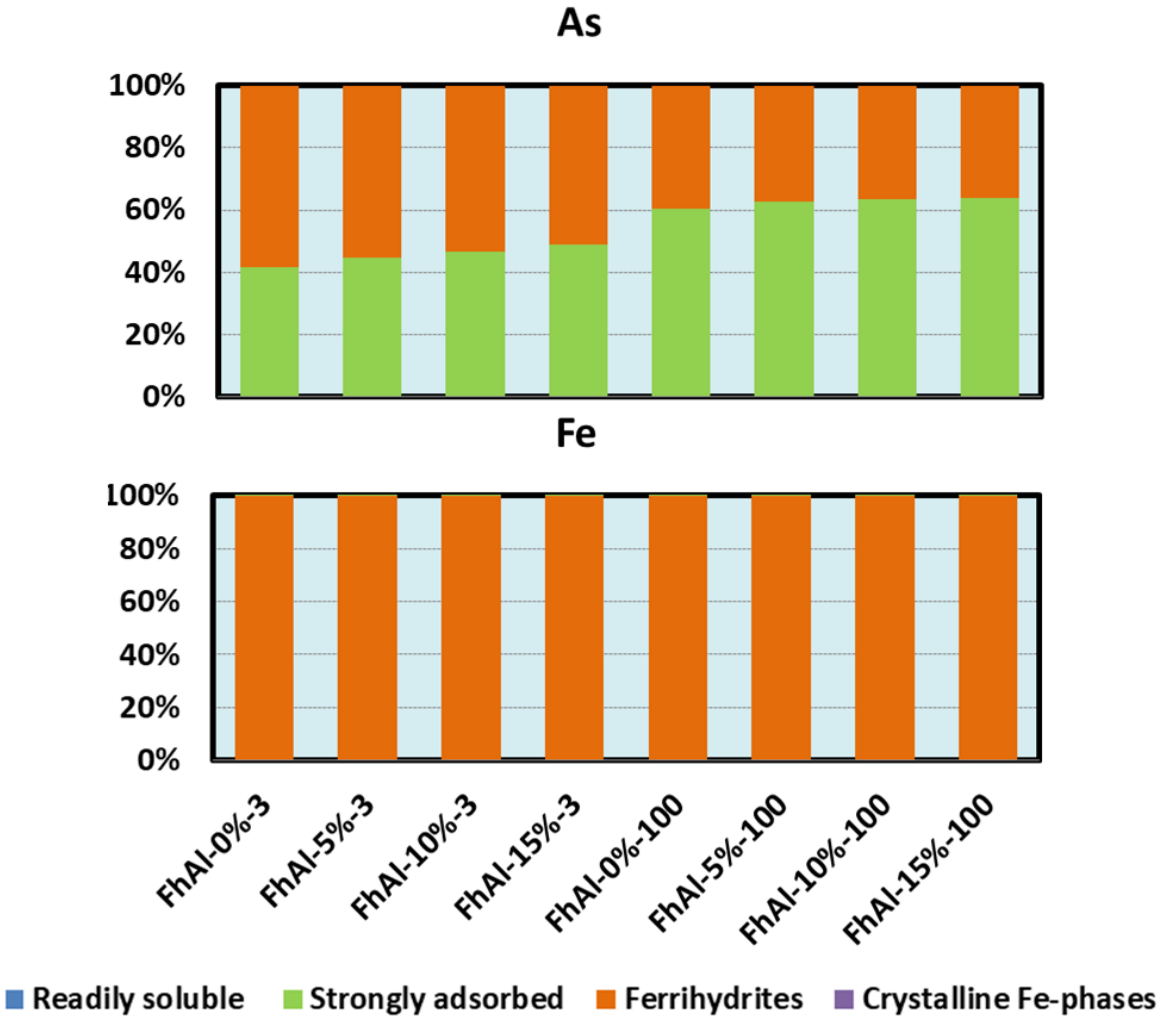

Figure 5.10: Arsenic and iron partitioning in the FhAl samples after adsorption ($[As]_0$ equals to 3 or 100 mg kg^{-1}), before aging.

After 4 and 8 days of aging, the sample FhAl-0%-3 ($[As]_0$ = 3 mg kg^{-1}) was submitted to SEP (Figure 5.11). The Fe partitioning clearly shows Fh phase transformations along the time, by the reduction of Fe associated with Fh. Figure 5.11 shows that aging, and consequently phase transformation, drastically reduces the As mobility. After 4 days of aging, more than 80% of As is just released by the solubilization of Fh and other more crystalline phases. This is a clear indication of As incorporation by the crystalline iron oxide and hydroxides phases, and its consequent immobilization, as shown by the decreasing liberation of soluble As during aging experiments (Figure 5.9).

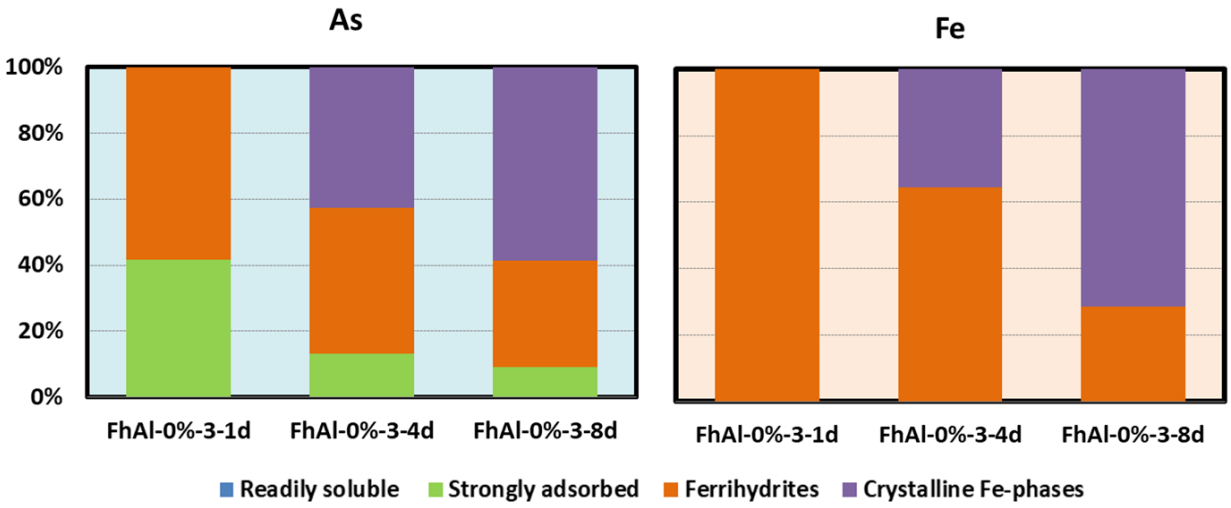

Figure 5.11: Arsenic and iron partitioning in Al-free ferrihydrite (FhAl-0%) before (1d) and after aging during 4 (4d) and 8 (8d) days, at 70 °C ($[As]_0$ = 3 mg kg^{-1} in the sorption experiments).

To evaluate the influence of Al in the immobilization of As, the SEP was also applied to samples aged during different times, but with similar Fh content before phase transformation (approximately 70% m/m). Before the SEP, the samples FhAl-0%-3, FhAl-5%-3, and FhAl-10%-3, were aged for 4, 8 and 16 days, respectively, (Figure 5.12). The phase distribution was estimated by Rietveld refinement and the results are in appendix C (table C.2). The iron partitioning shows that the Fh containing was similar, but slightly higher for samples with Al, indicating that more aging would be necessary for a perfect comparison. The As distribution shows that, differently from what was observed for samples without aging, the Al does not promote As mobility. In fact, the increase in Al-content reduces the strongly adsorbed As relatively to the As associated with the iron oxyhydroxides, promoting an even higher As fixation.

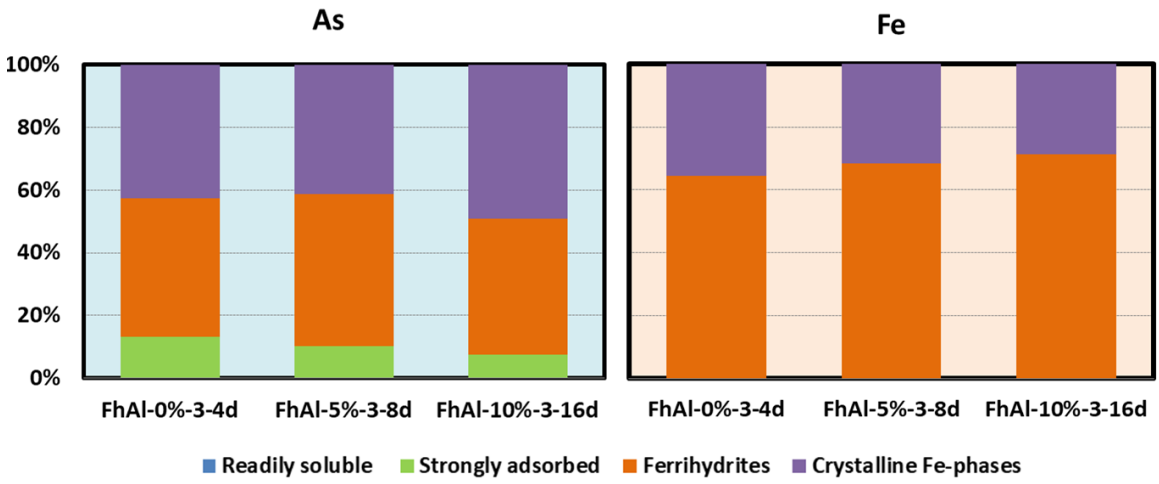

Figure 5.12: Arsenic and iron partitioning in the samples aged at 70 °C, $[As]_0$ = 3 mg kg^{-1}, during 4 days (FhAl-0%), 8 days (FhAl-5%), and 16 days (FhAl-10%).

5.3.5 Environmental implications

Six soils samples, containing iron oxyhydroxides with different Al content, were investigated by SEP. The samples were selected from a region with natural As anomaly. The As content was found to be 4304, 575, 841, 443, 324, and 405 mg kg^{-1} for samples K23, K22, K21, K40, K48, and K06, respectively. These values are significantly higher than the national guidelines (agricultural, 35 mg kg^{-1} and residential, 55 mg kg^{-1}). The detailed soil sampling and characterization are found elsewhere (ANTÔNIO, DAPHNE C. *et al.*, 2021; CIMINELLI *et al.*, 2018) and the mineralogical characterization is summarized in the appendix C (table C.3). The MLA characterization segregate the iron oxides and hydroxides phases by containing or not As. Aluminum was found just in the iron phases containing As, possible indicating a preference of As by Al-containing phases. The Figure 5.13-a shows As partitioning in the soil samples. Most of the As (73-93%) was associated with the Fe-crystalline phases, indicating low mobility of As in this soil, despite the higher content. Less than 10% As was classified as strongly adsorbed by the exchange reaction with phosphate solutions. And 4-18% As is associated with the less crystalline Fe (Al) oxyhydroxides. Approximately 95% As is associated with iron oxyhydroxides These findings corroborate those reported by Antônio and coworkers (2021), showing the low arsenic bioaccessibility, which indicates low potential risk to human health and the environment.

The table 3-3 shows the As containing in hematite crystals found in oxisol samples,

by EDS analysis. The increase in Al clearly increases the As association to the hematite (crystalline phases) and therefore As fixation. These findings indicate that the Al- substitution in ferrihydrites promotes the formation of mesocrystals by a mechanism of oriented aggregation, which entraps As within the crystal structures and then, reduces As mobility and bioacessibility. This mechanism, previously suggested from microscopy observation of mesocrystals in soils rich in As (FREITAS *et al.*, 2015), is now fully demonstrated by our results.

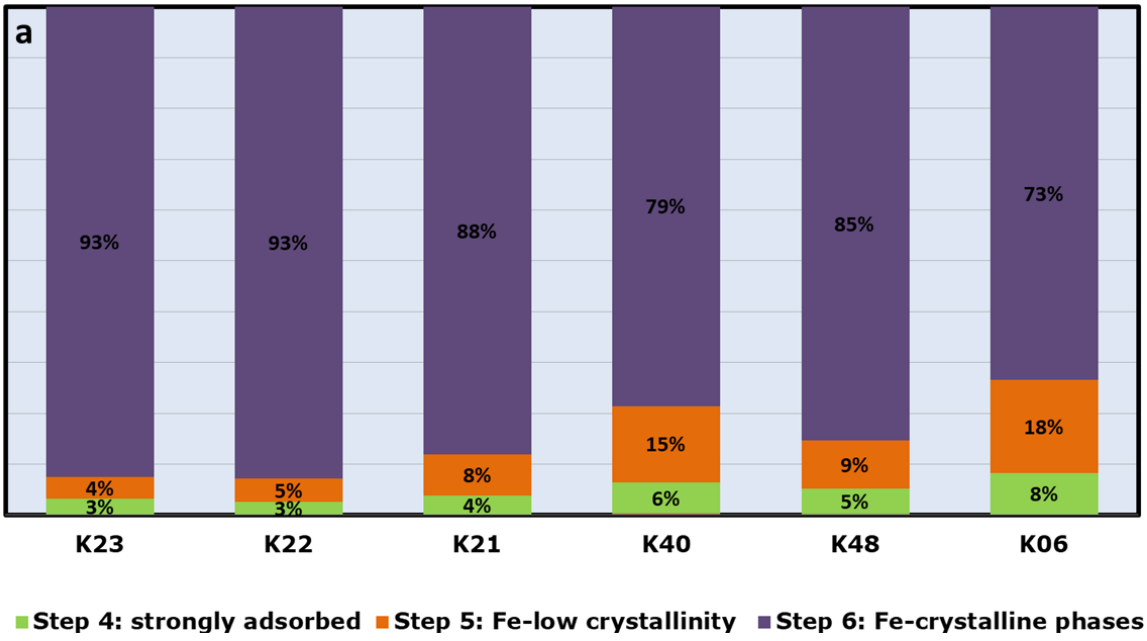

Figure 5.13: Arsenic partitioning in the soil samples.

5.4 Conclusion

In this work, the Al influence on As mobility from Al-containing iron oxyhydroxides, throughout its aging, was investigated. The Al-free Fh starts phase transformation after 30 days of aging at 30 °C. The Al-substitution delayed phase transformation and along 580 days the Fh samples containing 15, 20, and 25% mol Al remain unchanged. The Al introduction also inhibits the goethite formation and modify the mechanism of particle growth from predominantly Ostwald Ripening to Oriented Attachment. This is highlighted by the modification of the particles shape (from hexagonal and rhombohedral to disk shape) and the presence of mesocrystals in Fh with at least 10% mol Al. The formation of hematite's mesocrystals is favored by the

reduction of Fh solubility and increase in surface OH, both ascribed to the presence of Al. The As adsorption on Fh increases the time needed for phase transformation, but not the growth mechanism, once the particles formed kept the same characteristics of the As-free samples.

The sequential extraction protocol was used to determine the As partitioning in mobile, strongly adsorbed or associated with less or more crystalline iron oxyhydroxides. The Al-substitution was found to increase As mobility from fresh Fh. Conversely, the Al was found to promote As immobilization after Fh aging and phase transformation. Similar results were found in soil samples, in which the As associated with crystalline iron oxides increases with the Al content in these phases. It is suggested that the Al substitution induces the formation of Al-Fe-mesocrystals which entraps As inside its structures, reducing the As mobility.

A better understanding of As immobilization by Al-substituted iron oxides and hydroxides can contribute to a better management of arsenic residues.

6. FINAL CONSIDERATIONS

The use of ferrihydrites (Fh) in the removal of two contaminants with great harmful potential was studied in depth in this work. Arsenic and amoxicillin (AMX) were adsorbed on Fh containing Al, isomorphically substituted. The effect of Al on the adsorption and fixation capacity and possible mechanisms associated with these effects were evaluated. The adsorption capacity of AMX by pure ferrihydrite (up to 75 mg g-1) was superior to that of several other materials found in the literature. The presence of Al caused a negative effect, reducing adsorption by 28%. For the first time, the combination of spectroscopy in the infrared region with Fourier transform (FTIR), Raman spectroscopy and DFTB (Density Functional Based Tight Binding method), the latter in collaboration with theoretical researchers, was used to investigate the removal mechanism. from AMX by Fh. The results suggest the complexation of carboxyl with Fe in a bidentate binuclear configuration as the main adsorption mechanism of AMX in Fh. This conclusion is based on the differences between the wave numbers associated with the symmetrical and asymmetrical stretching of COO- (ΔCOO), before (ΔCOO = 351 cm-1) and after adsorption (ΔCOO = 333 cm-1), together with theoretical calculations that identified the energetically favorable configuration. This strong Fh-AMX interaction is important in the context of soils contaminated with AMX and rich in Fh, as it can minimize the transport of the antibiotic to groundwater, allowing its degradation by soil bacteria.

The characterization of Fh is challenging due to its small particle size (< 5 nm in those synthesized in this work) and large amount of structural defects. Isomorphic substitution, generally demonstrated in other materials by X-ray diffraction, for example, is not undisputed in the case of Fh. This work used, for the first time, the electron diffraction technique in a selected area to prove the isomorphic substitution of Fe by Al. It was also shown that such substitution increases the amount of hydroxyls on the surface of Fh by manipulating the SAD data (deviations from Vegard's rule) and using X-ray excited photoelectron spectroscopy (XPS) in the O (1s) region. The peak at ~531 eV, related to M-OH bonds, increased from 45% to 77% in the presence of 20% Al. This increase in OH on the surface of the Fh provided an increase of almost 30% in the adsorption of As. However, the Langmuir

constants (equations that best fit the adsorption profile) reduced from 0.55 to 0.17, at pH 5, and from 0.27 to 0.08, at pH 8, for 0% and 20% mol Al, respectively, which indicates a possible weakening in the interaction between As and Fh. These results emerge as a possible explanation for the increased adsorption of As with Al content, identified in soils rich in Fe oxyhydroxides containing Al.

Unlike AMX, degradation is not an alternative to arsenic removal. Thus, it becomes crucial to deepen the understanding of As retention by adsorbents over time, in order to enable their correct disposition. The transport of As in the environment can also be better understood from the determination of the mobility of As adsorbed on FhAl and its aging products, since FhAl are commonly found in soil. It was shown that the substitution of Fe for Al in Fh delays the phase transformation (from 30 days in samples without Al to 430 days in samples containing 15% Al), inhibits the formation of goethite in favor of hematite and alters the mechanism growth of the formed hematites. Even in the presence of As, which also delays the transformation of Fh, the growth mechanism is driven, under the observed conditions, by Al. The increase in Al also increases the mobility of As soon after adsorption, as shown by the sequential extraction assays and the reduction of the Langmuir constant. After aging, Al promotes As fixation, a phenomenon that was also observed in experiments with different soil samples. In these, the sequential extraction test showed the reduction of As mobility with the increase of the Al content present in the Fe oxide and hydroxide phases of the studied soils.

The results of this study make clear the importance of Fh in the removal and transport of AMX in the environment, as well as the benefits of the presence of Al in Fh for the removal and fixation of As. Whether these FhAls are synthetic, for industrial applications, or present in the soil, Al made it possible to increase the uptake of As and increase its fixation in the adsorption products over time, through the incorporation of As within oriented aggregates formed due to the presence of Al.

6.1.1 Suggestions for future investigations

(i) Investigate the removal and degradation of AMX in soils with different Fe oxyhydroxide contents.

(ii) To seek to detail, through high resolution microscopic and spectroscopic

techniques, the incorporation of As in the oriented aggregates of Fe oxyhydroxides containing Al.

(iii) To further study the complexation of As with the surface of FhAl particles, seeking to understand the weakening of the interaction during adsorption caused by the presence of Al.

(iv) Study the mobility of As associated with FhAl in complicating and common soil conditions, such as the presence of organic matter, the presence of Fe(II) or other materials that alter the redox potential of the medium.

(v) Study factors that accelerate the phase transformation of AlFh without increasing the mobility of As.

6.1.2 Publications

- Souza, T.G.F., Freitas, E.T.F., Mohallem, N.D.S., Ciminelli, V.S.T., 2021. Defects induced by Al substitution enhance As (V) adsorption on ferrihydrites. J. Hazard. Mater. 420, 126544.
- Souza, T.G.F., Olusegun, S.J., Galvao, B.R.L., Da Silva, J.L.F., Mohallem, N.D.S., Ciminelli, V.S.T. Mechanism and enhanced adsorption of amoxicillin by ferrihydrites: experimental and computational approaches (submitted manuscript)
- Souza, T.G.F., Freitas, E.T.F., Mohallem, N.D.S., Ciminelli, V.S.T., Influence of aluminium on the phase transformation and As(v) fixation by ferrihydrite nanoparticles (manuscript in preparation)

6.1.3 Contributions to additional publications

- Coelho, M. L. S. ; Souza, T. G. F. ; Coutinho, N. A. F. S. ; Caldeira, C. L. ; Ciminelli, V. S. T. . Efeito do envelhecimento na oxidação da arsenopirita. In: XXVIII ENTMME- Encontro Nacional de Tratamento de Minérios e Metalurgia Extrativa, 2019, Belo Horizonte. Anais do XXVIII Encontro Nacional de Tratamento de Minérios e Metalurgia Extrativa, 2019. v. 1.

- Freitas, E. T. F. ; Souza, T. G. F. ; Ciminelli, V. S. T. . Transmission electron microscopy techniques applied to the solid phase characterization of environmental samples. In: XXVIII ENTMME- Encontro Nacional de

Tratamento de Minérios e Metalurgia Extrativa, 2019, Belo Horizonte. Anais do XXVIII Encontro Nacional de Tratamento de Minérios e Metalurgia Extrativa, 2019. v. 1.

- Sunday J. Olusegun, Taiane G. F. Souza, Nelcy D. S. Mohallem, Virginia S. T. Ciminelli, Adsorption of As(III) and As(V), stability of biosilica based-ferrihydrite adsorbed arsenic and the oxidation of As(III) to As(V) at higher temperature. (manuscript in preparation)

- Sunday J. Olusegun, Taiane G. F. Souza, Guilhermina de O. Souza, Osial Magdalenaa, Nelcy D.S. Mohallem, Virginia S.T. Ciminelli, Krysinski Pawel, The mechanisms of adsorption and photo(degradation) of pharmaceuticals on iron-based materials: A comprehensive review. (submitted manuscript, under peer review)

7. CONSIDERAÇÕES FINAIS

O uso ferridritas (Fh) na remoção de dois contaminantes de grande potencial danoso foi estudado em profundidade neste trabalho. Arsênio e amoxicilina (AMX) foram adsorvidos em Fh contendo Al, isomorficamente substituído. O efeito do Al sobre a capacidade de adsorção e fixação e possíveis mecanismos associados a esses efeitos foram avaliados. A capacidade de adsorção de AMX por ferridrita pura (até 75 mg g^{-1}) foi superior a de diversos outros materiais encontrados na literatura. Já a presença de Al provocou um efeito negativo, reduzindo em 28% a adsorção. Pela primeira vez, a combinação das técnicas espectroscopia na região do infravermelho com transformada de Fourier (FTIR), espectroscopia Raman e DFTB (*Density Functional Based Tight Binding method*), esta última em colaboração com pesquisadores teóricos, foi utilizada para investigar o mecanismo de remoção da AMX por Fh. Os resultados sugerem a complexação da carboxila com o Fe em uma configuração bidentada binuclear como o principal mecanismo de adsorção de AMX em Fh. Esta conclusão é fundamentada nas diferenças entre os números de onda associados ao estiramento simétrico e assimétrico do COO^- (ΔCOO), antes (ΔCOO = 351 cm^{-1}) e após a adsorção (ΔCOO = 333 cm^{-1}), juntamente com cálculos teóricos que identificaram a configuração energeticamente favorável. Essa forte interação Fh-AMX é importante no contexto de solos contaminados com AMX e ricos em Fh, pois pode minimizar o carreamento do antibiótico para águas subterrâneas possibilitando sua degradação por bactérias do solo.

A caracterização de Fh é desafiadora devido ao seu pequeno tamanho de partículas (< 5 nm nas sintetizadas neste trabalho) e grande quantidade de defeitos estruturais.. A substituição isomórfica, geralmente demonstrada em outros materiais por difração de raios X, por exemplo, não é inconteste no caso da Fh. Este trabalho utilizou, pela primeira vez, a técnica de difração de elétrons em área selecionada para comprovar a substituição isomórfica de Fe por Al. Mostrou-se também que tal substituição aumenta a quantidade de hidroxilas na superfície das Fh através da manipulação dos dados de SAD (desvios da regra de Vegard) e do uso da espectroscopia de fotoelétrons excitados por raios X (XPS) na região O (1s). O pico em ~531 eV, relacionado às ligações M-OH, aumentou de 45% para 77% na

presença de 20% de Al. Esse aumento de OH na superfície das Fh proporcionou um aumento de quase 30% na adsorção de As. Porém, as constantes de Langmuir (equações que melhor se ajustaram ao perfil da adsorção) reduziram de 0,55 para 0,17, em pH 5, e 0,27 a 0,08, em pH 8, para 0% e 20% mol Al, respectivamente, o que indica um possível enfraquecimento na interação entra As e Fh. Estes resultados despontam como uma possível explicação para o aumento da adsorção de As com o teor de Al, identificados em solos ricos em oxihidróxidos de Fe contendo Al.

Diferentemente da AMX, a degradação não é uma alternativa na remoção de arsênio. Assim, torna-se crucial aprofundar a compreensão da retenção de As pelos adsorventes ao longo do tempo, a fim de viabilizar a correta disposição dos mesmos. O transporte de As no meio ambiente também pode ser melhor entendido a partir da determinação da mobilidade de As adsorvido nas FhAl e seus produtos de envelhecimento, uma vez que as FhAl são comumente encontradas no solo. Mostrou-se que a substituição de Fe por Al em Fh retarda a transformação de fases (de 30 dias nas amostras sem Al para 430 dias nas amostras contendo 15% de Al), inibe a formação de goethita em favor da hematita e altera o mecanismo de crescimento das hematitas formadas. Mesmo na presença de As, que também retarda a transformação da Fh, o mecanismo de crescimento é direcionado, nas condições observadas, pelo Al. O aumento de Al aumenta também a mobilidade do As logo após a adsorção, como mostram os ensaios de extração sequencial e a redução da constante de Langmuir. Já após o envelhecimento, o Al promove a fixação do As, fenômeno que também foi observado em experimentos com diferentes amostras de solos. Nestes, o ensaio de extração sequencial mostrou a redução da mobilidade de As com o aumento do teor de Al presente nas fases de óxidos e hidróxidos de Fe dos solos estudados.

Os resultados deste estudo deixam clara a importância das Fh na remoção e transporte de AMX no ambiente, bem como os benefícios da presença de Al em Fh para a remoção e fixação de As. Sejam estas FhAl sintéticas, para aplicações industriais, ou presentes no solo, o Al possibilitou aumentar a captação de As e aumentar sua fixação nos produtos de adsorção com o passar do tempo, pela incorporação de As dentro de agregados orientados formados devido à presença de

Al.

7.1.1 Sugestões para trabalhos futuros

(i) Investigar a remoção e degradação de AMX em solos com diferentes teores de oxihidróxidos de Fe.

(ii) Buscar detalhar através de técnicas microscópicas e espectroscópicas de alta resolução, a incorporação de As nos agregados orientados de oxihidróxidos de Fe contendo Al.

(iii) Estudar de maneira mais aprofundada a complexação de As com a superfície das partículas de FhAl, buscando compreender o enfraquecimento da interação durante a adsorção causada pela presença de Al.

(iv) Estudar a mobilidade do As associado a FhAl em condições complicadoras e comuns do solo, como presença de matéria orgânica, presença de Fe (II) ou outros materiais que alterem o potencial redox do meio.

(v) Estudar fatores que acelerem a transformação de fases de AlFh sem aumentar assim a mobilidade de As.

7.2 Publicações

7.2.1 Publicações geradas a partir dos resultados da tese

- Souza, T.G.F., Freitas, E.T.F., Mohallem, N.D.S., Ciminelli, V.S.T., 2021. Defects induced by Al substitution enhance As (V) adsorption on ferrihydrites. J. Hazard. Mater. 420, 126544.
- Souza, T.G.F., Olusegun, S.J., Galvao, B.R.L., Da Silva, J.L.F., Mohallem, N.D.S., Ciminelli, V.S.T. Mechanism and enhanced adsorption of amoxicillin by ferrihydrites: experimental and computational approaches (manuscrito submetido)
- Souza, T.G.F., Freitas, E.T.F., Mohallem, N.D.S., Ciminelli, V.S.T., Influence of aluminium on the phase transformation and As(v) fixation by ferrihydrite nanoparticles (manuscrito em elaboração)

7.2.2 Contribuições para outras publicações

- Coelho, M. L. S. ; Souza, T. G. F. ; Coutinho, N. A. F. S. ; Caldeira, C. L. ; Ciminelli, V. S. T. . Efeito do envelhecimento na oxidação da arsenopirita. In: XXVIII ENTMME- Encontro Nacional de Tratamento de Minérios e Metalurgia Extrativa, 2019, Belo Horizonte. Anais do XXVIII Encontro Nacional de Tratamento de Minérios e Metalurgia Extrativa, 2019. v. 1.

- Freitas, E. T. F. ; Souza, T. G. F. ; Ciminelli, V. S. T. . Transmission electron microscopy techniques applied to the solid phase characterization of environmental samples. In: XXVIII ENTMME- Encontro Nacional de Tratamento de Minérios e Metalurgia Extrativa, 2019, Belo Horizonte. Anais do XXVIII Encontro Nacional de Tratamento de Minérios e Metalurgia Extrativa, 2019. v. 1.

- Sunday J. Olusegun, Taiane G. F. Souza, Nelcy D. S. Mohallem, Virginia S. T. Ciminelli, Adsorption of As(III) and As(V), stability of biosilica based-ferrihydrite adsorbed arsenic and the oxidation of As(III) to As(V) at higher temperature. (manuscrito em elaboração)

- Sunday J. Olusegun, Taiane G. F. Souza, Guilhermina de O. Souza, Osial Magdalenaa, Nelcy D.S. Mohallem, Virginia S.T. Ciminelli, Krysinski Pawel, The mechanisms of adsorption and photo(degradation) of pharmaceuticals on iron-based materials: A comprehensive review. (manuscrito submetido em periódico da área e sob revisão dos pares)

REFERENCES

ADRA, A. *et al.* Arsenate and arsenite adsorption onto Al-containing ferrihydrites. Implications for arsenic immobilization after neutralization of acid mine drainage. *Applied Geochemistry*, v. 64, p. 2–9, 2016. Disponível em: <http://dx.doi.org/10.1016/j.apgeochem.2015.09.015>.

ADRA, A. *et al.* Arsenic scavenging by aluminum-substituted ferrihydrites in a circumneutral pH river impacted by acid mine drainage. *Environmental Science and Technology*, v. 47, n. 22, p. 12784–12792, 2013.

ADRIANO, W. S. *et al.* Adsorption of amoxicillin on chitosan beads: Kinetics, equilibrium and validation of finite bath models. *Biochemical Engineering Journal*, v. 27, n. 2, p. 132–137, dez. 2005. Disponível em: <https://linkinghub.elsevier.com/retrieve/pii/S1369703X05002299>.

AKSU DEMIREZEN, D.; YILDIZ, Y. Ş.; DEMIREZEN YILMAZ, D. Amoxicillin degradation using green synthesized iron oxide nanoparticles: Kinetics and mechanism analysis. *Environmental Nanotechnology, Monitoring and Management*, v. 11, n. February, 2019.

ANASTOPOULOS, I. *et al.* Removal of caffeine, nicotine and amoxicillin from (waste)waters by various adsorbents. A review. *Journal of Environmental Management*, v. 261, n. January, 2020.

ANDERSON, P. R.; BENJAMIN, M. M. Surface and Bulk Characteristics of Binary Oxide Suspensions. v. 24, n. 5, p. 692–698, 1990.

ANTÔNIO, DAPHINE CHIARA. *Daphne Chiara Antônio Bioacessibilidade de arsênio em amostras de solo em região de mineração de ouro Dissertação apresentada ao Programa de Pós-Graduação em Engenharia Metalúrgica , Materiais e de Minas da Escola de Engenharia da Universidade Federal de*. 2017. 1–118 f. Universidade Federal de Minas Gerais, 2017. Disponível em: <https://repositorio.ufmg.br/handle/1843/32350>.

ANTÔNIO, DAPHNE C. *et al.* Effects of aluminum and soil mineralogy on arsenic bioaccessibility. *Environmental Pollution*, v. 274, p. 116482, abr. 2021. Disponível em: <https://linkinghub.elsevier.com/retrieve/pii/S0269749121000609>.

BARRON, V.; HERRUZO, M.; TORRENT, J. Phosphate Adsorption by Aluminous Hematites of Different Shapes. *Soil Science Society of America Journal*, v. 52, n. 3, p. 647, 1988. Disponível em: <https://www.soils.org/publications/sssaj/abstracts/52/3/SS0520030647>.

BARRÓN, V.; TORRENT, J. Surface Hydroxyl Configuration of Various Crystal Faces of Hematite and Goethite. *Journal of Colloid and Interface Science*, v. 177, n. 2, p. 407–410, fev. 1996. Disponível em: <https://linkinghub.elsevier.com/retrieve/pii/S002197979690051X>.

BAZILEVSKAYA, E. *et al.* Aluminum coprecipitates with Fe (hydr)oxides: Does isomorphous substitution of Al3+ for Fe3+ in goethite occur? *Geochimica et Cosmochimica Acta*, v. 75, n. 16, p. 4667–4683, 2011.

BEBU, A. *et al.* IR, Raman, SERS and DFT study of amoxicillin. *Journal of Molecular Structure*, v. 993, n. 1–3, p. 52–56, 2011.

BOILY, J. F.; SONG, X. Direct identification of reaction sites on ferrihydrite. *Communications Chemistry*, v. 3, n. 1, 2020.

BOJARSKI, B.; KOT, B.; WITESKA, M. Antibacterials in Aquatic Environment and Their Toxicity to Fish. *Pharmaceuticals*, v. 13, n. 8, p. 189, 9 ago. 2020. Disponível em: <https://www.mdpi.com/1424-8247/13/8/189>.

BOLANZ, R. M. *et al.* The effect of antimonate, arsenate, and phosphate on the transformation of ferrihydrite to goethite, hematite, feroxyhyte, and tripuhyite. *Clays and Clay Minerals*, v. 61, n. 1, p. 11–25, 2013.

BOSMAN, M. *et al.* Mapping chemical and bonding information using multivariate analysis of electron energy-loss spectrum images. *Ultramicroscopy*, v. 106, n. 11- 12 SPEC. ISS., p. 1024–1032, 2006.

BOUKHELKHAL, A. *et al.* Adsorptive removal of amoxicillin from wastewater using wheat grains: equilibrium, kinetic, thermodynamic studies and mass transfer. *Desalination and Water Treatment*, v. 57, n. 56, p. 27035–27047, 1 dez. 2016. Disponível em: <https://www.tandfonline.com/doi/full/10.1080/19443994.2016.1166991>.

BOUYARMANE, H. *et al.* Parameters influencing ciprofloxacin, ofloxacin, amoxicillin and sulfamethoxazole retention by natural and converted calcium phosphates.

Journal of Hazardous Materials, v. 291, p. 38–44, jun. 2015. Disponível em: <http://dx.doi.org/10.1016/j.jhazmat.2015.02.049>.

BRITTAIN, H. G. (Org.). *Analytical Profiles of Drug Substances and Excipients*. 1. ed. San Diego: Academic Press, 1994. v. 23. Disponível em: <https://linkinghub.elsevier.com/retrieve/pii/S0099542808602373>.

BUDYANTO, S. *et al.* Studies of Adsorption Equilibria and Kinetics of Amoxicillin from Simulated Wastewater using Activated Carbon and Natural Bentonite. *Journal of Environmental Protection Science*, v. 2, p. 72–80, 2008.

CALBOREAN, A. *et al.* Raman and SERS investigations of trihydrate amoxicillin. *Journal of Optoelectronics and Advanced Materials*, v. 9, n. 3, p. 680–685, 2007.

CALDEIRA, C. L.; CIMINELLI, V. S. T.; OSSEO-ASARE, K. The role of carbonate ions in pyrite oxidation in aqueous systems. *Geochimica et Cosmochimica Acta*, v. 74, n. 6, p. 1777–1789, 2010.

CHADWICK, J. *et al.* A Mössbauer study of ferrihydrite and aluminium substituted ferrihydrites. *Journal of Magnetism and Magnetic Materials*, v. 61, n. 1–2, p. 88–100, set. 1986. Disponível em: <https://linkinghub.elsevier.com/retrieve/pii/0304885386900703>.

CHAI, L. *et al.* Tunable defects and interfaces of hierarchical dandelion-like NiCo2O4 via Ostwald ripening process for high-efficiency electromagnetic wave absorption. *Chemical Engineering Journal*, v. 429, n. May 2021, p. 132547, fev. 2022. Disponível em: <https://doi.org/10.1016/j.cej.2021.132547>.

CHELLIAPAN, S.; WILBY, T.; SALLIS, P. J. Performance of an up-flow anaerobic stage reactor (UASR) in the treatment of pharmaceutical wastewater containing macrolide antibiotics. *Water Research*, v. 40, n. 3, p. 507–516, fev. 2006. Disponível em: <https://linkinghub.elsevier.com/retrieve/pii/S0043135405006706>.

CHEN, J. S. *et al.* Building hematite nanostructures by oriented attachment. *Angewandte Chemie - International Edition*, v. 50, n. 3, p. 650–653, 2011.

CHEN, L. *et al.* Application of metal oxide heterostructures in arsenic removal from contaminated water. *Journal of Nanomaterials*, v. 2014, 2014.

CHEN, X. *et al.* Ferrihydrite enhanced the electrogenic hydrocarbon degradation in soil microbial electrochemical remediation. *Chemical Engineering Journal*, v. 446, n.

P1, p. 136901, out. 2022. Disponível em: <https://doi.org/10.1016/j.cej.2022.136901>.

CHITONGO, R.; OPEOLU, B. O.; OLATUNJI, O. S. Abatement of Amoxicillin, Ampicillin, and Chloramphenicol From Aqueous Solutions Using Activated Carbon Prepared From Grape Slurry. *CLEAN – Soil, Air, Water*, v. 47, n. 2, p. 1800077, 17 fev. 2019. Disponível em: <https://onlinelibrary.wiley.com/doi/10.1002/clen.201800077>.

CHOI, K.-J.; KIM, S.-G.; KIM, S.-H. Removal of antibiotics by coagulation and granular activated carbon filtration. *Journal of Hazardous Materials*, v. 151, n. 1, p. 38–43, fev. 2008. Disponível em: <https://linkinghub.elsevier.com/retrieve/pii/S0304389407007649>.

CHUN ZENG, H. Ostwald Ripening: A Synthetic Approach for Hollow Nanomaterials. *Current Nanoscience*, v. 3, n. 2, p. 177–181, 1 maio 2007. Disponível em: <http://www.eurekaselect.com/openurl/content.php?genre=article&issn=1573-4137&volume=3&issue=2&spage=177>.

CIMINELLI, V. S. T. *et al.* Low arsenic bioaccessibility by fixation in nanostructured iron (Hydr)oxides: Quantitative identification of As-bearing phases. *Journal of Hazardous Materials*, v. 353, n. February, p. 261–270, 2018.

CISMASU, A. C. *et al.* Composition et propriétés structurales des ferrihydrites naturelles. *Comptes Rendus - Geoscience*, v. 343, n. 2–3, p. 210–218, 2011. Disponível em: <http://dx.doi.org/10.1016/j.crte.2010.11.001>.

CISMASU, A. C. *et al.* Properties of impurity-bearing ferrihydrite I. Effects of Al content and precipitation rate on the structure of 2-line ferrihydrite. *Geochimica et Cosmochimica Acta*, v. 92, p. 275–291, 2012.

CISMASU, A. C. *et al.* Properties of impurity-bearing ferrihydrite II: Insights into the surface structure and composition of pure, Al- and Si-bearing ferrihydrite from Zn(II) sorption experiments and Zn K-edge X-ray absorption spectroscopy. *Geochimica et Cosmochimica Acta*, v. 119, p. 46–60, 2013.

CISMASU, A. C. *et al.* Properties of impurity-bearing ferrihydrite III. Effects of Si on the structure of 2-line ferrihydrite. *Geochimica et Cosmochimica Acta*, v. 133, p. 168–185, 2014. Disponível em: <http://dx.doi.org/10.1016/j.gca.2014.02.018>.

CONAMA. Resolution N^{o} 460/2013 (Change the CONAMA n^{o} 420/2009). Provides criteria and guiding values of soil quality for the presence of chemical substances and establishes guidelines for the environmental management of areas contaminated by these substances as a. p. 20, 2013.

CORNELL, R. M.; SCHWERTMANN, U. Introduction to the Iron Oxides. *The Iron Oxides*. Weinheim, FRG: Wiley-VCH Verlag GmbH & Co. KGaA, 2003. p. 1–7. Disponível em: <http://doi.wiley.com/10.1002/3527602097.ch1>.

CORNELL, ROCHELLE M.; SCHWERTMANN, U. *The Iron Oxides_ Structure, Properties, Reactions, Occurrences and Uses*. Second Edi ed. [S.l.]: Wiley-VCH Verlag GmbH & Co. KGaA, 2003.

COSTANZO, S. D.; MURBY, J.; BATES, J. Ecosystem response to antibiotics entering the aquatic environment. *Marine Pollution Bulletin*, v. 51, n. 1–4, p. 218–223, 2005.

DANNER, M.-C. *et al.* Antibiotic pollution in surface fresh waters: Occurrence and effects. *Science of The Total Environment*, v. 664, p. 793–804, maio 2019. Disponível em: <https://doi.org/10.1016/j.scitotenv.2019.01.406>.

DANTAS, M. S. S. *et al.* As(III) immobilization on gibbsite: Investigation of the complexation mechanism by combining EXAFS analyses and DFT calculations. *Geochimica et Cosmochimica Acta*, v. 83, p. 205–216, 2011. Disponível em: <http://dx.doi.org/10.1016/j.gca.2011.12.019>.

DAS, S.; ESSILFIE-DUGHAN, J.; HENDRY, M. J. Arsenate partitioning from ferrihydrite to hematite: Spectroscopic evidence. *American Mineralogist*, v. 99, n. 4, p. 749–754, 1 abr. 2014. Disponível em: <https://pubs.geoscienceworld.org/ammin/article/99/4/749-754/46102>.

DE FRANCO, M. A. E. *et al.* Removal of amoxicillin from water by adsorption onto activated carbon in batch process and fixed bed column: Kinetics, isotherms, experimental design and breakthrough curves modelling. *Journal of Cleaner Production*, v. 161, p. 947–956, set. 2017. Disponível em: <https://linkinghub.elsevier.com/retrieve/pii/S0959652617311496>.

DE YOREO, J. J. *et al.* Crystallization by particle attachment in synthetic, biogenic, and geologic environments. *Science*, v. 349, n. 6247, 2015.

DI IORIO, E. *et al.* Arsenate retention mechanisms on hematite with different morphologies evaluated using AFM, TEM measurements and vibrational spectroscopy. *Geochimica et Cosmochimica Acta*, v. 237, p. 155–170, set. 2018. Disponível em: <https://doi.org/10.1016/j.gca.2018.06.027>.

DODD, M. C. *et al.* Kinetics and mechanistic aspects of As(III) oxidation by aqueous chlorine, chloramines, and ozone: Relevance to drinking water treatment. *Environmental Science and Technology*, v. 40, n. 10, p. 3285–3292, 2006.

DRITS, V. A. *et al.* Structural Model for Ferrihydrite. *Clay Minerals*, v. 28, n. 2, p. 185–207, 9 jun. 1993. Disponível em: <https://www.cambridge.org/core/product/identifier/S0009855800026303/type/journal_article>.

DU, H. *et al.* Sorption of Pb(II) by Nanosized Ferrihydrite Organo-Mineral Composites Formed by Adsorption versus Coprecipitation. *ACS Earth and Space Chemistry*, v. 2, n. 6, p. 556–564, 2018.

DUARTE, G. *et al.* Evaluation of 10 years stability of concentrated arsenic-sulfide tailings. p. 423–425, 2016.

EKSTROM, E. B. *et al.* Contrasting effects of Al substitution on microbial reduction of Fe(III) (hydr)oxides. *Geochimica et Cosmochimica Acta*, v. 74, n. 24, p. 7086–7099, 2010. Disponível em: <http://dx.doi.org/10.1016/j.gca.2010.09.008>.

ELSTNER, M. *et al.* Self-consistent-charge density-functional tight-binding method for simulations of complex materials properties. *Physical Review B*, v. 58, n. 11, p. 7260–7268, 15 set. 1998. Disponível em: <https://link.aps.org/doi/10.1103/PhysRevB.58.7260>.

FAIVRE, D. *Iron Oxides From Nature to Applications*. Weinheim, Germany: Wiley-VCH, 2016.

FEAM. *Manual de Coleta de Solos para Valores de Referência de Qualidade no Estado de Minas Gerais*. Belo Horizonte: [s.n.], 2013.

FISCHER, W. R.; SCHWERTMANN, U. The formation of hematite from amorphous iron(III)hydroxide. *Clays and Clay Minerals*, v. 23, n. 1, 1975.

FRANKENBERGER, W. T. *Environmental Chemistry of Arsenic*. Marcel Dek ed. New York: CRC Press, 2001.

FREITAS, E. T. F. *et al.* Arsenic entrapment by nanocrystals of Al-magnetite: The role of Al in crystal growth and As retention. *Chemosphere*, v. 158, p. 91–99, set. 2016. Disponível em: <http://linkinghub.elsevier.com/retrieve/pii/S0045653516306841>.

FREITAS, E. T. F. *Mecanismo Inédito de Imobilização de Arsênio Baseado em Agregação Orientada de Nanopartículas Cristalinas de (Hidr)óxidos de Ferro e Alumínio: Evidências por Microscopia Eletrônica de Transmissão*. 2017. 1–143 f. Universidade Federal de Minas Gerais, 2017. Disponível em: <http://hdl.handle.net/1843/BUBD-AU9H42>.

FREITAS, E. T. F. *et al.* Natural attenuation of arsenic in the environment by immobilization in nanostructured hematite. *Chemosphere*, v. 138, p. 340–347, nov. 2015. Disponível em: <http://linkinghub.elsevier.com/retrieve/pii/S0045653515005950>.

FREUNDLICH, H. Über die Adsorption in Lösungen. *Zeitschrift für Physikalische Chemie*, v. 57U, n. 1, p. 1100–1107, 1 jan. 1907. Disponível em: <http://www.degruyter.com/view/j/zpch.1907.57.issue-1/zpch-1907-5723/zpch-1907-5723.xml>.

GLASAUER, S. M. *et al.* Inhibition of sintering by Si during the conversion of Si-rich ferrihydrite to hematite. *Clays and Clay Minerals*, v. 48, n. 1, p. 51–56, 2000.

GODDARD, A. *et al.* Effect of omeprazole on the distribution of metronidazole, amoxicillin, and clarithromycin in human gastric juice. *Gastroenterology*, v. 111, n. 2, p. 358–367, ago. 1996. Disponível em: <https://linkinghub.elsevier.com/retrieve/pii/S001650859600354X>.

GRENNI, P.; ANCONA, V.; BARRA CARACCIOLO, A. Ecological effects of antibiotics on natural ecosystems: A review. *Microchemical Journal*, v. 136, p. 25–39, jan. 2018. Disponível em: <https://doi.org/10.1016/j.microc.2017.02.006>.

GROSSL, P. R. *et al.* Arsenate and Chromate Retention Mechanisms on Goethite. 2. Kinetic Evaluation Using a Pressure-Jump Relaxation Technique. *Environmental Science & Technology*, v. 31, n. 2, p. 321–326, fev. 1997. Disponível em: <https://pubs.acs.org/doi/10.1021/es950654l>.

HA, J. *et al.* Interaction of aqueous Zn(II) with hematite nanoparticles and microparticles. Part 1. EXAFS study of Zn(II) adsorption and precipitation. *Langmuir*,

v. 25, n. 10, p. 5574–5585, 2009.

HANSEL, C. M. *et al.* Effect of adsorbed and substituted Al on Fe(II)-induced mineralization pathways of ferrihydrite. *Geochimica et Cosmochimica Acta*, v. 75, n. 16, p. 4653–4666, 2011. Disponível em: <http://dx.doi.org/10.1016/j.gca.2011.05.033>.

HAO, L. *et al.* A critical review on arsenic removal from water using iron-based adsorbents. *RSC Advances*, v. 8, n. 69, p. 39545–39560, 2018. Disponível em: <http://xlink.rsc.org/?DOI=C8RA08512A>.

HARRINGTON, R. *et al.* Neutron pair distribution function study of two-line ferrihydrite. *Environmental Science and Technology*, v. 45, n. 23, p. 9883–9890, 2011.

HARVEY, O. R.; RHUE, R. D. Kinetics and energetics of phosphate sorption in a multi-component Al(III)-Fe(III) hydr(oxide) sorbent system. *Journal of Colloid and Interface Science*, v. 322, n. 2, p. 384–393, 2008.

HAUSNER, D. B. *et al.* Ferrihydrite reactivity toward carbon dioxide. *Journal of Colloid and Interface Science*, v. 337, n. 2, p. 492–500, 2009. Disponível em: <http://dx.doi.org/10.1016/j.jcis.2009.05.069>.

HENKE, K. *Arsenic−Environmental Chemistry, Health Threats and Waste Treatment*. 1. ed. Chichester, UK: John Wiley & sons Ltd., 2009.

HENMI, T. *et al.* Poorly-ordered iron-rich precipitates from springs and streams on andesitic volcanoes. *Geochimica et Cosmochimica Acta*, v. 44, n. 2, p. 365–372, fev. 1980. Disponível em: <https://linkinghub.elsevier.com/retrieve/pii/0016703780901441>.

HIEMSTRA, T. Surface and mineral structure of ferrihydrite. *Geochimica et Cosmochimica Acta*, v. 105, p. 316–325, 2013. Disponível em: <http://dx.doi.org/10.1016/j.gca.2012.12.002>.

HIEMSTRA, T.; VAN RIEMSDIJK, W. H. A surface structural model for ferrihydrite I: Sites related to primary charge, molar mass, and mass density. *Geochimica et Cosmochimica Acta*, v. 73, n. 15, p. 4423–4436, 2009. Disponível em: <http://dx.doi.org/10.1016/j.gca.2009.04.032>.

HIEMSTRA, T.; ZHAO, W. Reactivity of ferrihydrite and ferritin in relation to surface

structure, size, and nanoparticle formation studied for phosphate and arsenate. *Environmental Science: Nano*, v. 3, n. 6, p. 1265–1279, 2016. Disponível em: <http://dx.doi.org/10.1039/C6EN00061D>.

HOMEM, V.; ALVES, A.; SANTOS, L. Amoxicillin removal from aqueous matrices by sorption with almond shell ashes. *International Journal of Environmental Analytical Chemistry*, v. 90, n. 14–15, p. 1063–1084, 10 dez. 2010. Disponível em: <http://www.tandfonline.com/doi/abs/10.1080/03067310903410964>.

HU, Y. *et al.* Aluminum affects heterogeneous Fe(III) (Hydr)oxide nucleation, growth, and ostwald ripening. *Environmental Science and Technology*, v. 48, n. 1, p. 299–306, 2014.

JAMBOR, J. L.; DUTRIZAC, J. E. Occurrence and Constitution of Natural and Synthetic Ferrihydrite, a Widespread Iron Oxyhydroxide. *Chemical Reviews*, v. 98, n. 7, p. 2549–2586, nov. 1998. Disponível em: <https://pubs.acs.org/doi/10.1021/cr970105t>.

JENTZSCH, T. L.; PENN, R. L. Influence of aluminum doping on ferrihydrite nanoparticle reactivity. *Journal of Physical Chemistry B*, v. 110, n. 24, p. 11746–11750, 2006.

JIA, B.; GAO, L. Growth of Well-Defined Cubic Hematite Single Crystals: Oriented Aggregation and Ostwald Ripening. *Crystal Growth & Design*, v. 8, n. 4, p. 1372–1376, abr. 2008. Disponível em: <http://pubs.acs.org/doi/abs/10.1021/cg070300t>.

JIA, Y. *et al.* Infrared spectroscopic and X-ray diffraction characterization of the nature of adsorbed arsenate on ferrihydrite. *Geochimica et Cosmochimica Acta*, v. 71, n. 7, p. 1643–1654, 2007.

JOHNSTON, C. P.; CHRYSOCHOOU, M. Mechanisms of Chromate, Selenate, and Sulfate Adsorption on Al-Substituted Ferrihydrite: Implications for Ferrihydrite Surface Structure and Reactivity. *Environmental Science and Technology*, v. 50, n. 7, p. 3589–3596, 2016.

JUNGCHAROEN, P. *et al.* Synthesis of Lignin-Modified Nanoscale Zerovalent Iron Applied to Arsenic Removal. v. 03, n. 09, p. 1–6, 2017. Disponível em: <www.academicfora.com>.

KHALIL, M. *et al.* Hydrothermal synthesis, characterization, and growth mechanism

of hematite nanoparticles. *Journal of Nanoparticle Research*, v. 16, n. 4, 2014.

KHARDORI, N.; STEVAUX, C.; RIPLEY, K. Antibiotics: From the Beginning to the Future: Part 2. *Indian Journal of Pediatrics*, v. 87, n. 1, p. 43–47, 2020.

KLEIN, A. R. *et al.* Probing the Fate of Different Structures of Beta-Lactam Antibiotics: Hydrolysis, Mineral Capture, and Influence of Organic Matter. *ACS Earth and Space Chemistry*, 2021.

KLEIN, E. Y. *et al.* Global increase and geographic convergence in antibiotic consumption between 2000 and 2015. v. 115, n. 15, p. 3463–3470, 2018.

KOYUNCU, I. *et al.* Removal of hormones and antibiotics by nanofiltration membranes. *Journal of Membrane Science*, v. 309, n. 1–2, p. 94–101, fev. 2008. Disponível em: <https://linkinghub.elsevier.com/retrieve/pii/S037673880700734X>.

KUBICKI, J. D. *et al.* Density functional theory modeling of chromate adsorption onto ferrihydrite nanoparticles. *Geochemical Transactions*, v. 19, n. 1, p. 8, 1 dez. 2018. Disponível em: <https://doi.org/10.1186/s12932-018-0053-8>.

KUMAR, R. *et al.* Emerging technologies for arsenic removal from drinking water in rural and peri-urban areas: Methods, experience from, and options for Latin America. *Science of The Total Environment*, v. 694, p. 133427, dez. 2019. Disponível em: <https://linkinghub.elsevier.com/retrieve/pii/S0048969719333467>.

KÜMMERER, K. Antibiotics in the aquatic environment - A review - Part I. *Chemosphere*, v. 75, n. 4, p. 417–434, 2009.

LADEIRA, A C Q *et al.* Mechanism of anion retention from EXAFS and density functional calculations: Arsenic (V) adsorbed on gibbsite. *Geochimica et Cosmochimica Acta*, v. 65, n. 8, p. 1211–1217, 2001.

LADEIRA, ANA C.Q.; CIMINELLI, V. S. T. Adsorption and desorption of arsenic on an oxisol and its constituents. *Water Research*, v. 38, n. 8, p. 2087–2094, 2004.

LADEIRA, ANA CLÁUDIA Q.; CIMINELLI, V. S. T.; NEPOMUCENO, A. L. Seleção de solos para a imobilização de arsênio. *Rem: Revista Escola de Minas*, v. 55, n. 3, p. 215–221, 2005.

LANGMUIR, I. THE ADSORPTION OF GASES ON PLANE SURFACES OF GLASS, MICA AND PLATINUM. *Journal of the American Chemical Society*, v. 40, n. 9, p. 1361–1403, set. 1918. Disponível em:

<https://pubs.acs.org/doi/abs/10.1021/ja02242a004>.

LI, B. *et al.* Mechanisms of arsenate and cadmium co-immobilized on ferrihydrite inferred from ternary surface configuration. *Chemical Engineering Journal*, v. 424, n. March, p. 130410, nov. 2021. Disponível em: <https://doi.org/10.1016/j.cej.2021.130410>.

LI, F.; GENG, D.; CAO, Q. Adsorption of As(V) on aluminum-, iron-, and manganese-(oxyhydr)oxides: equilibrium and kinetics. *Desalination and Water Treatment*, v. 56, n. 7, p. 1829–1838, 2015.

LI, H.; JENSEN, J. H. Improving the efficiency and convergence of geometry optimization with the polarizable continuum model: New energy gradients and molecular surface tessellation. *Journal of Computational Chemistry*, v. 25, n. 12, p. 1449–1462, set. 2004. Disponível em: <https://onlinelibrary.wiley.com/doi/10.1002/jcc.20072>.

LI, W. *et al.* Mechanisms on the morphology variation of hematite crystals by Al substitution: The modification of Fe and O reticular densities. *Scientific Reports*, v. 6, n. 1, p. 35960, 27 dez. 2016. Disponível em: <http://www.nature.com/articles/srep35960>.

LI, W. C. Occurrence, sources, and fate of pharmaceuticals in aquatic environment and soil. *Environmental Pollution*, v. 187, p. 193–201, abr. 2014. Disponível em: <https://linkinghub.elsevier.com/retrieve/pii/S0269749114000219>.

LIANG, Y. *et al.* Al-substitution-induced defect sites enhance adsorption of Pb2+ on hematite. *Environmental Science: Nano*, v. 6, n. 5, p. 1323–1331, 2019.

LIM, J. *et al.* Characterization of magnetic nanoparticle by dynamic light scattering. *Nanoscale Research Letters*, v. 8, n. 1, p. 381, 2013. Disponível em: <http://www.nanoscalereslett.com/content/8/1/381>.

LIMA, É. C.; ADEBAYO, M. A.; FERNANDO, M. M. *Chapter 3- Kinetic and Equilibrium Models of Adsorption in Carbon Nanomaterials as Adsorbents for Environmental and Biological Applications, C.P. Bergmann, F.M. Machado editors*. [S.l: s.n.], 2015.

LIU, J. *et al.* Aggregation of ferrihydrite nanoparticles: Effects of pH, electrolytes,and organics. *Environmental Research*, v. 172, n. January, p. 552–560, 2019.

LIU, L. *et al.* Analyzing the adsorptive behavior of Amoxicillin on four Zr-MOFs nanoparticles: Functional groups dependence of adsorption performance and mechanisms. *Journal of Environmental Management*, v. 268, n. May, p. 110630, 2020. Disponível em: <https://doi.org/10.1016/j.jenvman.2020.110630>.

LIU, YU-TING; HESTERBERG, D. Phosphate Bonding on Noncrystalline Al / Fe-Hydroxide Coprecipitates. p. 6283–6289, 2011.

LIU, YUAN *et al.* Ostwald Ripening-Mediated Grafting of Metal–Organic Frameworks on a Single Colloidal Nanocrystal to Form Uniform and Controllable MXF. *Journal of the American Chemical Society*, v. 141, n. 18, p. 7407–7413, 8 maio 2019. Disponível em: <https://pubs.acs.org/doi/10.1021/jacs.9b01563>.

LOU, X. W. (DAVID); ARCHER, L. A.; YANG, Z. Hollow Micro-/Nanostructures: Synthesis and Applications. *Advanced Materials*, v. 20, n. 21, p. 3987–4019, 3 nov. 2008. Disponível em: <https://onlinelibrary.wiley.com/doi/10.1002/adma.200800854>.

LOURENÇO, M. P. *et al.* Accurate SCC-DFTB Parametrization for Bulk Water. *Journal of Chemical Theory and Computation*, v. 16, n. 3, p. 1768–1778, 10 mar. 2020. Disponível em: <https://pubs.acs.org/doi/10.1021/acs.jctc.9b00816>.

LOURENÇO, M. P. *et al.* FASP: a framework for automation of Slater–Koster file parameterization. *Theoretical Chemistry Accounts*, v. 135, n. 11, p. 250, 18 nov. 2016. Disponível em: <http://link.springer.com/10.1007/s00214-016-2001-y>.

LŮ, J. *et al.* Adsorptive removal of phosphate by a nanostructured Fe-Al-Mn trimetal oxide adsorbent. *Powder Technology*, v. 233, p. 146–154, 2013. Disponível em: <http://dx.doi.org/10.1016/j.powtec.2012.08.024>.

LU, Y. *et al.* Ferrihydrite transformation under the impact of humic acid and Pb: Kinetics, nanoscale mechanisms, and implications for C and Pb dynamics. *Environmental Science: Nano*, v. 6, n. 3, p. 747–762, 2019.

LUENGO, C.; BRIGANTE, M.; AVENA, M. Adsorption kinetics of phosphate and arsenate on goethite. A comparative study. *Journal of Colloid and Interface Science*, v. 311, n. 2, p. 354–360, 2007.

MA, J. *et al.* Easy solid-phase synthesis of pH-insensitive heterogeneous CNTs/FeS Fenton-like catalyst for the removal of antibiotics from aqueous solution. *Journal of Colloid and Interface Science*, v. 444, p. 24–32, abr. 2015. Disponível em:

<http://dx.doi.org/10.1016/j.jcis.2014.12.027>.

MACKUĽAK, T. *et al.* Pharmaceuticals, drugs, and resistant microorganisms — environmental impact on population health. *Current Opinion in Environmental Science & Health*, v. 9, p. 40–48, jun. 2019. Disponível em: <https://linkinghub.elsevier.com/retrieve/pii/S2468584419300029>.

MALLET, M. *et al.* Investigation of phosphate adsorption onto ferrihydrite by X-ray Photoelectron Spectroscopy. *Journal of Colloid and Interface Science*, v. 407, p. 95–101, 2013. Disponível em: <http://dx.doi.org/10.1016/j.jcis.2013.06.049>.

MANCEAU, A.; GATES, W. P. Incorporation of Al in iron oxyhydroxides: implications for the structure of ferrihydrite. *Clay Minerals*, v. 48, n. 03, p. 481–489, 2013.

MANCEAU, A.; SKANTHAKUMAR, S.; SODERHOLM, L. PDF analysis of ferrihydrite: Critical assessment of the under-constrained akdalaite model. *American Mineralogist*, v. 99, n. 1, p. 102–108, 1 jan. 2014. Disponível em: <https://www.degruyter.com/document/doi/10.2138/am.2014.4576/html>.

MANCEAU, ALAIN. Comment on “roles of Hydration and Magnetism on the Structure of Ferrihydrite from First Principles”. *ACS Earth and Space Chemistry*, v. 3, n. 8, p. 1576–1580, 2019.

MASSEY, M. S. *et al.* Uranium incorporation into aluminum-substituted ferrihydrite during iron(<scp>ii</scp>)-induced transformation. *Environ. Sci.: Processes Impacts*, v. 16, n. 9, p. 2137–2144, 2014. Disponível em: <http://dx.doi.org/10.1039/C4EM00148F>.

MASUE-SLOWEY, Y.; LOEPPERT, R. H.; FENDORF, S. Alteration of ferrihydrite reductive dissolution and transformation by adsorbed As and structural Al: Implications for As retention. *Geochimica et Cosmochimica Acta*, v. 75, n. 3, p. 870–886, 2011. Disponível em: <http://dx.doi.org/10.1016/j.gca.2010.11.016>.

MASUE, Y.; LOEPPERT, R. H.; KRAMER, T. A. Arsenate and arsenite adsorption and desorption behavior on coprecipitated aluminum:iron hydroxides. *Environmental Science and Technology*, v. 41, n. 3, p. 837–842, 2007.

MAZZETTI, L.; THISTLETHWAITE, P. J. Raman spectra and thermal transformations of ferrihydrite and schwertmannite. *Journal of Raman Spectroscopy*, v. 33, n. 2, p. 104–111, 2002.

MCMAHON, G. *et al.* Application of Dual Beam FIB to the Metrology of Nanostructured Photovoltaic Devices. *Microscopy and Microanalysis*, v. 15, n. S2, p. 1392, 2009. Disponível em: <http://www.journals.cambridge.org/abstract_S1431927609097244>.

MICHEL, F. M.; EHM, L.; LIU, G.; *et al.* Similarities in 2- and 6-line ferrihydrite based on pair distribution function analysis of X-ray total scattering. *Chemistry of Materials*, v. 19, n. 6, p. 1489–1496, 2007.

MICHEL, F. M.; EHM, L.; ANTAO, S. M.; *et al.* The Structure of Ferrihydrite, a Nanocrystalline Material. *Science*, v. 316, n. 5832, p. 1726–1729, 22 jun. 2007. Disponível em: <https://www.sciencemag.org/lookup/doi/10.1126/science.1142525>.

MITCHELL, D. R. G. DiffTools: Electron diffraction software tools for DigitalMicrograph™. *Microscopy Research and Technique*, v. 71, n. 8, p. 588–593, 2008.

MOUSSAVI, G. *et al.* Preparation, characterization and adsorption potential of the NH4Cl-induced activated carbon for the removal of amoxicillin antibiotic from water. *Chemical Engineering Journal*, v. 217, p. 119–128, 2013. Disponível em: <http://dx.doi.org/10.1016/j.cej.2012.11.069>.

MÜLLER, K. *et al.* A comparative study of As(III) and As(V) in aqueous solutions and adsorbed on iron oxy-hydroxides by Raman spectroscopy. *Water Research*, v. 44, n. 19, p. 5660–5672, 2010.

NAKAMOTO, K. *Infrared and Raman Spectra of Inorganic and Coordination Compounds Part B: Applications in Coordination, Organometallic, and Bioinorganic Chemistry*. Hoboken, New Jersey: John Wiley & Sons, Inc., 2009.

NAMAYANDEH, A.; KABENGI, N. Calorimetric study of the influence of aluminum substitution in ferrihydrite on sulfate adsorption and reversibility. *Journal of Colloid and Interface Science*, v. 540, p. 20–29, 2019. Disponível em: <https://doi.org/10.1016/j.jcis.2019.01.001>.

NI, C. *et al.* Adsorption performance of Cr(VI) onto Al-free and Al-substituted ferrihydrites. *RSC Advances*, v. 6, n. 71, p. 66412–66419, 2016. Disponível em: <http://dx.doi.org/10.1039/C6RA09465A>.

NIEDERBERGER, M.; CÖLFEN, H. Oriented attachment and mesocrystals: Non-

classical crystallization mechanisms based on nanoparticle assembly. *Physical Chemistry Chemical Physics*, v. 8, n. 28, p. 3271–3287, 2006.

NIEHAUS, T. A.; ELSTNER, M.; *et al.* Application of an approximate density-functional method to sulfur containing compounds. *Journal of Molecular Structure: THEOCHEM*, v. 541, n. 1–3, p. 185–194, maio 2001. Disponível em: <https://linkinghub.elsevier.com/retrieve/pii/S0166128000007624>.

NIEHAUS, T. A.; SUHAI, S.; *et al.* Tight-binding approach to time-dependent density-functional response theory. *Physical Review B*, v. 63, n. 8, p. 085108, 6 fev. 2001. Disponível em: <https://link.aps.org/doi/10.1103/PhysRevB.63.085108>.

PANTUZZO, F.L.; CIMINELLI, V. S. T.; BRITO, W. NEW EVIDENCES FOR THE ROLE OF PRECIPITATION AND ADSORPTION DURING FE(III)-AS(V) COPRECIPITATION. In: YOUNG, C. A. *et al.* (Org.). . *Hydrometallurgy 2008: Proceedings of the Sixth International Symposium*. 1st. ed. Phoenix: Society for Mining, Metallurgy, and Exploration; Illustrated edition, 2008. p. 130–139.

PANTUZZO, FERNANDO L.; CIMINELLI, V. S. T. Arsenic association and stability in long-term disposed arsenic residues. *Water Research*, v. 44, n. 19, p. 5631–5640, 2010. Disponível em: <http://dx.doi.org/10.1016/j.watres.2010.07.011>.

PENKE, Y. K. *et al.* Aluminum substituted nickel ferrite (Ni-Al-Fe): A ternary metal oxide adsorbent for arsenic adsorption in aqueous medium. *RSC Advances*, v. 6, n. 60, p. 55608–55617, 2016.

PENN, R. L. Kinetics of oriented aggregation. *Journal of Physical Chemistry B*, v. 108, n. 34, p. 12707–12712, 2004.

PEZOTI, O. *et al.* NaOH-activated carbon of high surface area produced from guava seeds as a high-efficiency adsorbent for amoxicillin removal: Kinetic, isotherm and thermodynamic studies. *Chemical Engineering Journal*, v. 288, p. 778–788, mar. 2016. Disponível em: <http://dx.doi.org/10.1016/j.cej.2015.12.042>.

PINNEY, N.; MORGAN, D. Ab initio study of structurally bound water at cation vacancy sites in Fe- and Al-oxyhydroxide materials. *Geochimica et Cosmochimica Acta*, v. 114, p. 94–111, 2013a. Disponível em: <http://dx.doi.org/10.1016/j.gca.2013.03.032>.

PINNEY, N.; MORGAN, D. Thermodynamics of Al-substitution in Fe-oxyhydroxides.

Geochimica et Cosmochimica Acta, v. 120, p. 514–530, 2013b. Disponível em: <http://dx.doi.org/10.1016/j.gca.2013.05.045>.

PINTO, P. S. *et al.* Role of [FeOx(OH)y] surface sites on the adsorption of β-lactamic antibiotics on Al2O3 supported Fe oxide. *Journal of Hazardous Materials*, v. 317, p. 327–334, 2016. Disponível em: <http://dx.doi.org/10.1016/j.jhazmat.2016.05.095>.

PINTO, P. S.; LANZA, G. D.; LAGO, R. M. Controlled Dehydration of Fe(OH) 3 to Fe 2 O 3 : Developing Mesopores with Complexing Iron Species for the Adsorption of β - Lactam Antibiotics. v. 30, n. 2, p. 310–317, 2019.

PRASAD PANDA, A. *et al.* Understanding the As(III) oxidative performance of MnO2 polymorphs (α, β, and γ) and synthesis of an efficient nanocomposite of iron ore slime derived 2-line ferrihydrite and γ-MnO2 for sequestration of total arsenic from aqueous solution. *Chemical Engineering Journal*, v. 442, n. P1, p. 136075, ago. 2022. Disponível em: <https://doi.org/10.1016/j.cej.2022.136075>.

PUTRA, E. K. *et al.* Performance of activated carbon and bentonite for adsorption of amoxicillin from wastewater: Mechanisms, isotherms and kinetics. *Water Research*, v. 43, n. 9, p. 2419–2430, 2009. Disponível em: <http://dx.doi.org/10.1016/j.watres.2009.02.039>.

RAPPE, A. K. *et al.* UFF, a full periodic table force field for molecular mechanics and molecular dynamics simulations. *Journal of the American Chemical Society*, v. 114, n. 25, p. 10024–10035, 1 dez. 1992. Disponível em: <https://pubs.acs.org/doi/abs/10.1021/ja00051a040>.

RODRIGUEZ-HERRERA, R. *et al. Enzymes in the Pharmaceutical Industry for β - Lactam Antibiotic Production*. [S.l.]: Elsevier Inc., 2019. Disponível em: <https://doi.org/10.1016/B978-0-12-813280-7.00036-0>.

ROUQUEROL, J.; LLEWELLYN, P.; ROUQUEROL, F. Is the bet equation applicable to microporous adsorbents? [S.l: s.n.], 2007. p. 49–56. Disponível em: <https://linkinghub.elsevier.com/retrieve/pii/S0167299107800085>.

ROUT, K.; MOHAPATRA, M.; ANAND, S. 2-Line ferrihydrite: Synthesis, characterization and its adsorption behaviour for removal of Pb(ii), Cd(ii), Cu(ii) and Zn(ii) from aqueous solutions. *Dalton Transactions*, v. 41, n. 11, p. 3302–3312, 2012.

RUAN, H. D. *et al.* Infrared spectroscopy of goethite dehydroxylation. II. Effect of

aluminium substitution on the behaviour of hydroxyl units. *Spectrochimica Acta - Part A Molecular and Biomolecular Spectroscopy*, v. 58, n. 3, p. 479–491, 2002.

RUAN, H. D.; GILKES, R. J. Dehydroxylation of Aluminous Goethite: Unit Cell Dimensions, Crystal Size and Surface Area. *Clays and Clay Minerals*, v. 43, n. 2, p. 196–211, 1995. Disponível em: <http://www.clays.org/journal/archive/volume 43/43-2-196.pdf>.

SALVIANO, A. B. *et al.* Iron oxide nanoparticles supported on mesoporous mcm-41 for efficient adsorption of hazardous β-lactamic antibiotics. *Water, Air, and Soil Pollution*, v. 229, n. 3, p. 1–14, 2018.

SASSI, M.; CHAKA, A. M.; ROSSO, K. M. Ab initio thermodynamics reveals the nanocomposite structure of ferrihydrite. *Communications Chemistry*, v. 4, n. 1, p. 134, 20 dez. 2021. Disponível em: <http://dx.doi.org/10.1038/s42004-021-00562-7>.

SCHMIDT, M. W. *et al.* General atomic and molecular electronic structure system. *Journal of Computational Chemistry*, v. 14, n. 11, p. 1347–1363, 1 nov. 1993. Disponível em: <https://pubs.acs.org/doi/10.1021/ct600312f>.

SCHWERTMANN, U. *et al.* INFLUENCE OF ALUMINUM ON IRON OXIDES - 2. PREPARATION AND PROPERTIES OF Al-SUBSTITUTED HEMATITES. *Clays and Clay Minerals*, v. 27, n. 2, p. 105–112, 1979.

SCHWERTMANN, U; MURAD, E. EFFECT OF pH ON THE FORMATION OF GOETHITE AND.pdf. v. 31, n. 4, p. 277–284, 1983.

SCHWERTMANN, UDO *et al.* The effect of Al on Fe oxides. XIX. Formation of Al-substituted hematite from ferrihydrite at 25°C and pH 4 to 7. *Clays and Clay Minerals*, v. 48, n. 2, p. 159–172, 2000.

SCHWERTMANN, UDO; FRIEDL, J.; KYEK, A. Formation and properties of a continuous crystallinity series of synthetic ferrihydrites (2- to 6-line) and their relation to FeOOH forms. *Clays and Clay Minerals*, v. 52, n. 2, p. 221–226, 2004.

SCHWERTMANN, UDO; FRIEDL, J.; STANJEK, H. From Fe(III) Ions to Ferrihydrite and then to Hematite. *Journal of Colloid and Interface Science*, v. 209, n. 1, p. 215–223, jan. 1999. Disponível em: <https://linkinghub.elsevier.com/retrieve/pii/S0021979798958994>.

SEEHRA, M. S. *et al.* Structural investigations of synthetic ferrihydrite nanoparticles

doped with Si. *Solid State Communications*, v. 130, n. 9, p. 597–601, 2004.

SHERMAN, D. M.; RANDALL, S. R. Surface complexation of arsenic(V) to iron(III) (hydr)oxides: Structural mechanism from ab initio molecular geometries and EXAFS spectroscopy. *Geochimica et Cosmochimica Acta*, v. 67, n. 22, p. 4223–4230, 2003.

SHI, Q.; JING, C.; MENG, X. Competing Interactions of As Adsorption and Fe(III) Polymerization during Ferric Coprecipitation Treatment. *Environmental Science and Technology*, v. 52, n. 13, p. 7343–7350, 2018.

SILVA, J. *et al.* The role of Al-Goethites on arsenate mobility. *Water Research*, v. 44, n. 19, p. 5684–5692, 2010.

SMEDLEY, P. L.; KINNIBURGH, D. G. A review of the source, behaviour and distribution of arsenic in natural waters. *Applied Geochemistry*, v. 17, p. 517–568, 2002.

SOLDOOZY, S. *et al.* In Situ and Real-Time ATR-FTIR Temperature-Dependent Adsorption Kinetics Coupled with DFT Calculations of Dimethylarsinate and Arsenate on Hematite Nanoparticles. *Langmuir*, v. 36, n. 16, p. 4299–4307, 28 abr. 2020. Disponível em: <https://pubs.acs.org/doi/10.1021/acs.langmuir.0c00252>.

SOLTIS, J. A. *et al.* Phase Transformation and Particle-Mediated Growth in the Formation of Hematite from 2-Line Ferrihydrite. *Crystal Growth and Design*, v. 16, n. 2, p. 922–932, 2016.

SOUZA, T. G. F. *et al.* Defects induced by Al substitution enhance As (V) adsorption on ferrihydrites. *Journal of Hazardous Materials*, v. 420, n. January, p. 126544, 2021.

THOMMES, M. *et al.* Physisorption of gases, with special reference to the evaluation of surface area and pore size distribution (IUPAC Technical Report). *Pure and Applied Chemistry*, v. 87, n. 9–10, p. 1051–1069, 1 out. 2015. Disponível em: <http://www.degruyter.com/view/j/pac.2015.87.issue-9-10/pac-2014-1117/pac-2014-1117.xml>.

TRAN, H. N.; WANG, Y. F.; *et al.* Insights into the mechanism of cationic dye adsorption on activated charcoal: The importance of Π–Π interactions. *Process Safety and Environmental Protection*, v. 107, p. 168–180, 2017.

TRAN, H. N.; YOU, S.-J.; *et al.* Mistakes and inconsistencies regarding adsorption of contaminants from aqueous solutions: A critical review. *Water Research*, v. 120, p.

88–116, set. 2017. Disponível em: <http://dx.doi.org/10.1016/j.watres.2017.04.014>.

TRI, N. N.; NGUYEN, M. T.; TRUNG, N. T. A molecular level insight into adsorption of β-lactam antibiotics on vermiculite surface. *Surface Science*, v. 695, n. February, p. 121588, maio 2020. Disponível em: <https://doi.org/10.1016/j.susc.2020.121588>.

TUFO, A. E.; AFONSO, M. DOS S.; SILEO, E. E. Arsenic adsorption onto aluminium-substituted goethite. *Environmental Chemistry*, v. 13, n. 5, p. 838, 2016.

TÜYSÜZ, H. *et al.* Synthesis and Magnetic Investigation of Ordered Mesoporous Two-Line Ferrihydrite. *Journal of the American Chemical Society*, v. 130, n. 1, p. 280–287, jan. 2008. Disponível em: <https://pubs.acs.org/doi/10.1021/ja075528j>.

USEPA. Microwave assisted acid digestion of sediments, sludges, soils and oils - Method 3051a. p. 30, 2007. Disponível em: <http://digilib.unila.ac.id/11478/16/16. BAB II.pdf>.

USEPA. *Preparation of soil sampling protocols: Sampling techniques and strategies*. *Other Information: See also PB--83-206979*. [S.l: s.n.], 1992.

VEGARD, V. L. Die Konstitution der Mischkristalle und die Raumffillung der Atome. *Z. Physik*, v. 5, p. 17–21, 1921.

VIOLANTE, A. *et al.* Coprecipitation of Arsenate with Metal Oxides: Nature, Mineralogy, and Reactivity of Aluminum Precipitates. *Environmental Science & Technology*, v. 40, n. 16, p. 4961–4967, 2009. Disponível em: <http://pubs.acs.org/doi/abs/10.1021/es052321m>.

VIRARAGHAVAN, T.; SUBRAMANIAN, K. S.; ARULDOSS, J. A. Arsenic in drinking water - Problems and solutions. *Water Science and Technology*, v. 40, n. 2, p. 69–76, 1999. Disponível em: <http://dx.doi.org/10.1016/S0273-1223(99)00432-1>.

WANG, S. *et al.* Accurate determination of the As(v) coordination environment at the surface of ferrihydrite using synchrotron extended X-ray absorption fine structure spectroscopy and: Ab initio Debye-Waller factors. *Environmental Science: Nano*, v. 6, n. 8, p. 2441–2451, 2019.

WANG, W. *et al.* Facet-dependent adsorption of aluminum(<scp>iii</scp>) on hematite nanocrystals and the influence on mineral transformation. *Environmental Science: Nano*, v. 9, n. 6, p. 2073–2085, 2022. Disponível em: <http://xlink.rsc.org/?DOI=D2EN00062H>.

WANG, Z. *et al.* Coprecipitated arsenate inhibits thermal transformation of 2-line ferrihydrite: Implications for long-term stability of ferrihydrite. *Chemosphere*, v. 122, p. 88–93, mar. 2015.

WAYCHUNAS, G. A. *et al.* Surface chemistry of ferrihydrite: Part 1. EXAFS studies of the geometry of coprecipitated and adsorbed arsenate. *Geochimica et Cosmochimica Acta*, v. 57, n. 10, p. 2251–2269, 1993.

WAYCHUNAS, GLENN A.; DAVIS, J. A.; FULLER, C. C. Geometry of sorbed arsenate on ferrihydrite and crystalline FeOOH: Re-evaluation of EXAFS results and topological factors in predicting sorbate geometry, and evidence for monodentate complexes. *Geochimica et Cosmochimica Acta*, v. 59, n. 17, p. 3655–3661, 1995.

WAYCHUNAS, GLENN A.; KIM, C. S.; BANFIELD, J. F. Nanoparticulate iron oxide minerals in soils and sediments: Unique properties and contaminant scavenging mechanisms. *Journal of Nanoparticle Research*, v. 7, n. 4–5, p. 409–433, 2005.

WILKIE, J. A.; HERING, J. G. Adsorption of arsenic onto hydrous ferric oxide: Effects of adsorbate/adsorbent ratios and co-occurring solutes. *Colloids and Surfaces A: Physicochemical and Engineering Aspects*, v. 107, p. 97–110, 1996.

WOLSKA, E.; SZAJDA, W.; PISZORA, P. Effect of the anionic sublattice hydroxylation on the goethite → maghemite transformation in the AlxFe1-xOOH system. *Materials Letters*, v. 21, n. 2, p. 191–195, 1994.

XIE, A. *et al.* Ultrahigh adsorption of typical antibiotics onto novel hierarchical porous carbons derived from renewable lignin via halloysite nanotubes-template and in-situ activation. *Chemical Engineering Journal*, v. 304, p. 609–620, nov. 2016. Disponível em: <http://dx.doi.org/10.1016/j.cej.2016.06.138>.

XIU, W. *et al.* Change of arsenite adsorption mechanism during aging of 2-line ferrihydrite in the absence of oxygen. *Applied Geochemistry*, v. 88, p. 149–157, 2018. Disponível em: <https://doi.org/10.1016/j.apgeochem.2017.08.001>.

XUE, Q. *et al.* Arsenite and arsenate binding to ferrihydrite organo-mineral coprecipitate: Implications for arsenic mobility and fate in natural environments. *Chemosphere*, v. 224, p. 103–110, 2019. Disponível em: <https://doi.org/10.1016/j.chemosphere.2019.02.118>.

YANG, L.; DONAHOE, R. J. The form, distribution and mobility of arsenic in soils

contaminated by arsenic trioxide, at sites in southeast USA. *Applied Geochemistry*, v. 22, n. 2, p. 320–341, 2007.

YANG, Z. *et al.* Stability of Fe–As composites formed with As(V) and aged ferrihydrite. *Journal of Environmental Sciences (China)*, v. 100, p. 43–50, 2021a. Disponível em: <https://doi.org/10.1016/j.jes.2020.07.015>.

YANG, Z. *et al.* Stability of Fe–As composites formed with As(V) and aged ferrihydrite. *Journal of Environmental Sciences*, v. 100, p. 43–50, fev. 2021b. Disponível em: <https://doi.org/10.1016/j.jes.2020.07.015>.

YAZIDI, A. *et al.* Adsorption of amoxicillin and tetracycline on activated carbon prepared from durian shell in single and binary systems: Experimental study and modeling analysis. *Chemical Engineering Journal*, v. 379, n. July 2019, 2020.

YE, C. *et al.* Influence of Al(III) and Sb(V) on the transformation of ferrihydrite nanoparticles: Interaction among ferrihydrite, coprecipitated Al(III) and Sb(V). *Journal of Hazardous Materials*, n. October, p. 124423, out. 2020. Disponível em: <https://doi.org/10.1016/j.jhazmat.2020.124423>.

YE, J. *et al.* Emerging sustainable technologies for remediation of soils and groundwater in a municipal solid waste landfill site -- A review. *Chemosphere*, v. 227, p. 681–702, jul. 2019. Disponível em: <https://doi.org/10.1016/j.chemosphere.2019.04.053>.

YU, G. *et al.* Behaviors and fate of adsorbed Cr(VI) during Fe(II)-induced transformation of ferrihydrite-humic acid co-precipitates. *Journal of Hazardous Materials*, v. 392, p. 122272, jun. 2020. Disponível em: <https://linkinghub.elsevier.com/retrieve/pii/S0304389420302600>.

ZHA, S. XING *et al.* The removal of amoxicillin from wastewater using organobentonite. *Journal of Environmental Management*, v. 129, p. 569–576, nov. 2013. Disponível em: <http://dx.doi.org/10.1016/j.jenvman.2013.08.032>.

ZHANG, S.; LI, X.; CHEN, J. P. An XPS study for mechanisms of arsenate adsorption onto a magnetite-doped activated carbon fiber. *Journal of Colloid and Interface Science*, v. 343, n. 1, p. 232–238, mar. 2010. Disponível em: <http://dx.doi.org/10.1016/j.jcis.2009.11.001>.

ZHAO, J. *et al.* Ferrihydrite: Surface Structure and its Effects on Phase

Transformation. *Clays and Clay Minerals*, v. 42, n. 6, p. 737–746, 1994. Disponível em: <http://link.springer.com/10.1346/CCMN.1994.0420610>.

ZHENG, G. *et al.* Parameter Calibration of Transition-Metal Elements for the Spin-Polarized Self-Consistent-Charge Density-Functional Tight-Binding (DFTB) Method: Sc, Ti, Fe, Co, and Ni. *Journal of Chemical Theory and Computation*, v. 3, n. 4, p. 1349–1367, 1 jul. 2007. Disponível em: <https://pubs.acs.org/doi/10.1021/ct600312f>.

ZIBORDI-BESSE, L. *et al.* Ethanol and Water Adsorption on Transition-Metal 13-Atom Clusters: A Density Functional Theory Investigation within van der Waals Corrections. *Journal of Physical Chemistry A*, v. 120, n. 24, p. 4231–4240, 2016.

ZOPPI, A. *et al.* Al-for-Fe substitution in hematite: the effect of low Al concentrations in the Raman spectrum of Fe2O3. *Journal of Raman Spectroscopy*, v. 39, n. 1, p. 40–46, jan. 2008. Disponível em: <http://onlinelibrary.wiley.com/doi/10.1002/jrs.1831/abstract>.

APPENDIX A- CHAPTER 3 SUPPLEMENTARY INFORMATION

Table A.1: As(V) adsorption on AlFh-0 and AlFh-10 evaluated during 200 h, pH5 and 25 ^{o}C. Starting As (V) concentration of 10 mg L^{-1} and 0.1 M $NaNO_3$.

Time (h)	Adsorbed Arsenate (mean values) (mmol/m²)	
	AlFh-0	AlFh-10
0	0	0
1	0.00438	0.00438
3	0.00431	0.00453
6	0.00439	0.00485
10.5	0.00462	0.00476
22.5	0.00507	0.00532
34.5	0.00454	0.00533
47.25	0.00518	0.00547
72.75	0.00517	0.00576
96.75	0.0051	0.00552
120	0.0058	0.00603
191.5	0.00555	0.00611

Table A.2: Maxima adsorption capacity (Γmax), Langmuir constant (K_L), and determination coefficient (R^2) of the nonlinear fit to the Langmuir model for arsenate adsorption onto different AlFh samples. The R^2 for the fit to the Freundlich model is also presented. Experimental conditions were pH 5 and 8 ± 0.3, adsorbent mass 2.5 mg, initial concentrations of As varying from 0.1 to 0.7 mM, ionic strength 100 mM $NaNO_3$, equilibration time 150 h.

Sample	pH 5				pH 8			
	Γ_{max} (µmol.m^{-2})	K_L (kg. µmol^{1})	R^2_L	R^2_F	Γ_{max} (µmol.m^{-2})	K_L (kg. µmol^{-1})	R^2_L	R^2_F
AlFh-0	6.7 ± 0.4	0.55 ± 0.23	0.930	0.769	4.2 ± 0.1	0.27 ± 0.10	0.982	0.764
AlFh-5	6.7 ± 0.4	0.22 ± 0.08	0.938	0.773	4.4 ± 0.2	0.17 ± 0.06	0.971	0.656
AlFh-10	7.2 ± 0.4	0.18 ± 0.06	0.945	0.777	4.9 ± 0.1	0.13 ± 0.01	0.999	0.993
AlFh-15	8.6 ± 0.5	0.08 ± 0.02	0.930	0.773	5.1 ± 0.1	0.10 ± 0.01	0.997	0.998
AlFh-20	7.4 ± 0.4	0.17 ± 0.05	0.960	0.890	5.1 ± 0.1	0.08 ± 0.01	0.993	0.844

Table A.3: Relative area of deconvoluted peaks from XPS O (1s) scan of AlFh-X before As(V) adsorption.

Sample	Peak I (M-O)		Peak II (M-OH)		Peak III (H_2O)	
	Center (eV)	Area (%)	Center (eV)	Area (%)	Center (eV)	Area (%)
AlFh-0	529.0	50	530.4	45	532.5	5
AlFh-5	528.9	42	530.3	52	532.5	6
AlFh-10	529.0	24	530.3	70	532.5	5
AlFh-15	529.0	20	530.4	76	532.5	4
AlFh-20	529.2	21	530.7	77	532.5	2

Table A.4: Relative area of deconvoluted peaks from XPS As (3d) scan of AlFh-X after As(V) adsorption.

Sample	Peak I		Peak II	
	Center (eV)	Area (%)	Center (eV)	Area (%)
AlFh-0_As	44.6	99	46.5	1
AlFh-5_As	44.6	92	46.5	8
AlFh-15_As	44.7	85	46.5	15

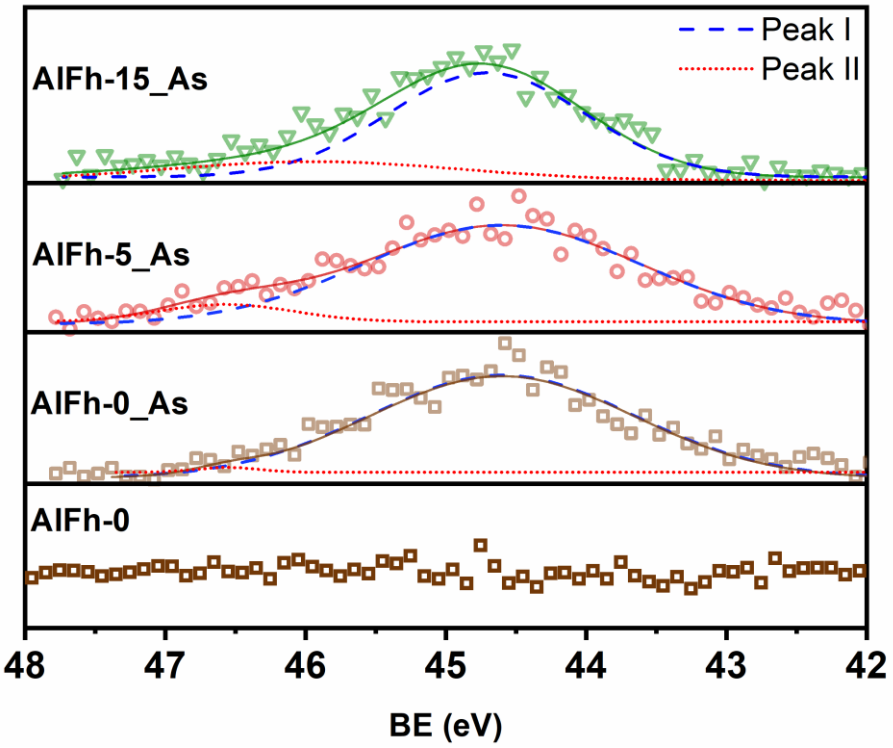

Figure A.1: XPS As (3d) scan of AlFh-X before and after As adsorption.

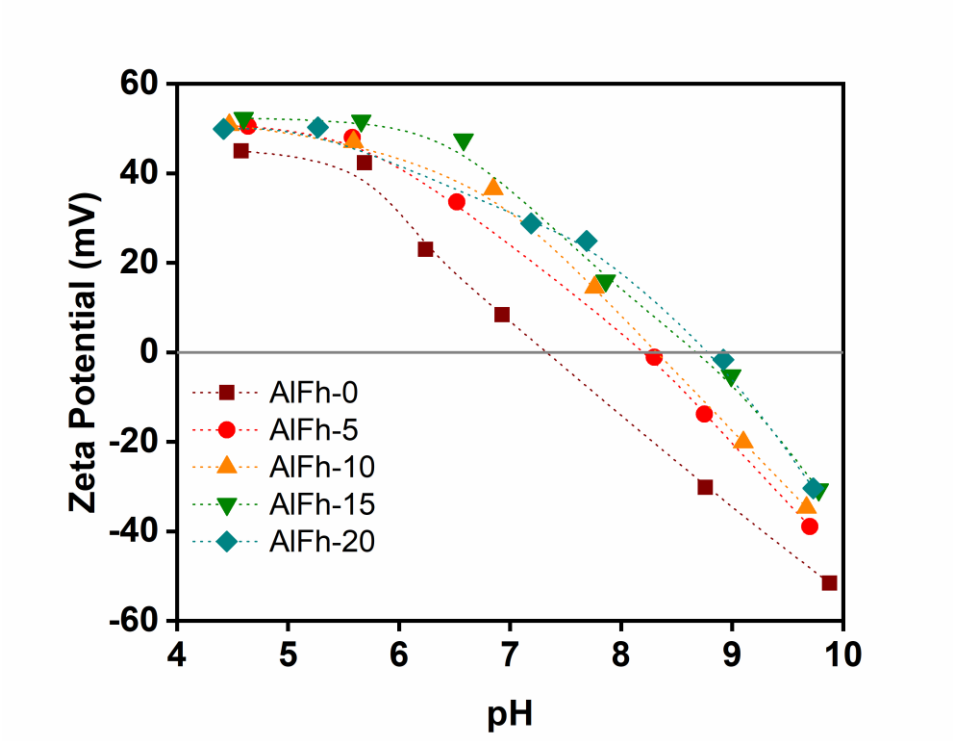

Figure A.2: Zeta potential of samples AlFh-X measured as function of pH.

APPENDIX B- CHAPTER 4 SUPPLEMENTARY INFORMATION

Adsorption isotherm

Langmuir, Freundlich and Liu isotherms are expressed in equations 1, 2 and 3 respectively.

$$q_e = \frac{q_{max} C_e K_L}{(1+K_L C_e)} \quad (1)$$

$$q_e = K_F C_e^{1/n_F} \quad (2)$$

$$q_e = \frac{q_{max}(C_e K_g)^{n_L}}{1+(C_e K_g)^{n_L}} \quad (3)$$

The various parameters of the equations are defined as follow; C_e is the equilibrium concentration in solution (mg L^{-1}), q_e is the amount of AMX adsorbed (mg g^{-1}), q_{max} is the maximum adsorption capacity (mg g^{-1}), K_L is Langmuir equilibrium constant (L mg^{-1}), K_F is the Freundlich constant (mg g^{-1} (mg $L^{-1})^{-1/nF}$), K_g is the Liu equilibrium constant (L mg^{-1}), n_F and n_L are the dimensionless exponent of Freundlich and Liu models, respectively.

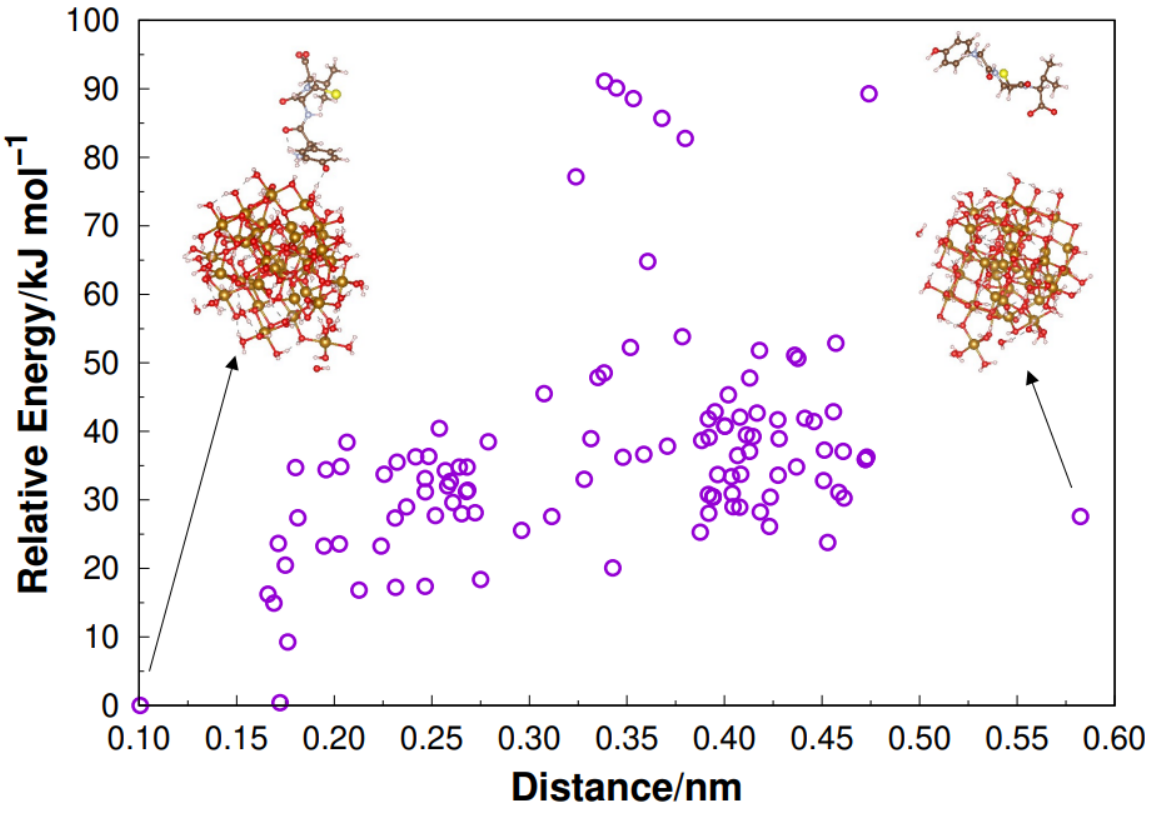

Figure B1: Relative energy of several physisorbed configurations as a functions of the particle-molecule distance.

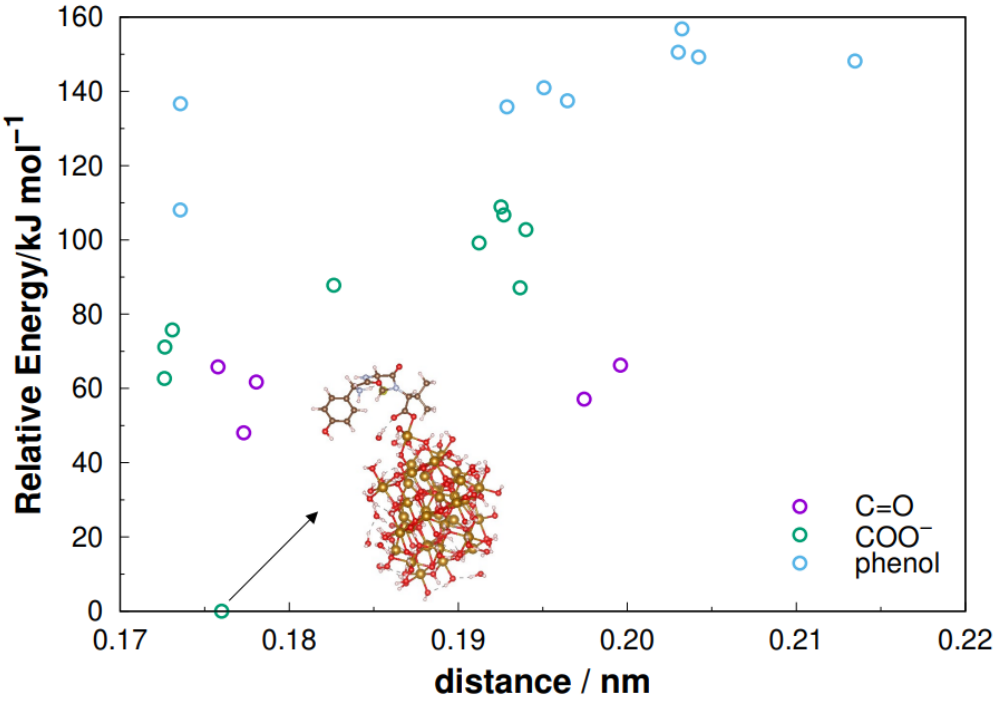

Figure B2: Relative energy of several monodentated adsorption configurations including a Fe-molecule chemical bond. Each color represents a different binding group in the molecule.

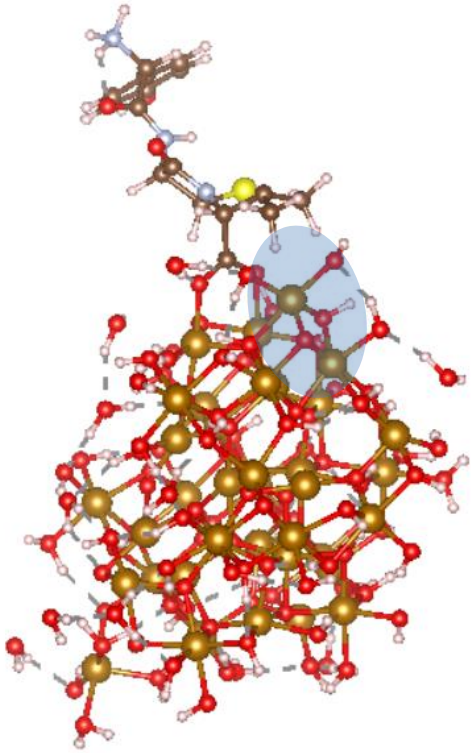

Figure B3: Computational predictions of CH_3-particle interaction.

Table B1: AMX adsorption in reuse tests and ASA_{BET} after calcination

Sample	Adsorption (mg g^{-1})- Cycles			ASA_{BET} (m^2 g^{-1})	Pore volume (cm^3/g)	Median pore size (nm)
	1	2	3			
Fh-0%Al	56	7	7	40 ± 3	0.130	14
Fh-10%Al	44	7	5	72 ± 7	0.165	9

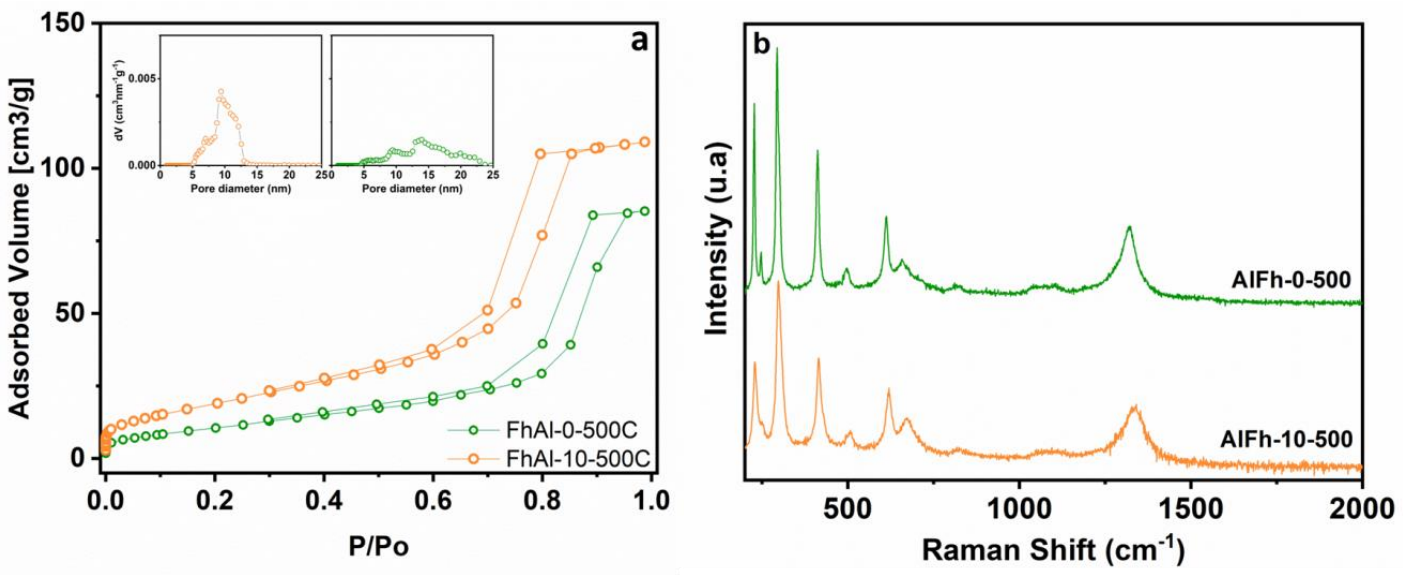

Figure B4: Isotherms of N_2 adsorption (a) and Raman spectra (b) from AMX adsorbed ferrihydrites after calcination.

APPENDIX C- CHAPTER 5 SUPPLEMENTARY INFORMATION

Table C.1: SEP conditions

Step	Fraction	Reagent	Procedure
1	Soluble	600 mL deionized water	Shaker/1h-25°C
2	Weakly bound As	25 mL 1 M $NaNO_3$	Shaker/1h-25°C
3	pH 5 acetate-soluble (Ca-oxides; Ca-arsenates)	25 mL NaOAc/HOAc (pH 5)	Shaker/1h-25°C
4	Strongly adsorbed	25 mL 0.1 M Na_2HPO_4/HNO_3 (pH 5)	Shaker/1h-70°C
5	Low-Crystallinity Iron oxyhydroxides (e.g. Ferrihydrite)	25 mL 0.4 M $NH_2OH.HCl$/0.25 M HCl	Shaker/1.5h-70°C
6	Crystalline Iron oxides/ hydroxides (e.g. hematite and goethite)	25 mL 4.2 M HCl/Asc. Ac. 0.66%/Na-citrate 0.88%	Shaker/2.5h-80°C
7	Residual	HCl/HNO_3/HF ¼ (4:2:2)mL	Micro-Wave digestion

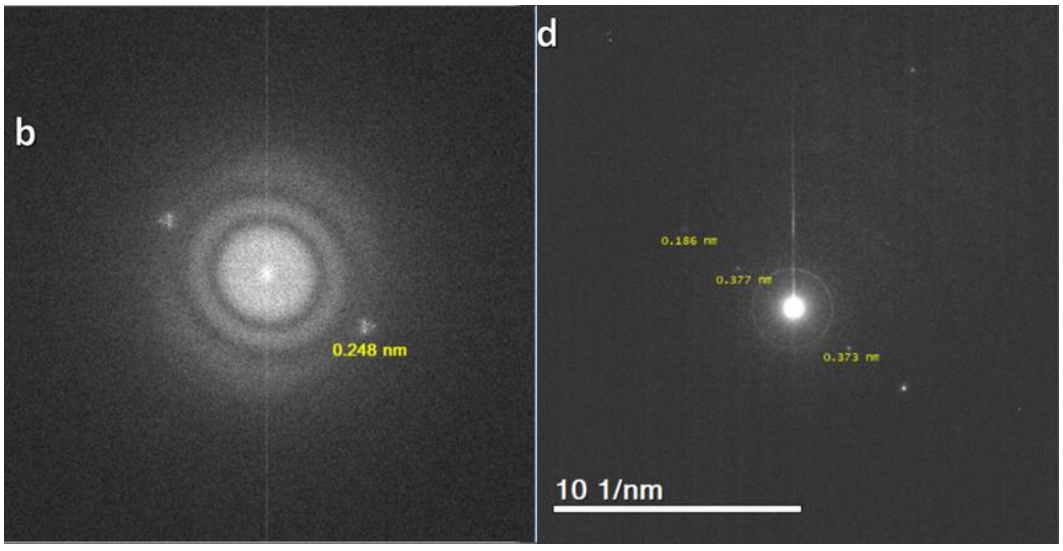

C.1: FFT of HRTEM of sample FhAl-0%-130d (b) and zero-loss filtered SAD of the sample FhAl-10%-130d (d) showing the presence of hematite mesocrystal $D_{(1,0,-2)}$= 0,368 nm.

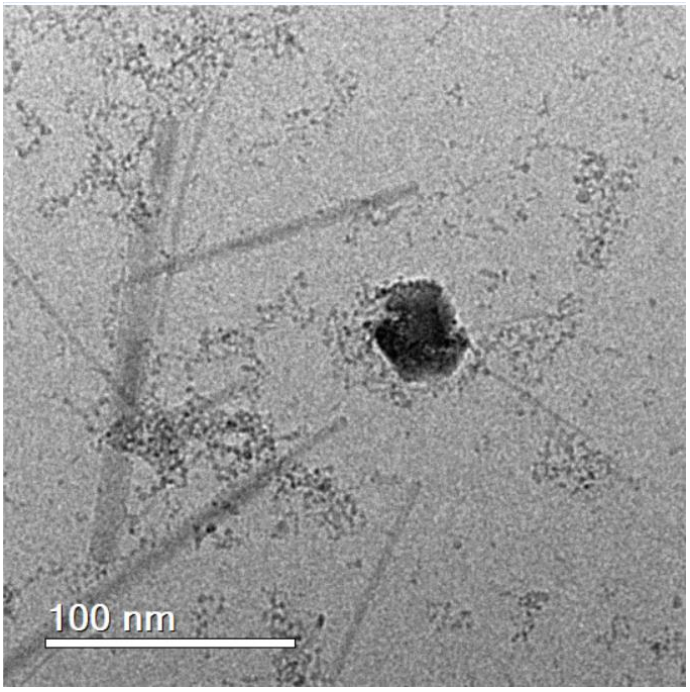

C.2: TEM of the sample FhAl-0%-130d.

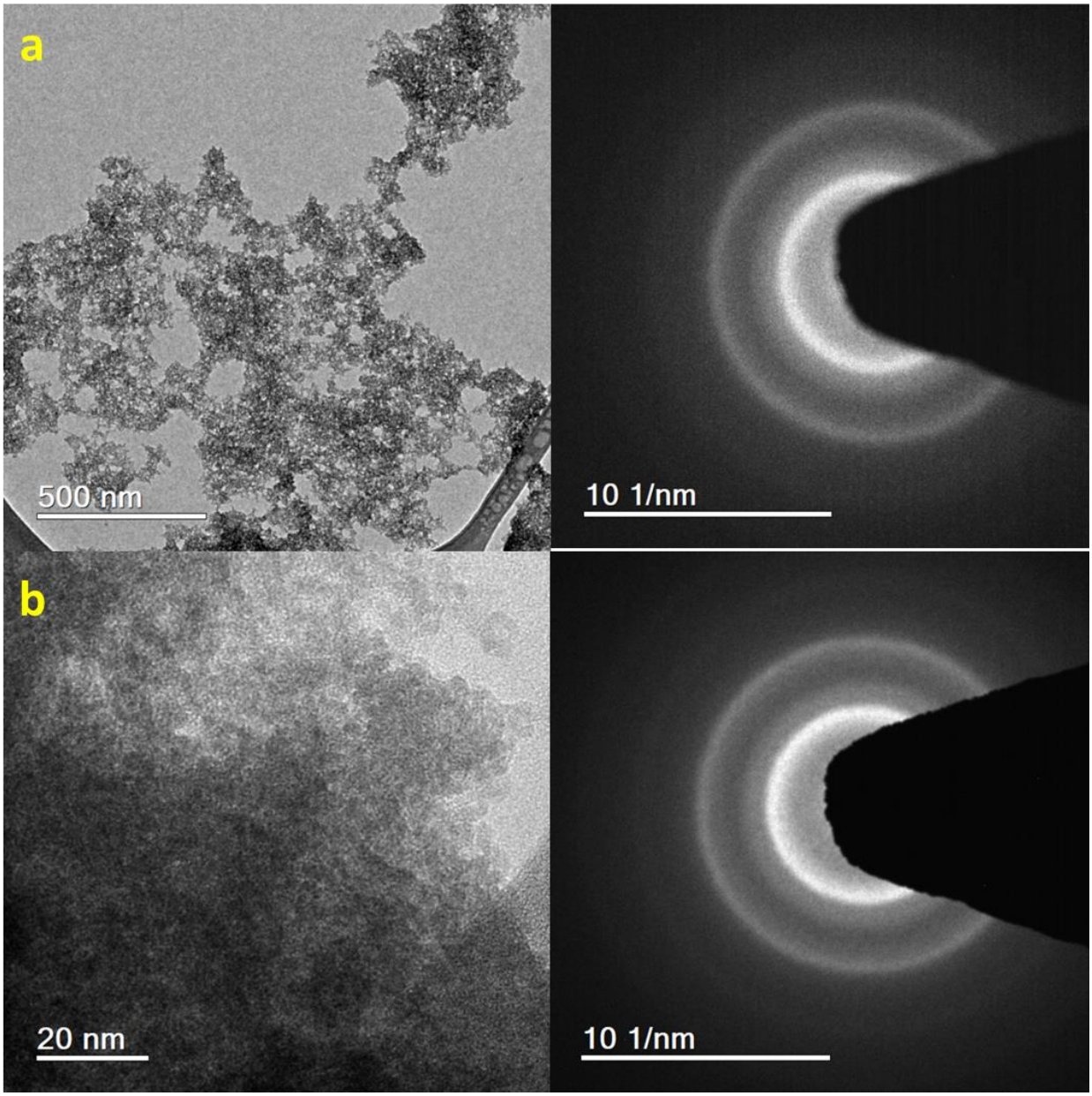

C.3: TEM images from the sample FhAl-0% and its SAD after aging for 30 (a) and 210 days (b).

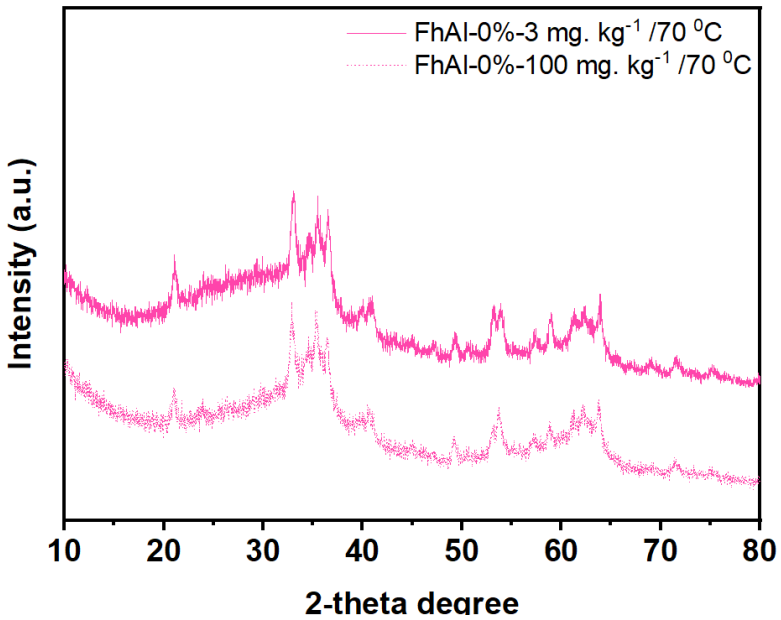

C.4: XRD from the sample FhAl-0%- 3/70 aged for 4 days and FhAl-0%- 100/70 aged for 20 days.

Table C.2: Phase distribution calculated by Rietiveld refinement

Sample	Fh (%m/m)	Hematite (%m/m)	Goetite (%m/m)
FhAl-0%-3-4d	67	16	17
FhAl-5%-3-8d	67	33	0
FhAl-10%-3-16d	71	29	0
FhAl-0%-100-20d	68	15	17
FhAl-5%-100-80d	69	31	0

Table C.3: Mineralogical characterization and Al distribuition through mineralogical phases by MLA

Sample	**K23**	**K22**	**K21**	**K40**	**K48**	**K06**
Mineral	Wt%	Wt%	Wt%	Wt%	Wt%	Wt%
Unknown	0.00	0.00	0.00	0.00	0.00	0.00
Low_Counts	0.00	0.00	0.00	0.00	0.00	0.00
No_XRay	0.00	0.00	0.00	0.00	0.00	0.00
Quartz	31.86	21.40	49.12	55.82	28.22	6.19
Fe Oxides/Hydroxides	23.77	29.58	1.37	1.41	6.68	0.71
Fe Oxides/Hydroxides-As	19.86	7.62	4.11	0.24	4.41	0.15
Anatase/Rutile	0.37	0.29	1.62	0.28	0.69	0.33
Monazite-(La)	0.47	0.31	0.60	0.07	0.13	0.01
Ilmenite	3.66	1.40	2.71	0.94	4.21	0.19
Pyrite	0.07	0.00	0.11	0.01	0.00	0.01
Arsenopyrite	0.00	0.00	0.00	0.00	0.00	0.00
Scorodite	0.00	0.00	0.00	0.00	0.00	0.00
Tourmaline	0.46	0.20	0.51	0.42	0.47	1.85
Mica/Clay Minerals	18.88	35.19	36.85	38.83	50.66	84.13
Zircon	0.53	0.46	0.04	0.04	0.06	0.15
Microcline	0.05	3.53	2.96	1.94	4.45	6.29
Total	100.0	100.0	100.0	100.0	100.0	100.0
Al-content in Fe Oxides/Hydroxides (%)	0	0	0	0	0	0
Al-content in Fe Oxides/Hydroxides-As (%)	0.938	0.379	0.182	0.028	0.196	0.007

APPENDIX D- ABSTRACT OF PUBLICATIONS IN COLLABORATION

EFEITO DO ENVELHECIMENTO NA OXIDAÇÃO DA ARSENOPIRITA[3]

Coelho, M.L.S. *, Souza, T.G.F., Coutinho, N.A.F.S., Caldeira, C.L., Ciminelli, V.S.T..**
Universidade Federal de Minas Gerais, Dept. de Engenharia Metalúrgica e de Materiais
Instituto Nacional de Ciência e Tecnologia em Recursos Minerais, Água e Biodiversidade – INCT-Acqua *e-mail: marina_luizacoelho@hotmail.com **ciminelli@demet.ufmg.br

Resumo

O estudo da cinética de oxidação da arsenopirita é de fundamental importância para elucidar as condições de estabilidade e de mobilização do arsênio no ambiente. O propósito dessa pesquisa consistiu na investigação do efeito do envelhecimento na liberação de arsênio de uma amostra de arsenopirita (FeAsS). Os ensaios foram conduzidos em coluna, sob fluxo contínuo por 24h, em meio circumneutro a alcalino (pH 5, 7 e 11) saturado em oxigênio para o material fresco e envelhecido em condições ambientais. A taxa de liberação do arsênio em pH 7 foi cerca de cinco vezes inferior ($10^{-9,3}$ mol.m^{-2}.s^{-1}) àquela observada em pH 5 ($10^{-8,8}$ mol.m^{-2}.s^{-1}) e pH 11 ($10^{-8,7}$ mol.m^{-2}.s^{-1}). A liberação de arsênio do material envelhecido foi cerca de 10 vezes superior à liberação do material fresco nas mesmas condições. Sugere-se que a dissolução de espécies oxidadas presentes na amostra de arsenopirita envelhecida aumentem a disponibilidade de Fe(III), mesmo em condições de pH em que essa espécie é insolúvel, favorecendo assim maior oxidação do sulfeto.

Palavras-chave: Envelhecimento, liberação de arsênio, arsenopirita, reatividade, oxidação.

Abstract

The study of the oxidation kinetics of arsenopyrite is of fundamental importance to elucidate the conditions of stability and the mobilization of arsenic in the environment. The purpose of this research was to investigate the effect of ageing on the release of arsenic from a sample of arsenopyrite (FeAsS). The tests were run in a column, under continuous flow for 24h, in an acid and alkaline medium (pH 5, 7 and 11) saturated in oxygen to fresh and aged material under ambient conditions. The rate of release of arsenic at pH 7 was about five times lower ($10^{-9,3}$ mol.m^{-2}.s^{-1}) than that observed at pH 5 ($10^{-8,8}$ mol.m^{-2}.s^{-1}) and pH 11 ($10^{-8,7}$ mol.m^{-2}.s^{-1}). The release of arsenic from the aged material was about 10 times greater than the release of the fresh material under the same conditions. It is suggested that the dissolution of oxidized species present in the sample of aged arsenopyrite increases the availability of Fe (III), even under pH conditions in which this species is insoluble, thus favoring the greater oxidation of the sulfide.

Keywords: Ageing, arsenic release, arsenopyrite, reactivity, oxidation.

[3] Published at XXVIII Encontro Nacional de Tratamento de Minérios e Metalurgia Extrativa, Belo Horizonte-MG, November, 4-8th, 2019

TRANSMISSION ELECTRON MICROSCOPY TECHNIQUES APPLIED TO THE SOLID PHASE CHARACTERIZATION OF ENVIRONMENTAL SAMPLES [4]

Freitas, E.T.F.[1], Souza, T.G.F[2], Mohallem, N.D.S[3], Ciminelli, V.S.T [2,4]
[1]Universidade Federal de Minas Gerais (UFMG), Center of Microscopy.
[2]Universidade Federal de Minas Gerais (UFMG), Department of Metallurgical and Materials Engineering, Aquous Processing Laboratory.
[3]Universidade Federal de Minas Gerais (UFMG), Department of Chemistry
[4]National Institute of Science and Technology on Minerals Resources, Water and Biodiversity, INCT-Acqua. email: ciminelli@demet.ufmg.br

Resumo

A caracterização de amostras ambientais é muito complexa devido à presença de muitas fases cristalográficas, tamanhos de partículas e composição elementar em concentrações até o nível de traços. Dentre as técnicas disponíveis para análise e caracterização em fase sólida, a microscopia eletrônica de transmissão (MET) é única na investigação da composição elementar e de fases de amostras nanométricas e até mesmo em escala atômica. No entanto, as técnicas de MET não devem ser usadas em estudos exploratórios de fases sólidas, uma vez que uma pequena parte da amostra é investigada. Em vez disso, seria necessário análises anteriores na amostra *bulk*. Por outro lado, o TEM é uma técnica muito poderosa para caracterizar completamente as fases sólidas com altas resoluções analíticas e espaciais. Neste trabalho, imagens de transmissão de alta resolução, difração de elétrons, espectroscopia de dispersão de energia por raios X e espectroscopia de perda de energia de elétrons são brevemente descritas para mostrar seu potencial para a caracterização de amostras ambientais.

Palavras-chave: Caracterização, amostras ambientais, MET, composição química, composição cristalográfica.

Abstract

The characterization of environmental samples is very complex due to the presence of many crystallographic phases, particles sizes and elemental composition in concentrations down to trace level. Amongst the available techniques for solid phase analyses and characterization, transmission electron microscopy (TEM) is unique on the investigation of both elemental and phase composition of samples down to nanometer and even atomic scale. However, TEM techniques are not to be used in exploratory studies of solid phases because just a very small part of the sample is investigated. It would be necessary previous bulk analyses of the sample. On the other hand, TEM is a very powerful technique to thoroughly characterize solid phases with high spatial and analytical resolutions. In this work high-resolution transmission imaging, electron diffraction, energy dispersive X-ray spectroscopy, and electron energy-loss spectroscopy are briefly described to show their potential on the characterization of environmental samples.

Keywords: Characterization, environmental samples, TEM, chemical composition, crystallographic composition.

[4] Published at XXVIII Encontro Nacional de Tratamento de Minérios e Metalurgia Extrativa, Belo Horizonte-MG, November, 4-8th, 2019

THE MECHANISMS OF ADSORPTION AND PHOTO(DEGRADATION) OF PHARMACEUTICALS ON IRON-BASED MATERIALS: A COMPREHENSIVE REVIEW[5]

Sunday J. Olusegun[a*], Taiane G. F. Souza [b], Guilhermina de O. Souza [d], Osial Magdalena[a,e] Nelcy D.S. Mohallem [d], Virginia S.T. Ciminelli [b,c], Krysinski Pawel [a]**

[a] Faculty of Chemistry, University of Warsaw, Pasteur Street 1, 02-093 Warsaw, Poland
[b] Department of Metallurgical and Materials Engineering, Universidade Federal de Minas Gerais, Belo Horizonte - MG, Brazil
[c] Acqua Institute, Brazil
[d] Chemistry Department, Laboratório de Materiais Nanoestruturados, Universidade Federal de Minas Gerais, Belo Horizonte - MG, Brazil
[e]Department of the Theory of Continuous Media, Institute of Fundamental Technological Research, Polish Academy of Sciences, Pawinskiego 5B Street, 02-106 Warsaw, Poland

Graphical abstract

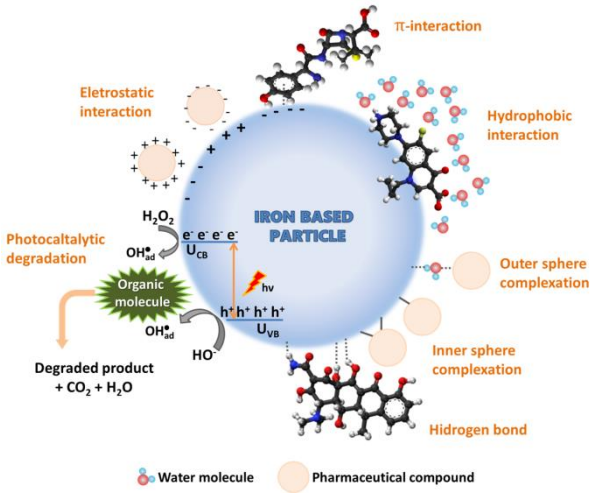

Abstract

Adsorption and photocatalytic degradation techniques for removing of various contaminants have received broad consideration and acceptance due to their advantages over conventional wastewater treatment techniques. Iron-based materials are among several groups of adsorbents, and photocatalysts that have proven to be effective in pharmaceuticals-based pollutants removal from wastewater. Besides unique physical properties like high surface area and specific affinity to particular compounds, some of them are biodegradable (or biocompatible) and can be easily separated by magnets after wastewater treatment for their further re-use. Pharmaceuticals removal is accompanied by several mechanisms, so there is a deep need for a better understanding of the complexity and development of the wastewater treatment within iron-based materials. Therefore, this review examined the mechanism of adsorption and photocatalysis degradation of the aqueous solutions of pharmaceuticals by iron-based materials. Fundamentals about mechanisms' complexity are also provided. We also addressed, the role of the material composition, and concentration used for effective water remediation. The overall idea of this review is to provide useful help to researchers on the mechanisms of adsorption and photocatalysis degradation of the selected pharmaceutical contaminants using iron-based materials. It summarizes the current understanding and the enhancement of the pharmaceutical treatment ways within nanostructure sorbents and catalysts, including the future development for a clean and safe environment.

[5] Manuscript submitted to Journal of Water Process Engineering, under revision.

REMOVAL AND SAFE DISPOSAL OF As(III) AND As(V) BY BIOSILICA BASED-FERRIHYDRITE[6]

Sunday J. Olusegun[a, b] *, Taiane G. F. Souza[a], Nelcy D. S. Mohallem[c], Virginia S. T. Ciminelli[a,b]**

[a] Department of Metallurgical and Materials Engineering,
[b] Acqua Institute, Brazil
[c] Chemistry Departament ,
Universidade Federal de Minas Gerais, Belo Horizonte - MG, Brazil
arewasegun@ufmg.br*; ciminelli@demet.ufmg.br**

Abstract

The ferrihydrite (Fh) 2-line and a composite of 2-line Fh and biosilica was synthetized and studied for the removal of As(III) and As(V). The biosilica was shown to increase specific surface area of the materials (251 and 281 m^2 g^{-1}) for samples with 0 and 15% of Si, respectively) and retard phase transformation when submitted to thermal treatments. The materials reach adsorption capacity better than most materials (140 and 86 mg kg^{-1}) for As(III) and As(V), respectively) following a kinetics of pseudo second order. The pH was shown to impact hugely on As (V) adsorption, but not on As (III), which is a oxyanion with charge zero in the pH of most adsorption. This results shows that the nature of interaction of As (III) and the Fh (containing or not biosilica) is not electrostatic. The products of adsorption were submitted to a thermal treatment (500 ^oC/ 2 h), which promoted the formation of ferric arsenate. The As adsorbed on Fh was shown to inhibit the phase transformation of Fh to hematite. The thermal treatment was shown also to oxide As(III) to As (V). The changes in the adsorption residues caused by the thermal treatment, as the formation of ferric arsenate, also impacted As mobility. The As associated with Fh increased from 42 to 95% of, by a sequential extraction protocol. Therefore, the proposed approach is an attractive alternative for As removal from aqueous solutions, by combining the high adsorption capacity of the adsorbent together with a residue treatment, which enables a safe disposal

[6] Manuscript in the final stage of preparation

BIOGRAFIA

Iniciei minha vida profissional aos 12 anos, criando modelos e costurando roupas no ateliê da minha mãe. Aprendi a costurar observando atentamente o que ela fazia e lendo revistas de modelagem. Acredito que neste momento se consolidavam na minha personalidade a curiosidade, a pro-atividade e o amor por aprender. Trabalhei no ateliê até os 17 anos, quando este encerrou suas atividades (devido à doença de minha mãe). O aprendizado lá adquirido se tornou hoje um *hobby*.

A busca pelo conhecimento me deu o terceiro lugar no vestibular da UFMG, onde cursei o bacharelado em química, apesar de sempre ter estudado em escolas públicas precárias. Durante a graduação colecionei boas notas, muitos amigos e muito aprendizado, inclusive a partir das atividades extracurriculares: participei de congressos, da organização da sala de química na mostra de profissões da UFMG, fui secretária do Centro de Estudos de Química (o "grêmio" da química à época) por 2 anos, dei aulas em cursinho pré-vestibular para alunos carentes, dei aulas no ensino médio na escola que me formou e fiz iniciação científica durante 3 dos 4 anos da graduação.

Minha primeira experiência foi no extinto laboratório de aniquilação de pósitrons, onde avaliava micro porosidade de xerogéis de sílica. Foi meu primeiro contato com o estudo dos materiais e suas estruturas. Em seguida trabalhei no CDTN, sintetizando e utilizando xerogéis de sílica para a liberação controlada de fármacos, onde participei do meu primeiro congresso e comecei a entender melhor como funcionava a pesquisa científica e a vida em um laboratório de química. Minha próxima iniciação científica foi no laboratório da prof.ª Nelcy (laboratório de materiais nanoestruturados-LMN), que participou, desde então, da minha vida acadêmica e profissional. No LMN aprendi muito sobre os nanomateriais: alumina, óxido de zinco e ferritas. Lá trabalhei com a síntese, dispersão, caracterização e aplicação desses materiais. Ao término da graduação fiquei no LMN por mais um ano como bolsista no Programa Institucional de Bolsas de Iniciação em Desenvolvimento Tecnológico e Inovação (PIBITI), dessa vez buscando implementar o scale-up para produção de óxidos nanoparticulados. Esses conhecimentos me deram base para atuar na Nanum Nanotecnologia S.A..

Assim, saí do LMN para trabalhar em uma start-up, a Nanum. Por lá foram 10 anos de muito conhecimento, profissional e pessoal. Na Nanum participei do desenvolvimento da síntese e dispersão de óxidos nanoparticulados, que geraram alguns pedidos de patentes. Desenvolvi também um ferrofluido aquoso, aplicado na produção de tintas de segurança, que gerou uma patente internacional. Com exceção do RH, passei por todas as áreas da empresa (controle de qualidade, produção- execução e gestão, estação de tratamento de efluentes, controle de estoque, importação de matéria prima, exportação de produtos, analista, coordenação, gerência e diretoria de pesquisa e desenvolvimento). Durante o período que atuava como coordenadora de P&D, fiz o mestrado em engenharia de materiais (sob orientação da Prof.ª Virginia e corientação da Prof.ª Nelcy) voltado à nanometrologia. O tamanho de nanopartículas foi determinado por diversas técnicas e suas incertezas e aplicações foram discutidas. Mais que o título de mestre, adquiri ali a certeza de voltar um dia para fazer doutorado, porém com dedicação exclusiva, onde poderia me dedicar mais a aprender. Aprofundar o conhecimento no uso e propriedades dos materiais, em especial na teoria e operação de técnicas de caracterização de materiais.

Em 2017, após o nascimento do meu primeiro filho, decidi então não mais retornar à Nanum, lugar de onde guardo grande carinho e amizades, iniciando em 2018 o doutorado em engenharia de materiais. É o fruto deste período de muito trabalho, incertezas e (o melhor) aprendizado, sob as dificuldades impostas pela pandemia que todos enfrentamos, que lhes foi apresentado nas páginas que antecedem esta biografia.

Publicações: 5 artigos em periódicos, 4 patentes/pedidos de patente e 7 trabalhos publicados em congressos.

Link para currículo Lattes: http://lattes.cnpq.br/8885131632047299